2009

USE OF SURFACE GEOPHYSICAL TECHNIQUES TO LOCATE A KARST CONDUIT IN THE CANE RUN - ROYAL SPRING BASIN, KENTUCKY

Ganesh N. Tripathi
University of Kentucky, Ganeshtripathi@hotmail.com

ABSTRACT OF THESIS

USE OF SURFACE GEOPHYSICAL TECHNIQUES TO LOCATE A KARST CONDUIT IN THE CANE RUN - ROYAL SPRING BASIN, KENTUCKY

Groundwater flow in karst terrains is difficult to map because it can be concentrated through conduits that do not necessarily coincide with the surface features. We applied electrical resistivity (ER) and self-potential (SP) techniques at three sites to locate an inferred trunk conduit feeding a major spring in the Inner Bluegrass region of Kentucky. Royal Spring is the primary water supply for the city of Georgetown; the upper part of its basin coincides with the Cane Run watershed. ER and SP profiles were perpendicular to the inferred trunk conduit orientation. ER profiles (972 m total length) were measured using a dipole–dipole electrode configuration with 2- to 3-m spacing. SP measurements were taken along those ER lines and an additional test profile (230 m) using one stationary reference electrode and another roving electrode at a fixed interval.

The low resistivity of water in the conduit, as compared to the high background resistivity of limestone bedrock, is the ER exploration target. A negative SP anomaly corresponds to a low ER anomaly for most of the profiles, but a few are not comparable. Five of seven SP profiles measured over a period of several months were found to be reproducible. Although the overall trends of the final SP profiles for different dates were similar, the SP magnitudes varied with the amount of precipitation and the average soil temperature. The low-resistivity anomalies in the 2D inverted sections and corresponding negative SP anomalies could be water-filled conduits, although mud-filled voids encountered during drilling suggest that these may be tributary conduits rather than the trunk conduit.

Ganesh N. Tripathi

July 24, 2009

0USE OF SURFACE GEOPHYSICAL TECHNIQUES TO LOCATE A KARST CONDUIT IN THE CANE RUN - ROYAL SPRING BASIN, KENTUCKY

By

Ganesh N. Tripathi

Dr. Alan E. Fryar

Director of Thesis

Dr. Alan E. Fryar

Director of Graduate Studies

July 24, 2009

Date

RULES FOR USE OF THESES

Unpublished theses submitted for the Master's degree and deposited in the University of Kentucky Library are as a rule open for inspection, but are to be used only with due regard to the rights of the authors. Bibliographical references may be noted, but quotations or summaries of parts may be published only with the permission of the author, and with the usual scholarly acknowledgements.

Extensive copying or publication of the thesis in whole or in part also requires the consent of the Dean of the Graduate School of the University of Kentucky.

A library that borrows this thesis for use by its patrons is expected to secure the signature of each user.

Name and Address Date

_____

_____

_____

_____

_____

_____

_____

_____

_____

_____

_____

_____

_____

THESIS

Ganesh Nath Tripathi

The Graduate School

University of Kentucky

2009

USE OF SURFACE GEOPHYSICAL TECHNIQUES TO LOCATE A KARST CONDUIT IN THE CANE RUN - ROYAL SPRING BASIN, KENTUCKY

THESIS

A thesis submitted in partial fulfillment of the
requirements for the degree of Master of Science in the
College of Arts and Sciences
at the University of Kentucky

By
Ganesh Nath Tripathi
Lexington, Kentucky
Director: Dr. Alan E. Fryar, Associate Professor of Earth and Environmental Sciences
Lexington, Kentucky
2009

ACKNOWLEDGEMENTS

I would like to thank Dr. Alan E. Fryar for his continuous support, guidance and encouragement throughout the project. Without his generous support this work would not have been completed. I would like to thank the UK College of Agriculture SB–271 program for their support to carry out this research. I would like to express my sincere thanks to committee members Dr. Edward Woolery for his guidance during ER data processing and Dr. James Dinger for coordinating the field work.

I would also like to thank members of the Kentucky Geological Survey, especially Mr. James C. Currens, Mr. Randy Paylor, Mr. Bart Davidson and Mr. Steve Webb for their help during data collection and providing project related informations. I really appreciate J. S. Strohmeyer, Schnabel Engineering South, for acquiring good ER field data for this project. I would like to thank Dr. James W. Ward for his invaluable suggestions during SP data analysis. I am equally thankful to my friends Mr. John Warden, Mr. Estifanos Haile and Mr. Prakash Dhakal for their help at the different stages of this project.

Finally, I would like to thank my brother Prashant Tripathi and my wife Kalpana Bhandari for helping me in data collection and supporting me during the entire study period.

TABLE OF CONTENTS

LIST OF TABLES

LIST OF FIGURES

Chapter 1. Introduction

1.1 Groundwater in Karst

Karst is a term commonly associated with carbonate rocks, but other soluble rocks, such as evaporites, gypsum and anhydrite, are also susceptible to development of karst features (Bakalowicz 2005). Karst is developed on carbonate rocks when mildly acidic water (containing dissolved CO_2) dissolves the rock mass along preferential flowpaths. Groundwater transports the dissolution products and simultaneously enlarges the flowpaths (joints, fractures, bedding surfaces, grain boundaries, etc.) thus creating voids and conduits (Bakalowicz 2005). The voids formed may be occluded with sediments deposited following high storm events.

In granular aquifers, groundwater flow paths are commonly delineated by mapping distribution of hydraulic heads from observation wells or piezometers. However, in karst aquifers flow paths are difficult to map because of the extreme heterogeneity of karstified rocks (Bakalowicz 2005). Multiple researchers have sought to define and characterize karst aquifer systems using different techniques (Romanov et al. 2002, White 2002, Motyka 1998, John et al. 2006, Kiraly 2003, White and White 2005). John et al. (2006) attempted to model heterogeneity in karst groundwater flow with a sequence of model cells that simulate the network of conduit flow. Kiraly (2003) explained the karstification process using a theoretical numerical model in terms of both hydrological and geological discontinuities that emphasizes the effect of karst channel network and epikarst zone. Motyka (1998) produced a conceptual model based on examples from Poland incorporating the role of sediment-filled karstic features in

groundwater flow. Similarly, Romanov et al. (2002) studied the interaction between fracture and conduit flow to produce a numerical model that simulates the karst aquifer. White (2002) and White and White (2005) discussed the karst aquifer modeling in terms of triple porosity or triple permeability model (groundwater flow in matrix, fractures and conduits).

1.2 Integrated Geophysical Techniques in Karst

Geophysical methods such as electrical resistivity (ER), self-potential (SP), ground penetrating radar (GPR), electromagnetic induction (EM), microgravity and seismic refraction/reflection can aid in identifying and delineating subsurface voids in karst terrains. For example, an integrated geophysical approach using multiple techniques, EM and ER (Ahmed and Carpenter 2003) and GPR and 2D ER tomography (Carpenter and Ekberg 2006), was useful for identifying features such as buried sinkholes, soil pipes and associated bedrock fractures in northern Illinois. Similarly, GPR and ER tomography were used to locate shallow subsurface cavities in the vicinity of Cairo, Egypt (El-Qady et al. 2005), and to identify a potentially unstable zone above a cave roof in southern Italy (Leucci and De Giorgi 2005). SP and ER responses over a thick conductor were tested on a laboratory model (Adeyemi et al. 2006). The authors concluded that SP was more efficient in locating and determining the orientation of a target in comparison to ER. Gravity, magnetic and GPR techniques were applied to detect underground cavities in northeast Spain (Mochales et al. 2008) and EM, gravity and SP were applied to study Kartchner Caverns State Park, Arizona (Lange 1999). Jardani et al. (2007) used SP and EM data to locate sinkholes and crypto-sinkholes. A microgravity survey in south Wales, United Kingdom, was able to identify confined and unconfined

conduits at varying depths (Styles et al. 2005). However, the authors emphasized the need for an integrated geophysical approach to validate the results. Researchers in Florida found that commercially available seismic refraction tomography software is capable of detecting typical undulating bedrock surfaces (Hiltunen et al. 2007). Similarly, seismic refraction tomography has been used to delineate possible karst conduits on the Oak Ridge Reservation, Tennessee (Sheehan et al. 2005).

The SP method has been widely used in groundwater flow studies due to its effectiveness in detecting subsurface water movement. The natural electric potential difference produced by streaming, or electrokinetic potential due to the underground movement of water, is more efficiently detected by the SP method than by any other geophysical technique. Laboratory experiments to study the streaming potential generated by water movement through different geologic media have been performed by Ahmed (1964) and Bogoslovsky and Ogilvy (1972). Ahmad (1964) investigated the streaming potential generated due to water movement through unconsolidated rock while the laboratory experiments on fissured media models by Bogoslovsky and Ogilvy (1972) expanded the scope of streaming potential to the study of karst groundwater flow. Unlike other geophysical techniques, relative SP amplitude along the same survey line varies significantly with time while preserving an overall trend, and in most cases the variations can be related to hydrogeological and meteorological parameters (Ernstson and Scherer 1986). Corwin (1990) has given a more detailed account of the SP field techniques in environmental and engineering applications. Either positive or negative SP expressions can be expected over the cave passages. These expressions could be related to the downward filtration effect through the cave walls and ceilings; movement toward the

surface by capillary action; streaming potential of flowing water in conduits; and/or the pH of the electrolyte (Lange and Kilty 1991, Ishido and Mizutani 1981). Lange and Kilty (1991) described many case studies of SP response over caverns in different parts of the United States and possible effects from artificial current sources such as cathodic protection devices on pipelines. In volcanic areas, Aubert and Atangana (1996) found a linear correlation between the unsaturated zone thickness and the range of negative SP anomalies. Those authors proposed a new concept of self-potential surface (SPS) that differentiates the unsaturated zone from the saturated and/or impermeable zone. Wanfang et al. (1999) developed a methodology to remove the topographic effect from SP data and applied it to identify discrete recharge zones for a karst aquifer. Concentrated vertical groundwater movement through sinkholes produces a significant negative anomaly for an uncontaminated karst aquifer. Several attempts have been made to quantify surface SP data to reproduce reliable subsurface information both in the lab and in the field. A new method to interpret the surface SP data quantitatively by determining the shape factor of an anomaly has been tested on synthetic data with and without noise component and implemented for a field data set (El-Araby 2004). Fagerlund and Heinson (2003) utilized the SP method in the laboratory and in the field to determine drawdown and other aquifer parameters.

There are very limited examples of ER being applied independently in karst studies. However, Schwartz and Schreiber (2009) quantified potential recharge through mantled sinkholes using differential electrical tomography. In most cases this method has been implemented in conjunction with other geophysical methods. The effectiveness of different electrode arrays in ER surveys differs with the properties of the geological

target, and depth and selection of an appropriate electrode array are of prime importance in getting reliable subsurface information (Zhou et al. 2002). Those authors compared Wenner, Schlumberger and dipole-dipole electrode arrays to study potential karst hazards associated with sinkholes and found the dipole-dipole array to be the most appropriate technique in such studies. Roth and Nyquist (2003) evaluated the applicability of the multi-electrode earth resistivity technique in karst, comparing several resistivity sections obtained from Wenner, dipole-dipole and Schlumberger arrays with the boring results, and found encouraging results in locating subsurface voids and determining bedrock depths with few limitations. In the Inner Bluegrass region of Kentucky, Bonita (1993) used the ER response to identify different geological formations and correlated their thicknesses with available standard stratigraphic sections. Graham (2000) studied the area to identify the water-bearing conduits supplying Royal Spring in the nearby city of Georgetown.

SP in conjunction with ER was found to be effective for locating sinkholes and crypto-sinkholes in chalk karst in northwestern France (Jardani et al. 2006). Those authors compared the SP results measured during spring and summer and found negative SP anomalies associated with the same sinkholes and crypto-sinkholes, but the number and magnitude of anomalies were reduced in the summer data. In a lab experiment, the SP technique was more reliable than ER in locating a thick conductor buried at different orientations (Adeyemi et al. 2006). In general, the usefulness of a geophysical technique can vary depending on the depth and geometry of the target feature, the composition and thickness of overlying soils, and whether the feature is water-filled or not.

1.3 Geology of the Region and the Study Area

The Inner Bluegrass region of central Kentucky is characterized by karstic features developed in the limestone bedrock on the surface and subsurface. The Cincinnati Arch, which is a major regional geological structure, controls the overall gentle dip of the bedrock strata. This north-south trending arch forms the Jessamine and Nashville domes along its axis, which are separated by a saddle in Cumberland County, Kentucky (Nosow et al. 1960). The general stratigraphic sequence of this area consists of the Ordovician-era High Bridge Group, Lexington Limestone and Clays Ferry Formation in ascending order. The High Bridge Group is sub-divided into the Camp Nelson Limestone, Oregon Limestone and Tyrone Limestone (Cressman 1965). The oldest exposed rock in the region can be found in the Kentucky River gorge at Camp Nelson. A disconformity separates the Lexington Limestone from the underlying Tyrone Limestone. The Lexington Limestone is sub-divided mainly on the basis of lithologic characteristics into 11 members (Cressman 1967).

The study area generally lacks exposed rock sections for stratigraphic studies. The nearest measured stratigraphic section, located in the area of the Vulcan quarry, is about 1.5 to 5 km away. A section of about 21 m has been measured at this location (Bonita 1993). On the basis of stratigraphic position and lithologic characteristics, the Lexington Limestone there was subdivided into the Millersburg, Tanglewood, Brannon, and Grier members (Fig. 1.1).

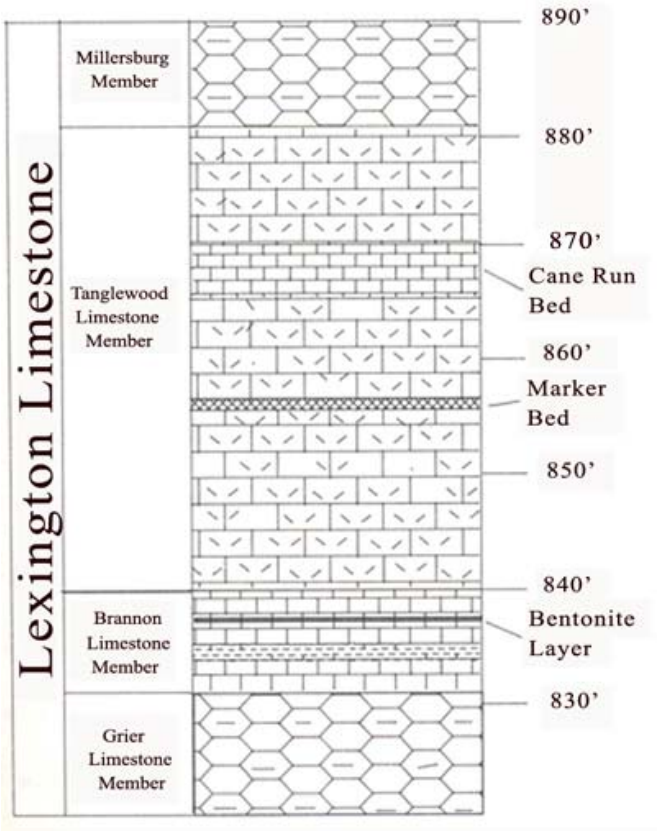

Figure 1.1. Stratigraphic section measured in Vulcan quarry (Bonita 1993).

The Grier Member is the oldest exposed unit of the Lexington Limestone in this area. It is characterized by nodular-bedded, fossiliferous calcisiltite and calcarenite which are poorly sorted (Cressman 1973). The Grier Member is locally intertongued with the Tanglewood Member which makes the contacts with the lower and upper unit of the sequence more complex. The Tanglewood Member is comprised of medium-grained, well-sorted bioclastic calcarenite containing bryozoan fragments and silicified brachiopods (Cressman 1973). Although the Brannon Member overlies the Tanglewood Member in normal stratigraphic sequence, the Brannon Member has been exposed between the Grier and Tanglewood Members in the study area (Bonita 1993). The Brannon Member is characterized by interbedded shale and fine-grained argillaceous

limestone in nearly equal proportions. The total thickness of the unit measured in the Vulcan quarry was about 2.7 m, including an 8 cm thick bentonite bed (Bonita 1993). The youngest exposed member of the Lexington Limestone in the quarry, the Millersburg Member, is composed of fossiliferous limestone and shale. The beds are generally discontinuous with irregular surfaces resembling nodules, as in the Grier Member.

1.4 Hydrogeology of the Study Area

Because of the dissolution of the Lexington Limestone, groundwater flow tends to be channeled through a network of tributary conduits to a main conduit and thence to a spring. Karst aquifers receive direct recharge through sinkholes and swallets in addition to infiltration. Surface water and groundwater basins do not necessarily coincide with each other. Several groundwater basins have been identified within the Inner Bluegrass region (Thrailkill et al. 1982, Currens et al. 2002). Generally, shallow subsurface (epikarstic) flow characterizes interbasin areas and deeper subsurface flow through the integrated conduit system characterizes groundwater basin areas (Thrailkill et al. 1982). Palmquist and Hall (1961) prepared hydrogeologic maps of the region. Faust (1977) used data from more than 500 wells to construct the first hydraulic-head map of the region.

One of the largest groundwater basins in the Inner Bluegrass region, and perhaps the most studied, is the Royal Spring basin. Royal Spring, which is the main water supply for the city of Georgetown, emerges from the Grier Member of the Lexington Limestone. Prior investigations of the Royal Spring basin have been tended to use tracer techniques and wells (Thrailkill et al. 1982, Hamilton 1950, Matson 1909). In particular, Sullivan (1983) studied the relationship between velocity and discharge, conduit geometry and

type of flow using fluorescent dyes. Spangler et al. (1982) reported that all of their dye introduction points (mainly swallets) were within the Grier or Tanglewood member and interpreted the conduit or conduits to have developed within a narrow stratigraphic interval. Thrailkill and Gouzie (1984) conducted preliminary field studies to determine discharge and travel time in the basin and also tried to estimate the trunk conduit geometry. Paylor and Currens (2004) determined and mapped groundwater travel times to Royal Spring for a range of discharge values.

Although geophysical exploration techniques can complement hydraulic studies in estimating the geometry, depth and orientation of conduits, geophysical studies of the Royal Spring basin have been few and incomplete. Bonita (1993) performed an ER survey and fracture trace analysis in the basin. The results from the fracture trace analysis were inconsistent and did not show the preferential flow direction of groundwater. Bonita (1993) utilized the resistivity data to establish the subsurface lithostratigraphy of the area and correlated it with the standard lithostratigraphic section. The author concluded that the groundwater basin underlies highly fractured areas and the interbasin underlies less fractured areas. Graham (2000) tested the ER survey technique on a known karst feature (Marshall Spring, Scott County) and applied it at the Kentucky Horse Park. A drillhole in the area encountered a water-bearing conduit, which the author interpreted to feed Royal Spring.

Despite multiple previous studies, the trunk conduit that drains the Royal Spring basin remains largely unmapped. Locating the trunk conduit is important for understanding the potential susceptibility of Royal Spring to non-point source pollution (for example, from urban and agricultural runoff into sinkholes) and point source

pollution (such as from chemical spills along highways crossing the groundwater basin). Integrated geophysical investigations could reduce the number and expense of drillholes needed to locate the conduit at various points. However, the depth, geometry and water content of the conduit may limit the usefulness of certain geophysical techniques.

1.5 Objectives

Electrical resistivity and self-potential geophysical techniques were applied to delineate the major karst conduit that supplies water to Royal Spring at Georgetown. The geophysical studies were intended to constrain the probable location of conduit for drilling. We hypothesized that water flowing through the conduit will produce a low resistivity anomaly and negative SP anomaly. The three sites selected for this study were the UK Agricultural Research Farm north of Interstate 64, along Berea Road and the Kentucky Horse Park. These sites were selected based on the locations of sinkhole and dye tracer results (Spangler et al. 1982, Paylor and Currens 2004). The first two sites are located in northern Fayette County and the latter is located in southern Scott County (Fig. 1.2).

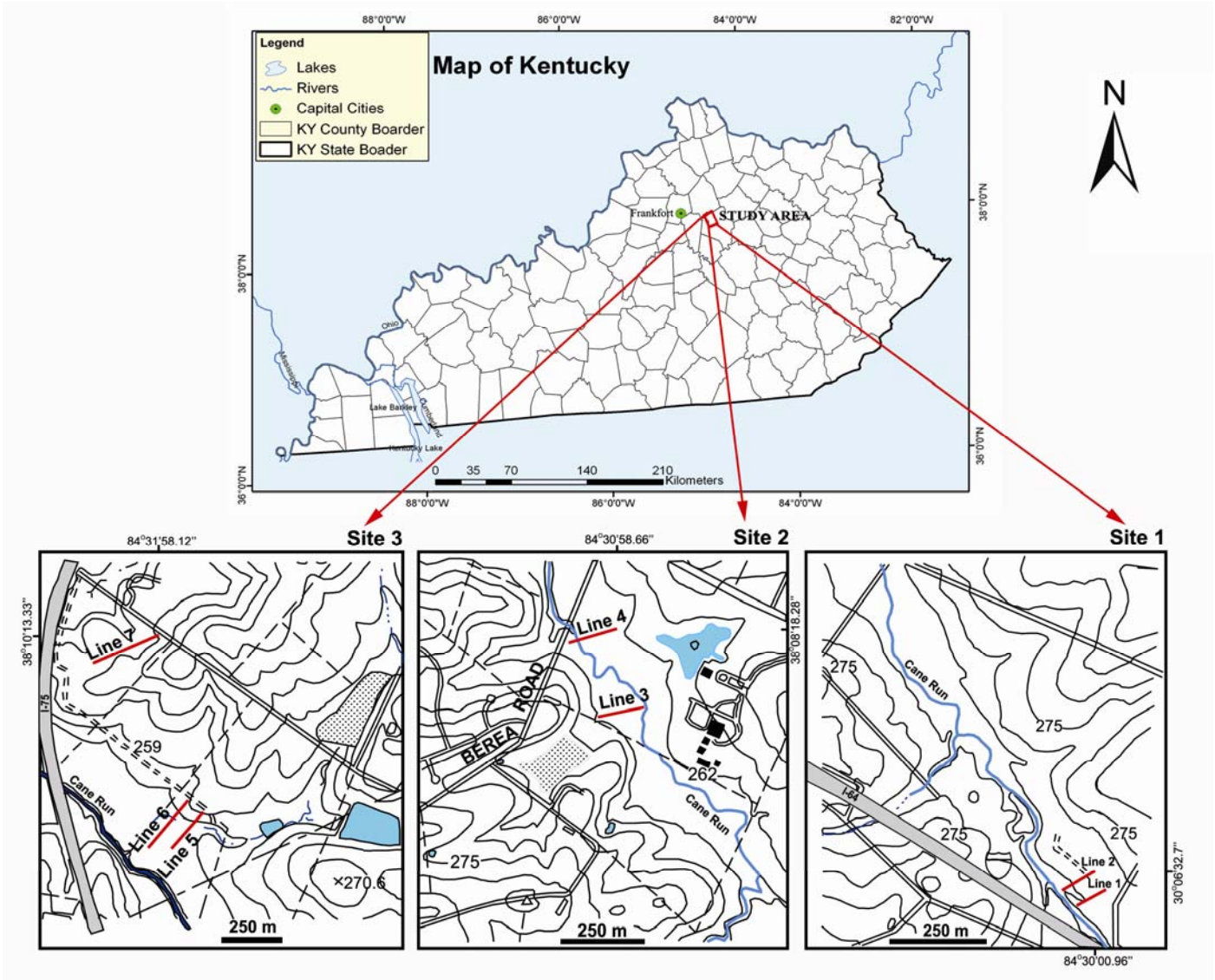

Figure 1.2. Map showing geophysical survey lines at study sites (1, UK Agricultural Research Farm; 2, Berea Road; 3, Kentucky Horse Park). (Contour interval: 3 m).

Chapter 2. Methods

Two electrical surveying methods, one using natural currents and other using artificially generated currents, have been implemented in the present study. We used the self-potential method (measuring potential difference due to natural currents flowing within the Earth's surface) and electrical resistivity method (measuring the resistance to current artificially injected into the ground) in an attempt to locate the karst conduit within the Royal Spring groundwater basin. Both techniques are briefly discussed under different sub-topics in this chapter.

2.1 Electrical Resistivity

2.1.1 Basic principles

The systematic use of electrical resistivity techniques to investigate the sub-surface goes back to about 1920 (Parasnis 1986). The fundamental principle of the resistivity method is based on Ohm's law, which states that current (I) passing through any two points in a circuit is directly proportional to the potential difference (dv) and inversely proportional to the resistance (R) between them. The resistance (R) of any medium or conductor depends on the length (l) and cross-section area (A) through which the current is passing. These two relations are expressed as equations 1 and 2 below:

$$I = dv/R \quad \text{..... (1)}$$

and

$$R = \rho l/A \quad \text{..... (2)}$$

where ρ is the constant of proportionality, known as the *resistivity* of the medium through which the current is passing. This fundamental law of electricity developed for a current flowing through any conducting media has been implemented to measure Earth resistance.

Utilizing the above-mentioned relations, the apparent resistivity of the subsurface can be determined with different surface electrode configurations. The apparent resistivity of a homogeneous isotropic medium due to a single current electrode at the surface can be represented by the following relation (equation 3) (Telford et al. 1983, Parasnis 1986):

……. (3)

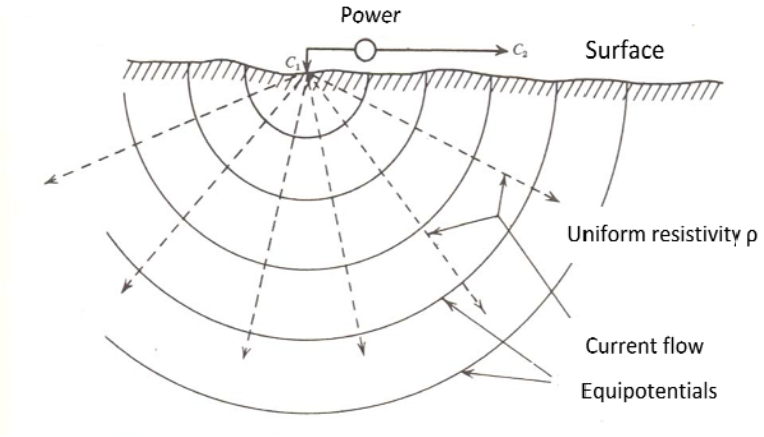

Figure 2.1. Current flow lines and equipotentials due to single-current electrode at surface (Telford et al. 1983).

Similarly, the potential at any point due to two current electrodes at the surface can be derived by calculating the potential due to each current electrode individually and summing to get the total potential at that point. If we have two potential electrodes

measuring potential difference between the two current electrodes, then this is equal to the difference between the total potential at each electrodes due to the two current sources (Fig. 2.2). This can be represented by equation 4 below (Telford et al. 1983):

$$\Delta V = \frac{I\rho}{2\pi}\left\{\left(\frac{1}{r1} - \frac{1}{r2}\right) - \left(\frac{1}{r3} - \frac{1}{r4}\right)\right\} \quad \text{..... (4)}$$

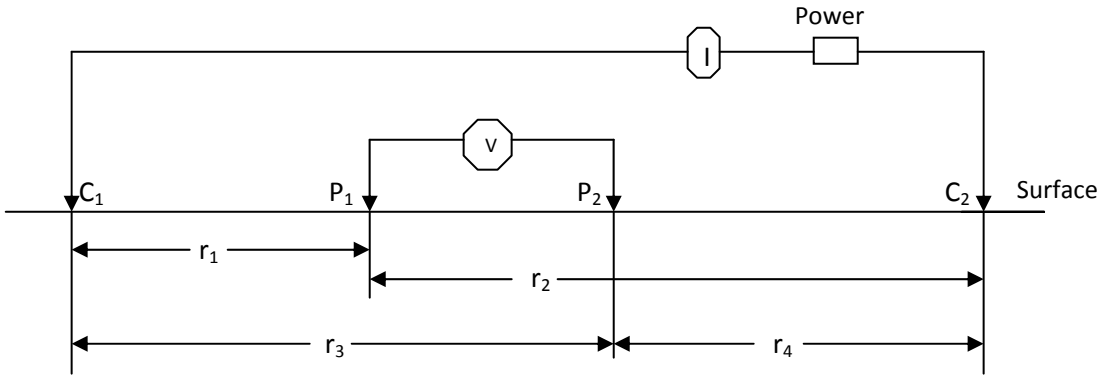

Figure 2.2. Representative electrode arrangements for four-electrode spreads commonly used in resistivity field work. (Modified from Telford et al. 1983, Fig. 8.3.)

The detailed derivation of the above-mentioned equations can be found in standard textbooks, such as Telford et al. (1983), Parasnis (1986), and others.

2.1.2 Data acquisition (Field methods)

In this method, artificially generated current is injected into the ground through a pair of metal electrodes (current electrodes) and the resulting potential difference is measured by another pair of electrodes (potential electrodes). Various electrode configurations have been proposed by many researchers. The Wenner and Schlumburger arrays have been the most popular. In a Wenner array, the electrodes are spread at uniform distance along a line with the current electrodes at the two ends and the potential

electrodes in the middle of the array. All four electrodes are extended away from a fixed center with equal electrode spacing for depth exploration (sounding) while all four electrodes are moved along a line with constant electrode separation for mapping. In the Schlumberger array, the distance between the potential electrodes placed at the middle of the array is much less than the distance between the current electrodes at both ends. The Wenner array is commonly used to map the lateral variation while the Schlumberger array is mostly used to explore greater depths.

A resistivity survey with fixed electrode spacing and moving along a constant distance to map lateral variation is termed resistivity profiling or mapping, whereas a resistivity survey undertaken with increasing electrode spacing for each measurement to explore greater depth is called electrical sounding or drilling (Telford et al. 1983). We used the dipole-dipole array (Fig. 2.3) for this study. In comparison to the Wenner and Schlumberger methods, the dipole-dipole method has greater sensitivity to vertical resistivity boundaries and is more capable of detecting subsurface voids filled with water (Zhou et al. 2002). Roth and Nyquist (2003) evaluated several multi-electrode configurations and concluded the dipole-dipole configuration is most reliable and capable of providing subsurface detail in karst areas.

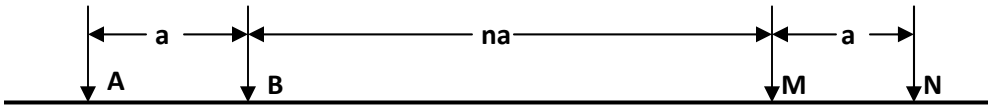

Figure 2.3. Dipole-dipole spread. A, B and M, N are current and potential electrode pairs,respectively, separated by a constant distance ‘a’. (Modified from Parasnis (1986), Fig. 4.13(c)).

We collected resistivity data at three different sites within the Inner Bluegrass region. Resistivity data along two lines at each site were collected using an eight-channel

SuperSting (R8/IP) multi-electrode earth resistivity meter, a product of Advanced Geosciences Inc. (AGI). The two lines at the first site (Fig. 1.2) were surveyed at 2-m electrode spacing and the other four resistivity lines at the remaining two sites were surveyed at 3-m electrode spacing. The survey lines were expected to run perpendicular to the inferred trunk conduit. The relative distances between the current and potential electrode pairs were increased for each measurement in order to sample greater depth. The maximum separation between current and potential dipole was set at six times the dipole (current or potential) spacing for data with better resolution (Loke 2001).

2.1.3 Data processing

The electrical resistivity survey data obtained were processed using EarthImager 2D version 2.2.0 (AGI, Austin, Texas) to get the inverted resistivity sections for all the survey lines. EarthImager 2D is a professional (commercial) software for resistivity and IP inversion. The resistivity data file format collected by the SuperSting is directly compatible with this software. In the initial setting menu in the settings window, the definition of the y-axis and orientation of the vertical axis need to be set before reading the data file while other settings can be set after reading the data file. As a first attempt at noisy data removal, the bad electrodes were identified and removed using the electrode editor submenu of the edit main menu. Thresholds for all the criteria of noisy data removal in the initial setting window were set (Table 2.1). Any data beyond these thresholds will automatically be removed in the inversion. Noisy data can also be removed manually by selecting with mouse clicks and deleting the data. Damped least-squares, smooth model inversion and robust least-squares inversion are three available options in the software to invert the resistivity data. The robust inversion method was

chosen for the inversion of the entire data set but the other two methods of inversion were also tested during data processing. The robust least-squares inversion method is more efficient in inverting noisy data as compared to the smoothness constrained least-squares inversion (Dahlin and Zhou 2004). In robust inversion the model is produced by minimizing the absolute value of data misfit (L1-norm), while in the smooth inversion it is obtained by minimizing the square of data misfit (L2-norm) (Dahlin and Zhou 2004).

Table 2.1. Inversion settings applied to data

<table>
<tr><td colspan="6">Initial Settings</td></tr>
<tr><td colspan="6">Data Removing Thresholds</td></tr>
<tr><td>Minimum Voltage (mV)</td><td>Minimum abs(V/I)-Ohm</td><td>Maximum Repeat Error (%)</td><td>Minimum Apparent Resistivity (Ohm-m)</td><td>Maximum Apparent Resistivity (Ohm-m)</td><td>Maximum Reciprocal Error</td></tr>
<tr><td>0.2</td><td>0.0005</td><td>3</td><td>1</td><td>10,000</td><td>5</td></tr>
<tr><td colspan="6">Forward Modeling settings</td></tr>
<tr><td>Forward Modeling Method</td><td>Forward Equation Solver</td><td>Type of Boundary Condition</td><td>Number of Mesh Divisions</td><td>Thickness Incremental Factor</td><td>Depth Factor</td></tr>
<tr><td>Finite Element</td><td>Cholesky Decomposition</td><td>Dirichlet</td><td>2</td><td>1.1</td><td>1.1</td></tr>
<tr><td colspan="6">Resistivity Inversion Settings</td></tr>
<tr><td rowspan="3">Stop Criteria</td><td colspan="4">Number of Iterations</td><td>8</td></tr>
<tr><td colspan="4">Maximum RMS Error (%)</td><td>3</td></tr>
<tr><td colspan="4">Error Reduction (%)</td><td>5</td></tr>
<tr><td colspan="5">Stabilizing Factor/Damping Factor</td><td>10</td></tr>
<tr><td colspan="4">Starting Model</td><td colspan="2">Average Apparent Resistivity</td></tr>
<tr><td colspan="5">Model Parameter Width</td><td>1</td></tr>
<tr><td colspan="5">Model Parameter Height</td><td>1</td></tr>
<tr><td colspan="5">Resolution</td><td>0.2</td></tr>
<tr><td colspan="5">Horizontal/Vertical Roughness Ratio</td><td>1.5</td></tr>
</table>

A finite-element forward modeling method was used to create a model setting Cholesky decomposition as a forward equation solver with the Dirichlet boundary condition. The number of mesh divisions was set to 2 between two electrodes. The thickness incremental factor and depth factor were set to 1.1 with the assumption that the thickness of the layers increases with depth.

In the resistivity inversion settings, the stop criteria were set with maximum number of iterations at 8, 3 % RMS error and 5 % error reduction. The inversion terminates on meeting one of the criteria in these settings. Both the stabilizing and damping factors were set to 10 and the robust data conditioner and robust model conditioner were set to 1 to avoid over-smoothing in the resulting model. For resolution factor the default value of 0.2 was accepted. The average apparent resistivity pseudosection was set to starting model for the inversion of all the data sets. Minimum resistivity was set to 1 ohm and maximum resistivity was set looking at the pseudosection after reading the data file. The horizontal/vertical roughness ratio was set to 1.5 to enhance the effect of lateral variations along the survey profile.

The inversion process progresses iteratively by taking the average apparent resistivity pseudosection as a starting model, to find a best fit between measured and predicted resistivity values and finally to produce the inverted resistivity section. In each iteration the model is adjusted to match the measured pseudosection utilizing a least squares optimization technique (Roth and Nyquist 2003).

2.1.4 Survey equipment

The following details on survey equipment have been summarized from the instruction manual for the SuperSting^{TM} with Swift^{TM} automatic resistivity and IP system (AGI 2005). As the name suggests, it collects data eight times faster than the single channel meter because of its ability to measure the potential between nine electrodes simultaneously for each current injection. Unlimited numbers of electrodes can be used with this instrument, which makes resistivity data acquisition less labor-intensive and time-consuming for large area coverage.

Figure 2.4. Eight-channel SuperSting R8/IP resistivity meter used for the survey.

This instrument consists of 12-V DC batteries, a switch box, 56 stainless-steel electrode stakes and a passive electrode cable (Swift cable). Six different electrode arrays (resistance, Schlumberger, Wenner, dipole-dipole, pole-dipole and pole-pole) are currently supported by this instrument. A command file must be loaded and stored in the instrument RAM before creating a new data file for any measurements. The command file controls the SuperSting to perform within a user-defined electrode configuration. It

can be created either using the “command creator module” of the SuperSting Administrator or manually by using any text editor. Separate command files are created for measurements with different electrode configurations. For each survey a new data file is created that works with a particular command file.

After the electrodes are laid out on the ground, the batteries inject the DC current through two current electrodes and the other two electrodes are used to measure the potential difference. The instrument was set up for automatic survey creating a data file with the appropriate command file. The unit of measurement was selected as meter and the electrode spacing was entered. If the survey line is longer than the electrode cable the roll-along survey option is chosen. We used the roll-along survey technique along three out of six survey lines (two at the Kentucky Horse Park [Lines 5 and 6, Fig. 1.2] and one at the Berea Road soccer field site [Line 4, Fig. 1.2]). The contact resistance test was performed before taking the measurements to assure good contact between electrodes and the ground. The switch box connected to the instrument changes the current and potential electrode position for each measurement according to the survey configuration set in the command file.

2.2 Self-Potential Method

The SP method is very simple, cost-effective and less sophisticated than other geophysical methods. This method measures the natural electrical potential of the ground surface generated by various sources. Clearly defined sources of the SP are mainly the fluid and heat fluxes, diffusion between regions of different chemical composition, and redox reactions between ore bodies and their surroundings (Fagerlund and Heinson

2003). Flow of fluids through the subsurface media produces electrokinetic or streaming potential that is different from areas without this kind of fluid movement. Similarly, diffusion and mineralization potentials are produced in areas with different chemical composition and mineralized ore bodies, respectively. The high sensitivity of SP method compared to other geophysical techniques, particularly in the measurement of streaming potential due to groundwater flow, has been found to be more efficient than any other geophysical technique (Lange and Kilty 1991, Fagerlund and Heinson 2003, Stevanovic and Dragisic 1998, Aubert and Atangana 1996). We used the SP method because of its inferred sensitivity to groundwater flow within a conduit.

2.2.1 Theory of streaming potential

Streaming or electrokinetic potentials result during the flow of any fluid through or against a solid medium. Helmholtz in the 19th century found that an electrolyte flowing through a capillary tube generates an electric potential difference between its ends. He was first to study this kind of phenomenon in detail (Parasnis 1986). This basic principle of streaming potential has been applied successfully in the study of groundwater flow. The motion of ions in the flowing liquid is the main source of this potential. The electric field (Vm^{-1}) due to the ions in motion can be obtained by solving equation 5 below (Parasnis 1986):

$$E = \frac{\varepsilon \rho \zeta}{4\pi\mu} p \quad \text{..... (5)}$$

where ε is the dielectric constant of the electrolyte, ρ is the resistivity of the electrolyte, ζ is the streaming potential, p is the pressure gradient and μ is the dynamic viscosity of the electrolyte.

Along the solid-liquid interface, excess charge accumulates to form an electrical double layer that generates streaming potential in the flowing liquid. According to the Gouy-Chapman model (Fig. 2.5), the uniform surface charge in the solid medium is balanced by the excess charge of opposite sign in the liquid phase. In the diffuse layer the charge density is maximum nearest the solid wall and decreases linearly to zero at some distance away from the interface. In the Stern model, an additional layer (the Stern layer) has been defined between the interface and the diffuse layer. According to this model, the layer next to the solid surface accommodates more adsorbed ions. Consequently, the potential in the Stern layer increases linearly and approaches zero at the diffuse layer. Figure 2.6 depicts this principle.

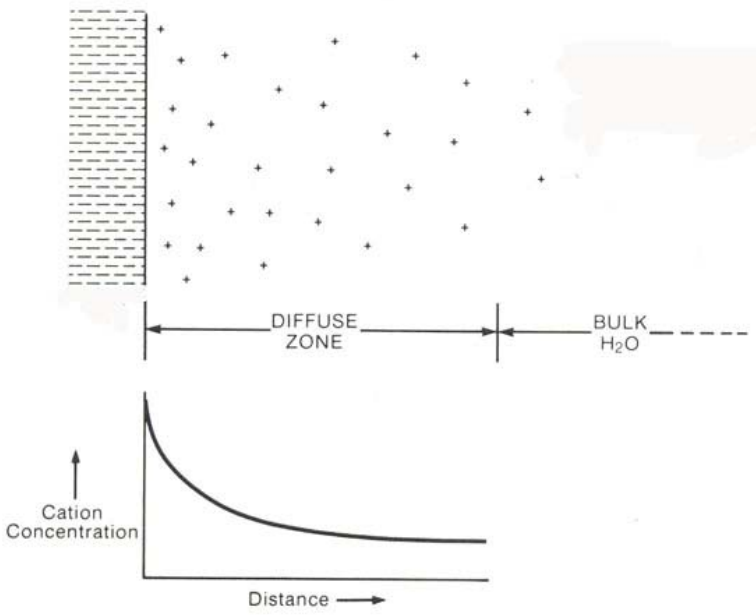

Figure 2.5 Gouy-Chapman model showing electrical double layer at clay-water interface (Eslinger and Pevear 1988).

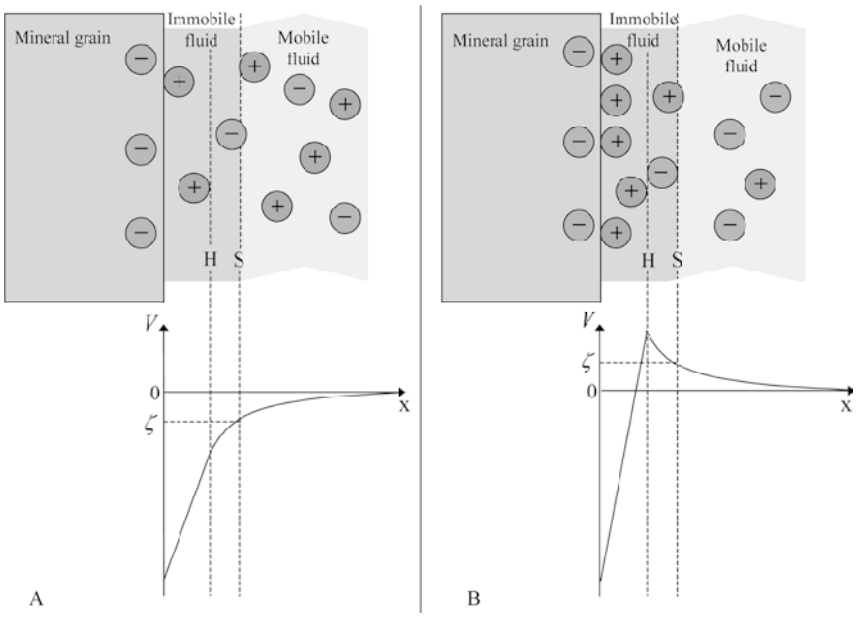

Fig. 2.6. Stern model showing electrical double layer at a rock-water interface (Fagerlund and Heinson 2003).

The electric potential (V) is shown as a function of distance (x) from the pore wall. The hydrodynamic slipping plane (S) separates the mobile and immobile phases of the liquid. The potential at this plane is the zeta or streaming potential (ζ). Depending on the amount of specific adsorption in the Stern layer between the pore wall and plane H, ζ can be positive (B) or negative (A). For a negative ζ, more positive than negative ions are transported with the fluid (Fagerlund and Heinson 2003).

2.2.2 Data acquisition

The gradient and fixed-base survey configurations are the main configurations widely used to collect SP data along a survey profile (Telford et al. 1983, Parasnis 1986, Corwin 1990). In the gradient array, the two non-polarizing electrodes are connected through a digital multi-meter with a fixed length cable and moved along the survey line. After each measurement, the trailing electrode occupies the position of leading electrode

for the new measurements and the process is continued to cover the entire survey length. As its name suggests, the fixed-base survey is performed by keeping one electrode (reference or base electrode) at a fixed base station while the other electrode (roving electrode) is moved at a constant interval to cover the entire survey line. The fixed-base array has many advantages over the gradient array: it lowers the level of cumulative error, can be conducted by a single operator, offers flexibility in reoccupying the previous stations, and offers better data reproducibility because stations with anomalous readings can be repeated (Corwin 1990). We used the fixed-base configuration for all of our survey lines, moving the roving electrode every 3.05 m (10 feet) or 4.57 m (15 feet) from the previous station. The base electrode (reference electrode) is buried about 30 cm and the roving electrode was placed about 15 to 20 cm below the ground surface. The holes were watered only in case of extremely dry soil, taking caution not to generate any kind of infiltration effect, to make a good contact between the electrodes and the ground. Two lines at Site 1 were measured every 3.05 m and the other lines were measured every 4.57 m from the base station. The base station was reoccupied every half an hour to correct for possible electrode drift caused by the temporal effect. As reported by Ernstson and Scherer (1986), we also observed a direct temperature effect on the electrodes during the day, particularly during sunny days. We tried to avoid this effect by putting the electrodes in shade. The fluctuation in meter readings increased as we moved farther away from the base station. At each station the minimum and maximum SP values were recorded for 2 to 3 minutes in accordance with the site condition (more sampling time for higher fluctuation in SP readings). The mean value is the representative SP for that station. The measurements were taken two to four times on different dates at each site.

2.2.3 Data processing

The SP data collected in the field were smoothed taking the moving average of the SP value along each survey line. This technique filters the high frequency noise from the data. SP varies with site conditions, such as temperature variation, electrode drift and polarization, rainfall, construction activity, topography, and water table depth (Corwin 1990). SP variations could be significant even for an hour-long survey, as well as over a period of months or years (Corwin 1990). The drift in the SP data is mainly the result of temporal variation in temperature and change in soil moisture content during the course of measurements. The temporal drift for each measurement should be corrected with the drift data collected during the survey. We used equation 6 to correct for the drift, which assumes a linear drift between successive base station readings (Wanfang et al. 1999):

$$V_{cj} = V_j - \left[V_{pi} + \frac{(T_j - T_{pi})(V_{ni} - V_{pi})}{T_{ni} - T_{pi}} + V_0\right] \quad \text{..... (6)}$$

where V_{cj} is drift-corrected SP; V_j is measured voltage at time T_j on line j; V_{pi} and V_{ni} are previous and subsequent readings at base station i at times T_{pi} and $T_{ni,}$ respectively; and V_o is the first base-station reading.

Where topography is irregular, the SP data vary inversely relative to changes in elevation (Telford et al. 1983, Ernstson and Scherer 1986, Aubert and Atangana 1996). We used the topographic correction method described by Wanfang et al. (1999) to remove the probable topographic effect on the data from site 3 at the Kentucky Horse Park, where topographic relief is 5.13 and 3.7 m for Lines 5 and 6, respectively. Topographic effects for other two sites were not calculated because relief at those sites is

less than 1 m. The topographic effect for each SP data point is calculated using equation 7 (Wanfang et al. 1999):

$$V_j^{te} = K_j\left(h_j - h_{0j}\right) \quad \text{..... (7)}$$

where V_j is the potential at elevation h_j along line j; K_j is the topographic correction factor; and h_{oj} is elevation of the first measurement.

The data obtained after processing were plotted against the distance along the survey line to get the final SP profile for analysis and interpretation.

2.2.4 Survey equipment

The components required for SP measurements were assembled from different sources. The instrumentation includes two non-polarizing electrodes, a digital multi-meter, and connecting cable, as well as a shovel to dig holes for electrodes, distilled or de-ionized water to clean electrodes between measurements, and a connecting cable about 220 m long with a reel. Non-polarizing electrodes were selected in order to avoid possible polarization while using ordinary metal stakes as electrodes (Telford et al. 1983, Parasnis 1986). Copper-copper sulfate half-cell electrodes were used, in which the copper rod is submerged in a supersaturated copper sulfate solution inside a container with a porous ceramic base that establishes contact between the electrode and the soil. A digital multi-meter with high input impedance value of 10 M-ohm was used to measure the potential difference (mV) between the reference and roving electrodes. An 18-gauge insulated connecting cable was used to connect two electrodes with the multi-meter.

Chapter 3. Interpretation and Discussion

3.1 Electrical Resistivity Data Interpretation

The resistivity data were interpreted to reflect the subsurface based on the response of underlying material to the injected currents. In the past, plots of resistivity data against the electrode spacing along the survey line were matched with theoretically calculated master curves to find the layer parameters such as apparent resistivity, layer thickness and the depth to the layer interface. Nowadays, with the development of sophisticated data acquisition and data processing techniques, it has become less time-consuming and labor-intensive to model the subsurface with resistivity data. As the measured apparent resistivity is the result of the cumulative effect of subsurface media, the inhomogeneous and anisotropic nature of real Earth material introduces ambiguity in interpretation.

All the sounding data gathered from the field applying the dipole-dipole electrode configuration were used to produce an inverted resistivity section along each survey profile. The inverted resistivity sections were interpreted on the basis of resistivity ranges that can be attributed to different Earth materials. The average apparent resistivity values measured during this study and in the study of Graham (2000) are constraints to distinguish the anomaly from the background resistivity values. The area is predominantly underlain by the Lexington Limestone and the discontinuity in the high resistivity layer along the profile is interpreted as due to the change in rock mass qualities (such as fractures, moisture content, etc.) along the profile. The average depth of

penetration varies with the properties of overburden soil and bedrock quality. The elevation changes between Royal Spring and the study sites are the major constraints on the probable target depths, i.e. the inferred conduit in the area.

3.1.1 ER line 1, University of Kentucky Agricultural Research Farm (Site 1)

This ER line is located within the University of Kentucky Agricultural Research Farm site north of Interstate 64. The ER data were collected along the NE–SW trending line with total profile length of 86 m. The model was adjusted from trial to trial during inversion by setting a threshold value of 12% relative data misfit for data removal and finally the data were inverted to get the resistivity section along the profile. Poorly-fit data above this threshold, 44 out of 515 points, were removed for this line. The effective depth of penetration for the section is around 15 m, which is equivalent to about 17% of the profile length. In general, the image gets distorted below 14 – 25% of the total survey length (AGI 2007) depending on the field condition.

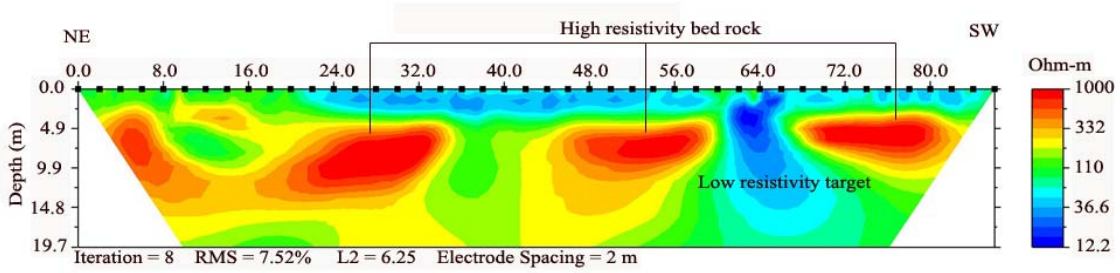

Figure 3.1. Interpreted inverted ER section along line 1 at the University of Kentucky Agricultural Research Farm (Site 1).

The inverted resistivity section shows a pronounced low-resistivity anomaly at approximately 14 m depth, between stations 60 and 70 m along the transect (Fig. 3.1). The apparent resistivity ranges between 10 and 50 ohm-m, which falls within the typical

resistivity range of fresh groundwater (Palacky 1987). Between stations 0 and 20 m the data suggest a very thin soil cover over weathered bedrock, whereas the remaining profile exhibits a relatively thick soil overburden. The thin soil cover was subsequently verified by direct soil probes. Beyond station 20 m, the topmost soil extends to the end of the profile and it attains maximum thickness of almost 3 m between stations 36 and 38 m. A resistivity range of about 30 – 75 ohm-m characterizes this layer. This layer is underlain by another 2- to 3-m thick layer of intermediate resistivity ranging from about 80 to 240 ohm-m, which continues throughout the profile except below the stations 35 to 42 m and 60 to 66 m. This layer is exposed almost at the surface between stations 0 and 20 m and the bottom of the layer is present at 2.5 m depth at the NE end of the profile, while it continues beneath most of the rest of the profile at a consistent depth of about 4.5 m. The lowermost distinguishable layer, with a higher resistivity ranging from about 240 to 678 ohm-m, appears throughout the section except in two places where it is interrupted by relatively low resistivity zones. These zones are interpreted as the result of poor rock-mass quality due to fractures and joints or the void being filled with clay-rich sediments, while the exceptionally low-resistivity anomaly has been treated as the water-bearing target. The thickness of this anomaly varies from 8 to 12 m and the top and bottom of the layer are located between 3 and 15 m depth from the surface.

3.1.2 ER line 2 (Site 1)

ER line 2 is located in the same field at site 1 and 93 m west of ER line 1. This line, 88 m long, runs almost parallel to the first resistivity line. The inverted resistivity section shows a close correlation with ER line 1. All three distinct layers on both of the sections at this site are closely correlated. The data above 24% relative data misfit, 52 out

of 512 points, were removed before inverting to get the final resistivity section (Fig. 3.2). The effective depth of penetration for the section is also around 15 m, which is equivalent to about 17% of the profile length.

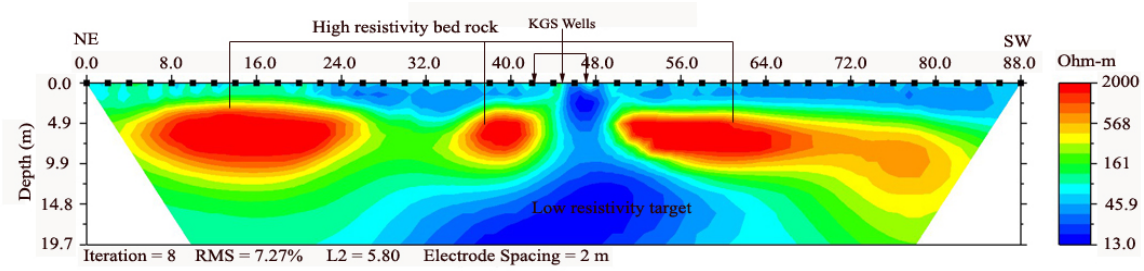

Figure 3.2. Interpreted inverted ER section along line 2 at the UK Agricultural Research Farm (Site 1).

The inverted resistivity section shows a pronounced low-resistivity anomaly centered at approximately 15 m depth between stations 42 and 50 m along the transect (Fig. 3.2). The apparent resistivity (between 10 and 100 ohm-m) falls within the typical resistivity range of fresh groundwater. Between stations 0 and 22 m the data suggest a very thin soil cover over weathered bedrock, whereas the remaining profile exhibits a relatively thick soil overburden. The topmost low-resistivity layer in this section strikes SW and attains its maximum thickness (to a depth of about 4.5 m) at the end of the profile. A resistivity range of about 32 – 80 ohm-m characterizes this layer. This layer is underlain by another 1- to 4-m thick layer of intermediate resistivity ranging from about 80 to 318 ohm-m, which continues throughout the profile except below the stations 44 to 48 m. This layer is exposed almost at the surface between stations 0 and 22 m. The bottom of the layer is present at 4.8 to 7.5 m along the ends of the profile and the layer thins between the stations 24 to 58 m. The lowermost distinguishable layer, with a higher

resistivity ranging from about 318 to 530 ohm-m, appears along the NE end of the profile from about 0 to 24 m and along the SW end from about 50 to 88 m, with a localized high-resistivity anomaly at about 36 to 42 m along the profile. The intervening low-resistivity zone is interpreted as fractures, joints or clay fills, while the exceptionally low-resistivity anomaly (from about 36 to 50 m along the profile) has been treated as the water-bearing target. The thickness of this anomaly varies from 5 to 10 m and the top and bottom of the anomaly are located between 2.5 and 17 m depth from the surface.

3.1.3 ER line 3, Berea Road (Site 2)

ER line 3 at the Berea Road site, west of Cane Run, is 135 m long and oriented NE–SW . The resistivity section along this line also shows three distinct layers with low, intermediate and high resistivities. The poorly-fit data above 15% (69 of 553) relative data misfit were removed before final inversion to get the inverted resistivity section along the profile (Fig. 3.3). The effective depth of penetration for the section is around 25 m which is equivalent to about 18% of the profile length.

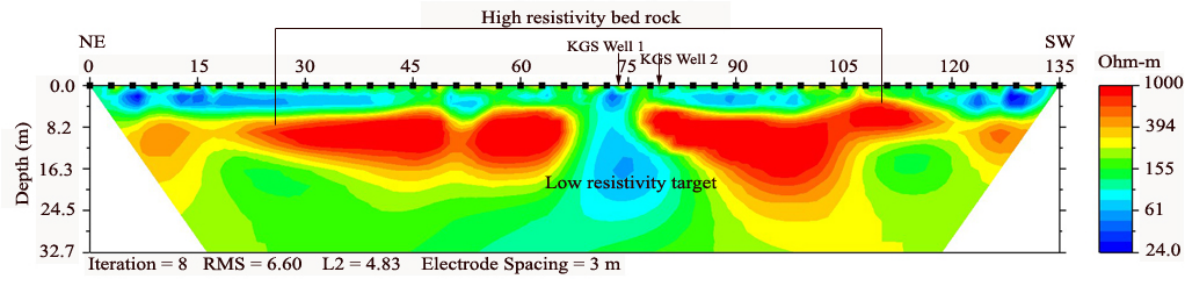

Figure 3.3. Interpreted inverted ER section along Line 3 at Berea Road (Site 2).

The inverted resistivity section shows a pronounced low-resistivity anomaly at approximately 16.6 m depth between stations 69 and 81 m along the transect (Fig. 3.3).

The resistivity of the center of the anomaly is 56.9 ohm-m, which falls within the typical resistivity range of fresh groundwater. The topmost low-resistivity layer, approximately 24 to 110 ohm-m, is not continuous throughout the section, but it stands out as a layer with different electrical properties compared to the layers underlying it. This layer is undifferentiable between stations 42 to 81 m and 99 to 120 m. The second or intermediate-resistivity layer, with values ranging from 110 to 275 ohm-m, is less distinct but continuous along the profile. This layer is thinner than in the sections at site 1. The thickness of the layer varies from 2 to 4 m and its bottom extends to a depth of 8 m below the surface at the NE end of the section. The lowermost distinguishable layer, with resistivity ranging from about 275 to 800 ohm-m, appears throughout the section except between stations 66 to 81 m, where it is interrupted by a relatively low-resistivity zone. The relatively low-resistivity zone is interpreted as the result of poor rock mass quality while the exceptionally low-resistivity anomaly has been treated as the water bearing target. The thickness of this anomaly varies from 4 to 20 m and the top and bottom of the anomaly are located between 2 and 26 m depth below the surface.

3.1.4 ER line 4 (Site 2)

ER line 4 at the Berea Road soccer field site, east of Cane Run, is 249 m long and runs NE–SW. The resistivity section along this line also shows three distinct layers with low, intermediate and high resistivities. The poorly-fit data above 5% (66 of 1242 points) relative misfit were removed to get the inverted resistivity section along the profile (Fig. 3.4). The effective depth of penetration for the section is about 20 m, which is equivalent to only about 8% of the profile length. The relatively shallow effective depth of

penetration compared to the total survey length could be the result of highly conductive soil overburden.

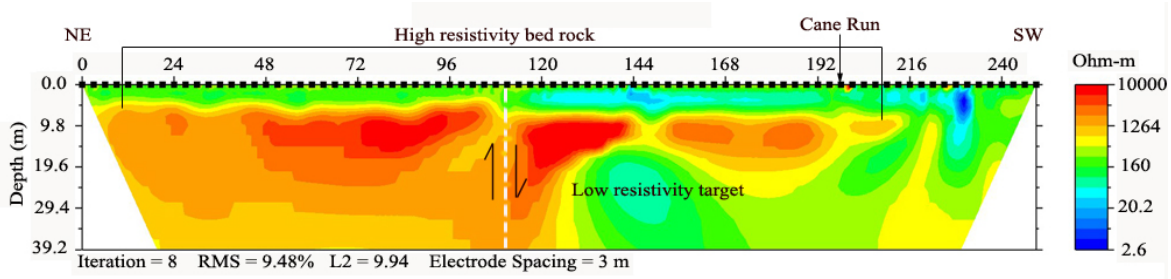

Figure 3.4. Interpreted inverted ER section along line 4 at Berea Road soccer field (Site 2).

The inverted section shows a pronounced low-resistivity anomaly at approximately 19 m depth (top of the anomaly), between stations 141 and 147 m along the transect (Fig. 3.4). The resistivity of the center of the anomaly is 20 ohm-m, which falls within the typical resistivity range of fresh groundwater. Unlike the other sections, line 4 shows only two distinguishable layers, with vast difference in their electrical properties. The topmost intermediate-resistivity layer, approximately 100 to 550 ohm-m, overlies a layer with apparent resistivity ranging from about 550 to 2400 ohm-m, surrounding even higher discrete resistivity zones reaching up to 3700 ohm-m. The topmost layer is continuous throughout the profile with discrete low-resistivity zones along both sides of Cane Run. The high- to very high-resistivity layer toward the NE part of the profile continues to station 144 m, beyond which it thins significantly toward the SW part of the profile and is absent beneath Cane Run. Between stations 105 and 111 m, the high- to very-high resistivity layer is vertically offset about 3 m downward, which is clearly seen on the section. The consistency of the layer to the NE and SW directions and identical resistivity range of rock units on both sides of the offset (discontinuity) indicates

that a fault passes through the profile (Fig. 3.4). The average depths to the top of the high resistivity layer to the NE and SW sides of the fault plane are 4.5 and 7.5 m, respectively.

3.1.5 ER line 5, Kentucky Horse Park (Site 3)

ER line 5 is a 165-m long, NE–SW profile near the Barton well at the Kentucky Horse Park. The resistivity section along this line can be tentatively divided into three layers of distinct ER responses (low, medium and high resistivity). These ranges do not necessarily correspond with the ranges used to categorize resistivity layers in other sections. The poorly-fit data above 15% (43 of 739) relative misfit were removed to get the inverted resistivity section along the profile (Fig. 3.5). The effective depth of penetration for the section is around 25 m, which is equivalent to about 15% of the profile length.

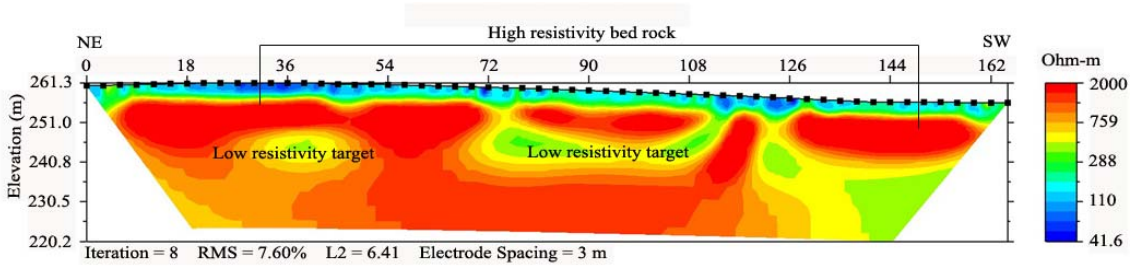

Figure 3.5. Interpreted inverted ER section along line 5 at the Kentucky Horse Park (Site 3). Note that ER is plotted versus elevation rather than depth because relief along the line warranted correction for elevation differences.

The inverted resistivity section shows three anomalous low-resistivity zones at about the same depths from the surface. The first anomaly (441 ohm-m, against 1000 to 2000 ohm-m background resistivity) is located at approximately 16.8 m depth between stations 33 and 42 m (Fig. 3.5). The other two low-resistivity anomalies (about 345 ohm-

m) lie between 75 to 108 m and at 123 m along the transects. This last anomaly is located close to a sinkhole and has an ER response typical of a sinkhole, but there is no surface expression. The low-resistivity zone extending from the surface into the underlying bedrock might indicate the ongoing process of new sinkhole formation. The topmost low-resistivity layer (41 to 200 ohm-m) above the very high resistivity layer (1300 to 2000 ohm-m) in the section is indistinct and discontinuous. The top of the intermediate layer of moderate resistivity (200 to 520 ohm-m) is unclear, but the bottom of the layer is consistent almost all along the profile length at about 5 m depth (256 m MSL) from the surface. The thickness of the very high-resistivity layer, which is continuous to 120 m along the profile, varies from 5 to 15 m and its bottom occurs at 10 to 20.5 m depth.

3.1.6 ER line 6 (Site 3)

The data along ER line 6 were collected using the roll-along survey technique and the two sets of measurements were processed separately as ER line 6(a) and 6 (b) (Figs. 3.6(a) and (b)). The composite ER line 6 runs 249 m NE–SW and almost parallel to ER line 5. The poorly-fit data above 10.5% (38 of 762 points) relative misfit were removed to get the inverted resistivity section along the profile (Fig. 3.6(a)). The effective depth of penetration for the section is around 20 m, which is equivalent to about 12% of the profile length.

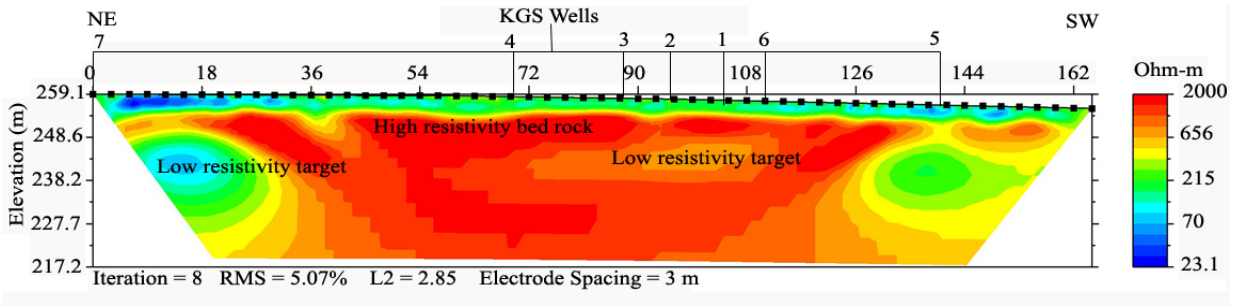

Figure 3.6(a). Interpreted ER section along line 6(a) at the Kentucky Horse Park (Site 3). Note that ER is plotted versus elevation rather than depth because relief along the line warranted correction for elevation differences.

Three zones of low-resistivity anomalies surrounded by high-resistivity background are distinctly visible along line 6(a) (Fig. 3.6(a)). The first low-resistivity anomaly (107.6 ohm-m), between 14 and 17 m distance along the profile, is located at about 15.4 m depth. The second low-resistivity anomaly (around 500 ohm-m, compared to 1000 to 1600 ohm-m background) is located at about 15 m depth and lies between stations 72 to 111 m along the profile. The third anomaly (293 ohm-m), at the SW end of the profile (129 to 150 m) is located only about 3 m from a sinkhole. The resistivity section along this line shows a similar response to that of ER line 5 to a depth of about 5 m from the surface. The topmost low-resistivity (22 to 141 ohm-m) layer is indistinct and discontinuous. The intermediate-resistivity (141 to 440 ohm-m) layer is continuous throughout the section. The bottom of this layer is almost consistent at around 5 m below the ground surface. This layer is underlain by a high-resistivity layer (440 to 1320 ohm-m) with discrete very high resistivity (1320 to 1630 ohm-m) zones.

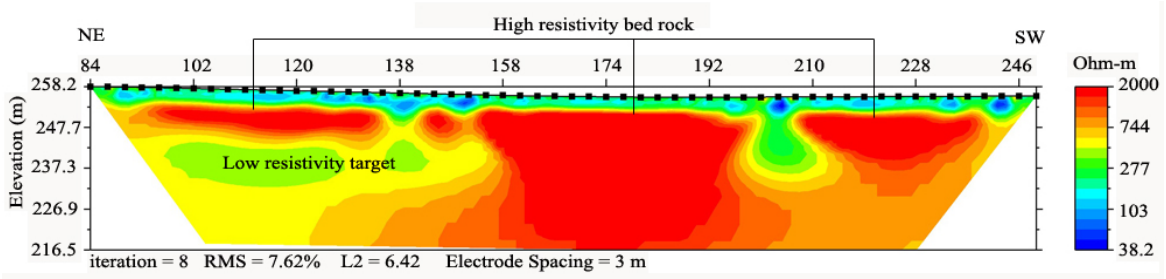

Figure 3.6(b). Interpreted ER section along line 6(b) at the Kentucky Horse Park (Site 3). Note that ER is plotted versus elevation rather than depth because relief along the line warranted correction for elevation differences.

Line 6(b) is the continuation of line 6(a) toward the SW and it overlaps the station at 84 m. The poorly-fit data above 19.5% (5 of 762 points) relative data misfit were removed from the data set before the inversion to produce the final resistivity section (Fig. 6(b)). The effective depth of penetration for the section is around 22 m, which is equivalent to about 13% of the profile length.

Line 6(b) shows two distinct anomalous low- to medium-resistivity (190 to 500 ohm-m) zones compared to high-resistivity (500 to 1800 ohm-m) surroundings. The anomaly at the NE end, extending between stations 99 to 126 m along the profile, is located at about 15 to 20 m depth. This anomalous zone (around 200 ohm-m) is immediately overlain by high-resistivity (up to 1800 ohm-m) bed rock. The anomaly below the station at 138 m may reflect sinkhole formation because of its proximity (about 3 m) to the sinkhole at the ground surface. A typical sinkhole-like resistivity signature is also visible in the section between 198 and 210 m, but there is no surface expression. The topmost layer is indistinct with isolated low-resistivity (38 to190 ohm-m) patches throughout the section. An intermediate layer of medium-resistivity (190 to 500 ohm-m) continues throughout the section. The contact between the medium-resistivity layer and

underlying high-resistivity layer (500 to 1800 ohm-m) occurs throughout the section at an average depth of about 5 m from the surface.

Table 3.1. Details of ER profiles.

Site name and number	Profile number	Survey date	Profile length (m)	Electrode spacing (m)	Number of electrodes	Survey method
University of Kentucky Agricultural Research Farm (Site 1)	ER line 1	6/11/2008	86	2	44	Dipole-dipole
	ER line 2	6/10/2008	88	2	45	Dipole-dipole
Berea Road (Site 2)	ER line 3	6/10/2008	135	3	46	Dipole-dipole
	ER line 4	6/10/2008	249	3	84	Dipole-dipole
Kentucky Horse Park (Site 3)	ER line 5	6/11/2008	165	3	54	Dipole-dipole
	ER line 6	6/9/2008	249	3	84	Dipole-dipole

3.2 Self-Potential Data Interpretation

SP data were collected along ER lines at all three sites for comparison with ER responses and were collected on multiple dates as a check on reproducibility. SP measurements were repeated at half-hour intervals at the base stations and used to correct for the electrode drift during the course of measurements. The SP data along lines 5, 6 and 7 were corrected for elevation due to the irregular topography. The topographic correction factors (K) for lines 5 and 6 (0.97 and 0.69, respectively) were determined by linear regression because these lines exhibit linear topography along the transect with

almost constant slope between the stations. Since line 7 exhibits irregular topography, values of K were individually determined to calculate the topographic effect for each set of SP readings (-0.72 for August 7, 2008, 0.79 for August 29, 2008, and -0.55 for March 18, 2009, respectively). Moving averages for SP data were calculated to remove the high-frequency noise. The averaged data were plotted against the electrode spacing along each survey profile and the subsurface geology was interpreted based on negative or positive SP anomalies.

3.2.1 SP Line 1, University of Kentucky Agricultural Research Farm (Site 1)

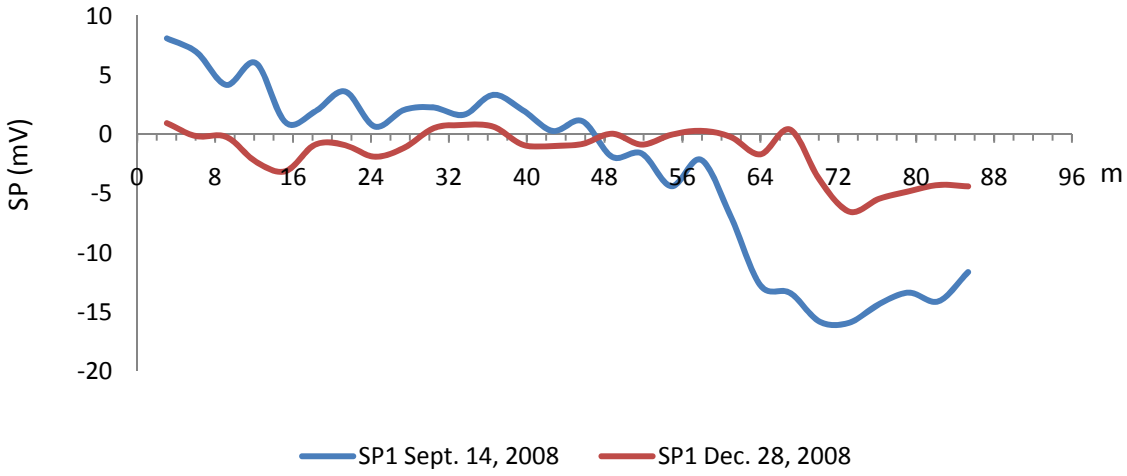

Figure 3.7. SP plot along line 1 at the UK Agricultural Research Farm (Site 1).

The processed SP data collected on September 14 and December 28, 2008, show similar trends with a major anomaly along the transect but with different SP values. The SP profiles show a monotonous response between 0 and 60 m and a negative anomaly across the remainder of the profile. The September anomaly is 13 mV more negative than the average background SP (3 mV) while the December anomaly is 5 mV less than the average background SP (2 mV). The total precipitation and average soil temperature for

the week preceding each measurement during September and December were 1.1 cm and 23 °C and 5.8 cm and 3.8 °C, respectively (Table 3.2). The low precipitation and high soil temperature during September measurements suggest drier field conditions than for the December measurements.

3.2.2 SP line 2 (Site 1)

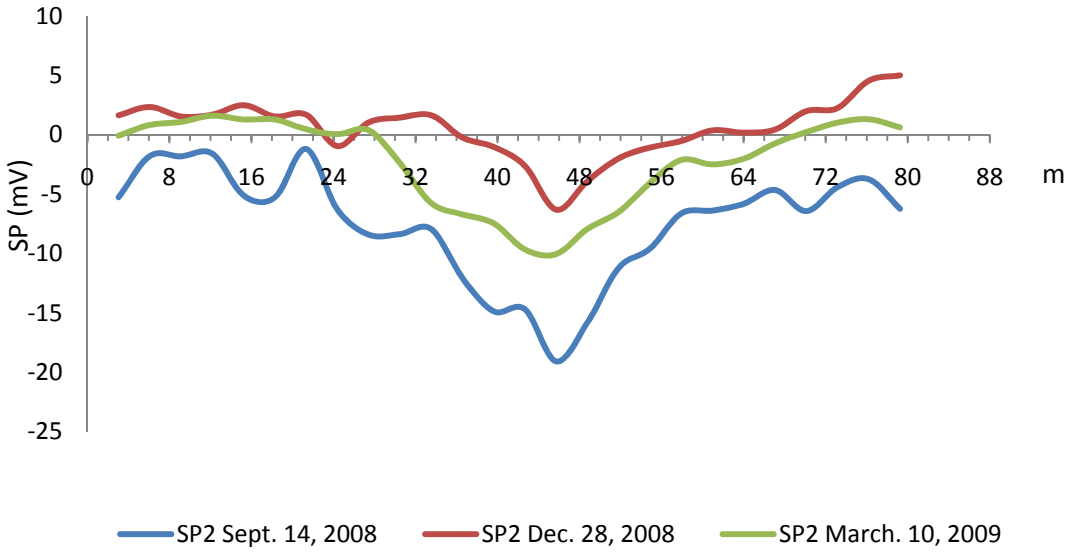

Figure 3.8. SP plots along line 2 at the UK Agricultural Research Farm (Site 1).

SP data acquired on three different dates in September 2008 through March 2009 show similar trends, with a significant negative anomaly between stations 40 and 50 m. The anomaly was 11.5 mV more negative than the average background SP in September (-7.5 mV), 6.5 mV more negative than the background SP in December (0.5 mV) and 7.8 mV more negative than the background SP in March (-2.2 mV).

The total precipitation and average soil temperature for each week preceding SP measurements were 1.1 cm and 23 °C in September, 5.8 cm and 3.8 °C in December, and

0.4 cm and 6.9 °C in March (Table 3.2). The difference between September and December responses was qualitatively similar for SP lines 1 and 2. The intermediate SP response for March is consistent with relatively mild temperature compared to late summer and early winter.

3.2.3 SP line 3, Berea Road (Site 2)

SP line 3 was surveyed on two dates in November 2008 and one in March 2009. The first two measurements were done along the same line while the third measurement was made along a parallel line with 3-m offset to the north.

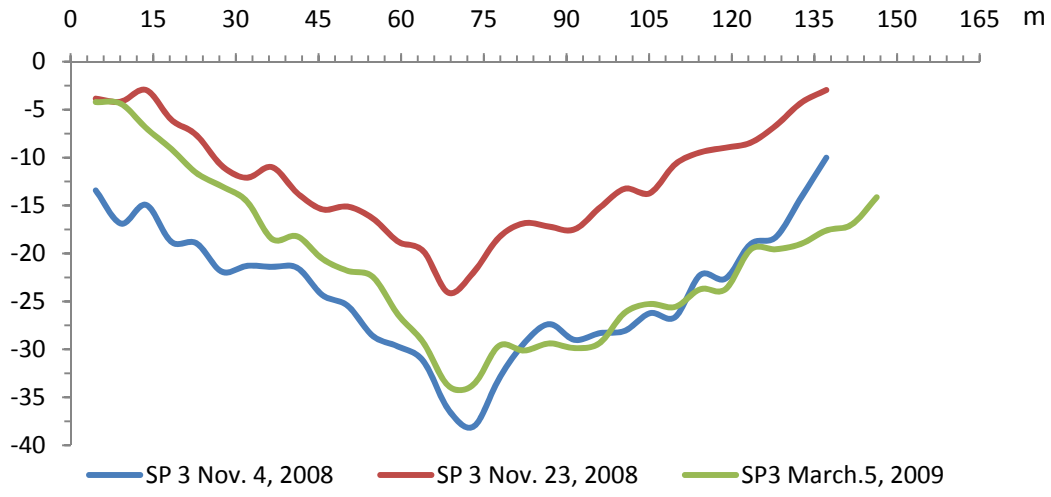

Figure 3.9. SP plots along line 3 at Berea Road (Site 2).

The negative SP anomaly for all three SP plots falls between stations 60 and 80 m, but the anomalous target is likely to lie between 68 and 73 m along the profile. The differences between the average background SP and the anomaly are -14.1 mV for the November 4, 2008, data, -11.8 mV for the November 23, 2008, data and -12.9 mV for the March 5, 2009 data.

The total precipitation and average soil temperature for each week preceding SP measurements were 0.0 cm and 11.1 °C (for November 4 data), 0.0 cm and 4.4 °C (for November 23 data), and 1.5 cm and 3.6 °C (for March 5 data), respectively (Table 3.2). Considering the relatively short time interval (19 days) between the first two sets of measurements and the 3-m offset between those transects and the March transect, the SP responses for all three surveys along line 4 are similar.

3.2.4 SP line 4 (Site 2)

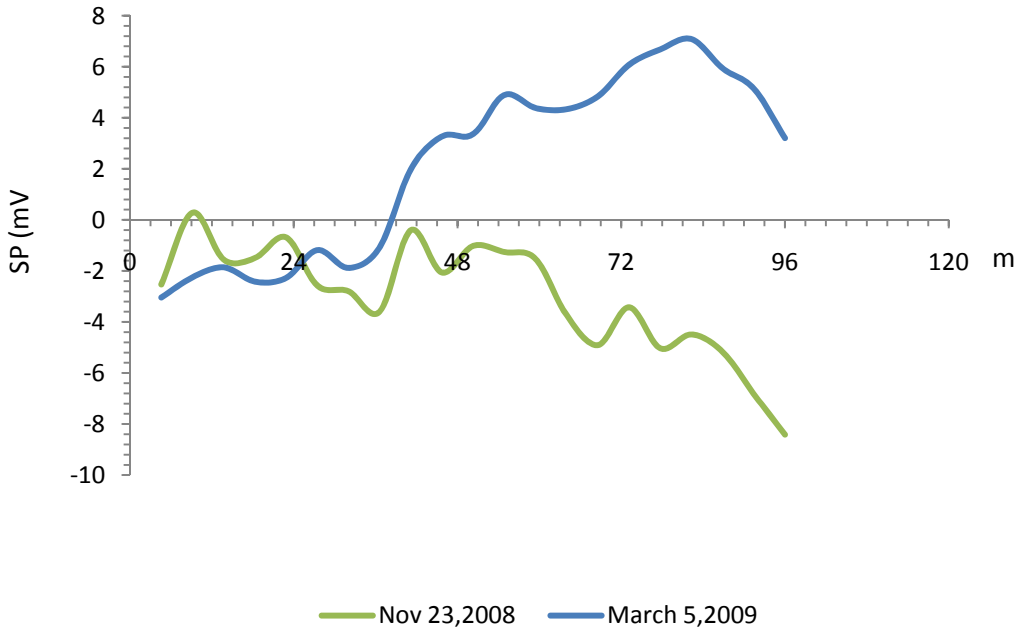

Figure 3.10. SP plots along line 4 at Berea Road soccer field (Site 2).

In contrast to SP lines 1 through 3, the shapes of SP curves along line 4 vary markedly over time, with a pronounced positive anomaly beyond about 40 m for the March 5, 2009, survey and pronounced negative anomaly beyond about 60 m for the November 23, 2008, survey. The total precipitation and average soil temperature for each week preceding measurements were 0.0 cm and 4.4 °C (for November data) and 1.5 cm

and 3.6 °C (for March data), respectively (Table 3.2). Since the profiles collected on different dates diverged, the SP data along line 4 are not utilized to delineate the conduit.

3.2.5 SP line 5, Kentucky Horse Park (Site 3)

SP measurements were collected multiple times along this line as well but only one set of data (collected on March 8, 2009) was processed and interpreted. The data collected on other dates did not correspond to each other or with the parallel SP line 6 that is only about 10 m away from line 5, perhaps because of instrument malfunction resulting from damage to the porous ceramic base.

The SP profile shows an overall negative anomaly between 25 and 130 m (Fig. 3.11). Discrete negative SP peaks occur at 34 m, 64 m, 96 m and 122 m. The difference between maximum and minimum SP values ranges from about 5 to 6 mV along this profile and these values are relatively small as compared to other SP lines.

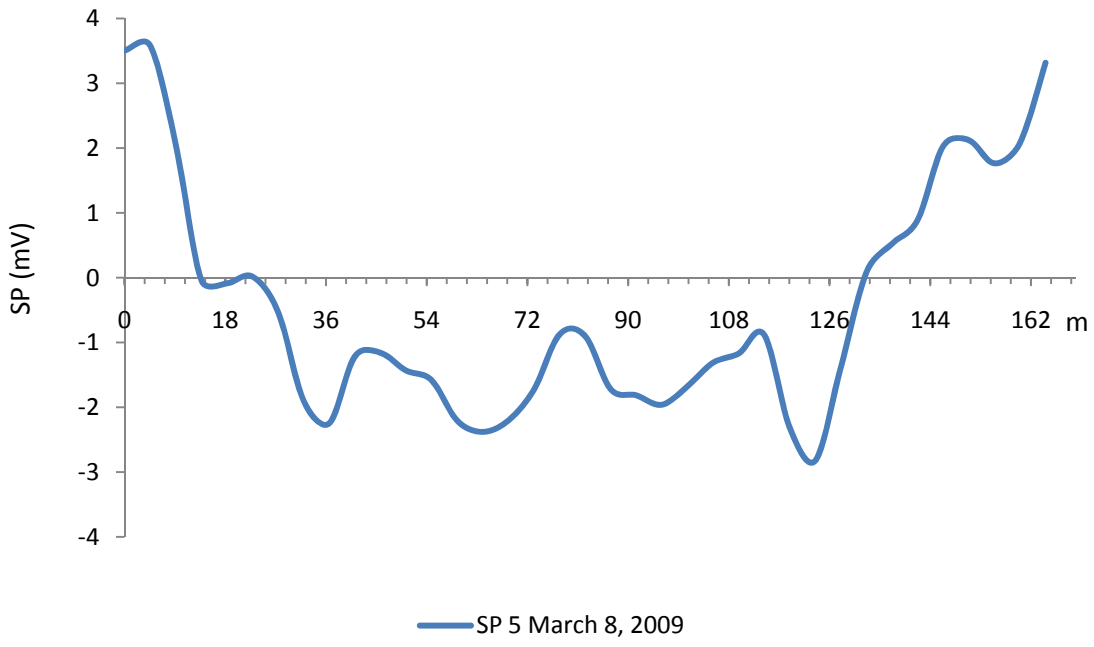

Figure 3.11. SP plot along line 5 at the Kentucky Horse Park (Site 3).

3.2.6 SP line 6 (Site 3)

Although SP measurements were made on more than two dates, only two sets of measurements were processed for analysis (Fig. 3.12) because of meter malfunction and electrode damage. The SP profile for November 2, 2008, shows several negative anomalies, including a broad anomaly from about 50 to 100 m, which is centered around 70 m, and sharp anomalies at about 115 m, 150 m, and 200 m. In comparison, the SP profile for March 8, 2009, is generally convex downward, with relatively subtle negative anomalies at about 85 m, 115 m, and 140 m. The total precipitation and average soil temperature for the week preceding each set of measurements were 1.0 cm and 10.8 °C for November and 0.4 cm and 4.4 °C for March, respectively (Table 3.2). The SP response was generally more negative with higher amplitude for data taken during the relatively dry, mild period (i.e., in November vs. March).

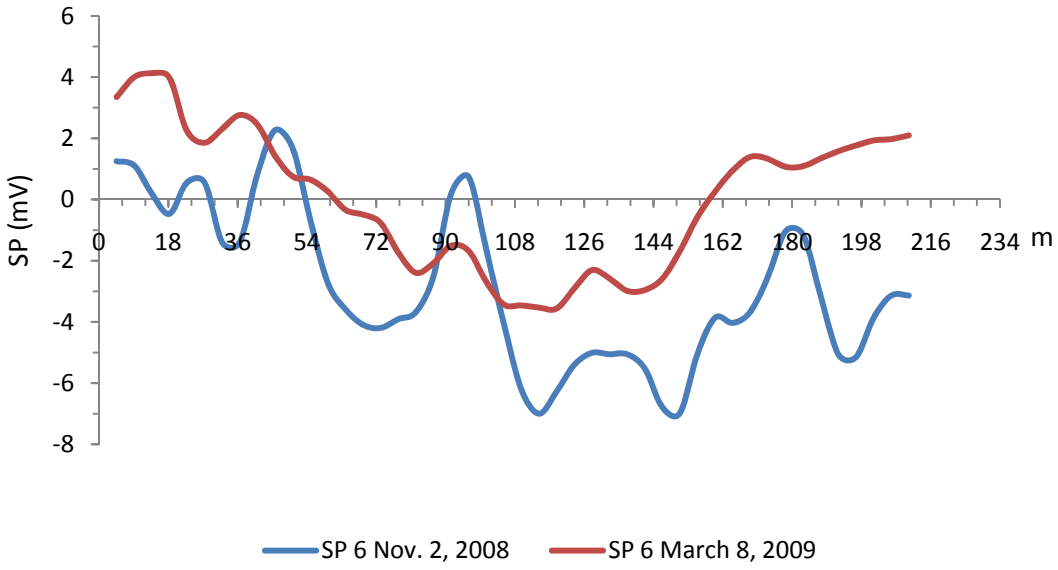

Figure 3.12. SP plots along line 6 at the Kentucky Horse Park (Site 3).

3.2.7 SP line 7, Kentucky Horse Park (Site 3)

SP line 7 is located at the north end of the Kentucky Horse Park near Interstate 75. It runs approximately parallel to and about 300 m north of the SP lines 5 and 6 at this site. This line was surveyed multiple times on different dates to check SP data reproducibility but ER data were not collected along this line.

In contrast to the other lines, the SP responses along line 7 tended to be convex upward (Fig. 3.13). A consistent negative anomaly for all the SP plots, surveyed at different dates, falls around 150 m. The difference between average background SP and this anomaly was 7 mV for August 29, 2008, 6.7 mV for September 12, 2008, and 6.25 mV for March 18, 2009.

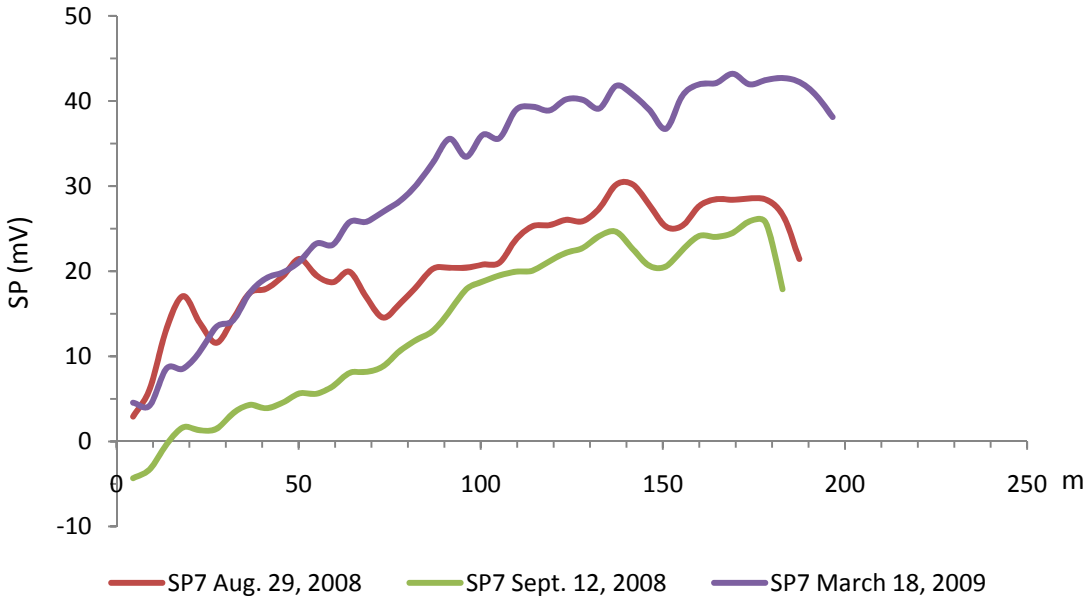

Figure 3.13. SP plots along line 7 at the Kentucky Horse Park (Site 3).

Although the overall trends in the profiles are similar, the SP magnitudes vary by as much as 15 mV at individual survey points. The total precipitation and average soil temperature for the week preceding each set of measurements were 0.9 cm and 24.4 °C for August 29, 2008, 0.04 cm and 23 °C for September 12, 2008, and 0.4 cm and 7.7 ° C for March 18, 2009, respectively (Table 3.2). The March SP profile, which reflected wetter and cooler conditions, is more positive than the September profile, while the August response is intermediate between the two subsequent profiles beyond 50 m.

Table 3.2. Precipitation and soil temperature data (Station: Spindletop).

SP line	Survey date	Precipitation duration	Total precip. (in.)	Total precip. (cm)	One-week avg. soil T. (grass),deg. Fahrenheit	One-week avg. soil T, deg. Celsius
Line 1	09/14/2008	09/08/08 - 09/14/08	0.43	1.1	73.5	23
	12/ 28/2008	12/22/08 - 12/28/08	2.27	5.8	39	3.8
Line 2	09/ 14/2008	09/08/08 - 09/14/08	0.43	1.1	73.5	23
	12/ 28/2008	12/22/09 - 12/28/08	2.27	5.8	39	3.8
	03/10/2009	03/04/09 - 03/10/09	0.16	0.4	44.5	6.9
Line 3	11/ 04/2008	10/29/08 - 11/04/08	0	0	52	11.1
	11/23/2008	11/17/08 - 11/23/08	0	0	40	4.4
	03/05/2009	02/27/09 - 03/05/09	0.61	1.5	38.5	3.6
Line 4	11/23/2008	11/17/08 - 11/23/08	0	0	40	4.4
	03/0 5, 2009	02/27/09 - 03/05/09	0.61	1.5	38.5	3.6
Line 5	03/08/2009	03/02/09 - 03/08/09	0.16	0.4	40.5	4.7
Line 6	11/02/2008	10/27/08 - 11/02/08	0.39	1	51.5	10.8
	03/08/2009	03/02/09 - 03/08/09	0.27	0.7	40.5	4.7
Line 7	08/07/2008	08/01/08 - 08/07/08	0.51	1.3	78	25.5
	08/29/2008	08/23/08 - 08/29/08	0.35	0.9	76	24.4
	09/12/2008	09/06/08 - 09/12/08	0.01	0	73.5	23
	03/18/2009	03/12/09 - 03/18/09	0.16	0.4	46	7.7

Source: UK Agricultural Weather Center (2009).

3.3 Comparison of ER and SP Results

3.3.1 UK Agricultural Research Farm (Site 1)

The inverted resistivity section and residual SP plot along Line 1 (Fig. 3.14) at this site show a pronounced low resistivity and negative SP anomaly at approximately 14 m depth, between stations 60 to 70 m along the transects (Fig. 3.14). However, a hole drilled into this anomaly at 63.5 m did not encounter a solution conduit. The well log indicates that it could be a soil-filled sinkhole (James Dinger, Kentucky Geological Survey, personal correspondence). The identification of metallic objects in a hole dug during an SP survey is consistent with the negative SP response. Between stations 0 and 20 m, the data suggest very thin soil cover over weathered bedrock, which was subsequently verified by direct soil probes. The inverted resistivity section and the SP plots show a pronounced anomaly at approximately 17 m depth between stations 40 and 50 m along line 2 (Fig. 3.15). However, a borehole drilled into the anomaly did not encounter a solution conduit.

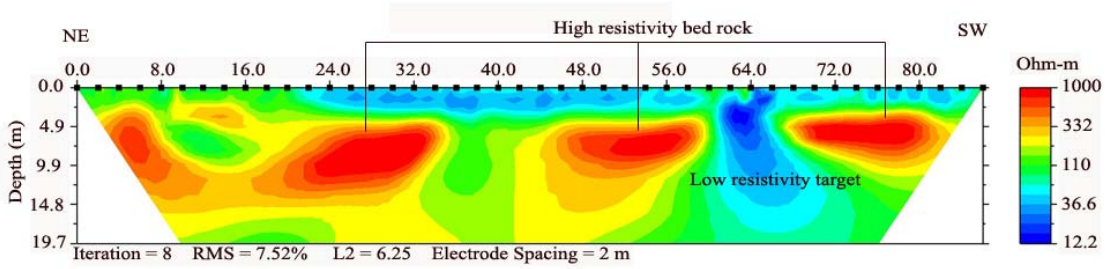

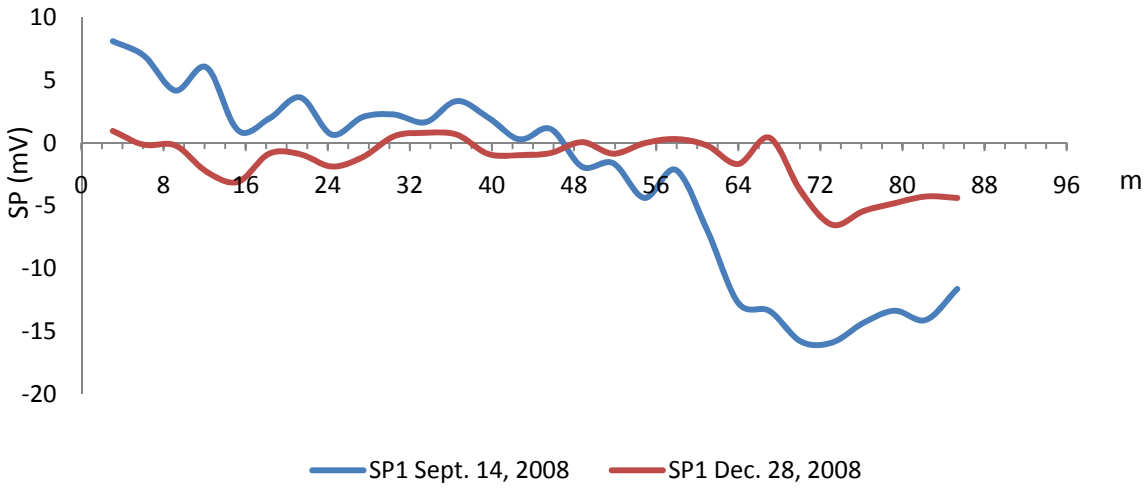

Figure 3.14. ER and SP profiles along line 1 at the University of Kentucky Agricultural Research Farm (Site 1).

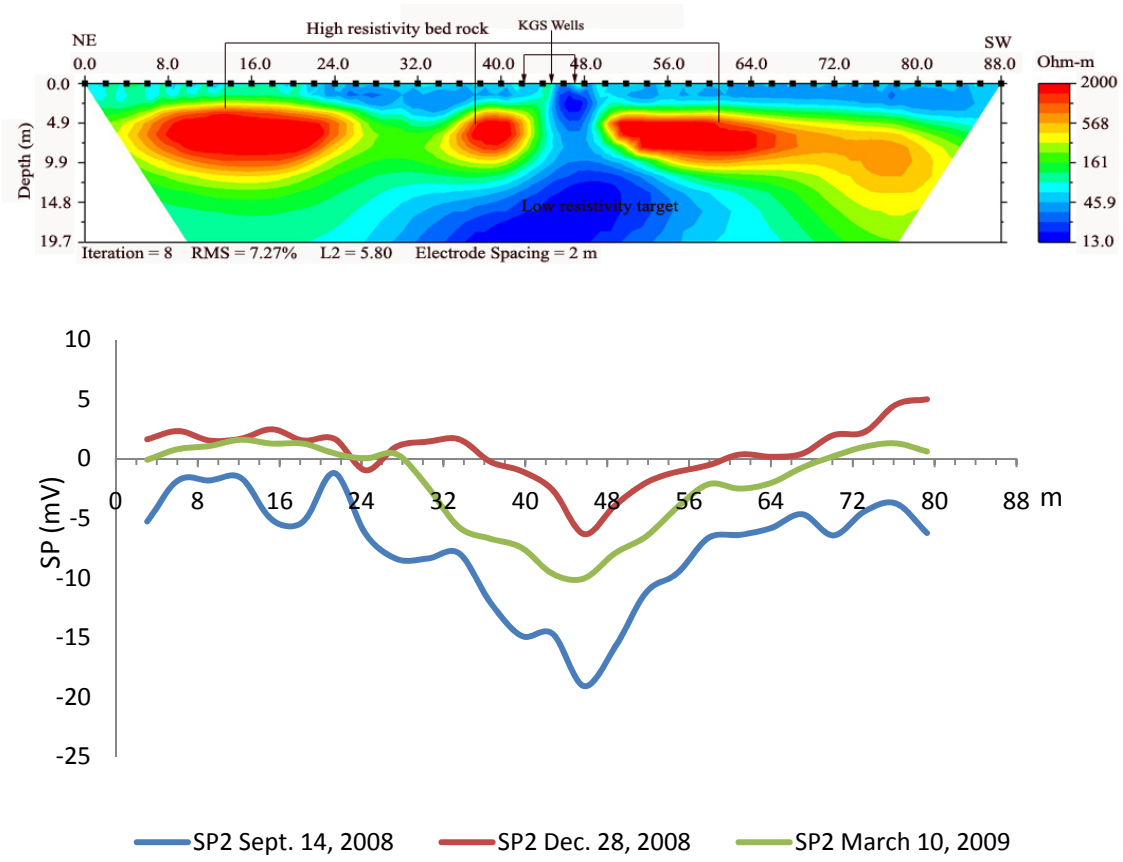

Figure 3.15. ER and SP responses along line 2 at UK Agricultural Research Farm (Site 1)

3.3.2 Berea Road (Site 2)

The plots along line 3 (Fig. 3.16) at this site show a pronounced low resistivity and negative SP anomaly at approximately 16.6 m depth between stations 69 and 81 m (Fig. 3.16). Two holes (#1 at 72 m and #2 at 80 m along line 3) drilled into this target encountered a water-bearing conduit, whereas two holes drilled off the transect were dry. The static water levels measured (James Currens, Kentucky Geological Survey, personal communication) in both wells were 15.7 m below the ground surface. The low-resistivity layer at the top of the section is interpreted as soil overburden and might be the flood plain deposit of Cane Run.

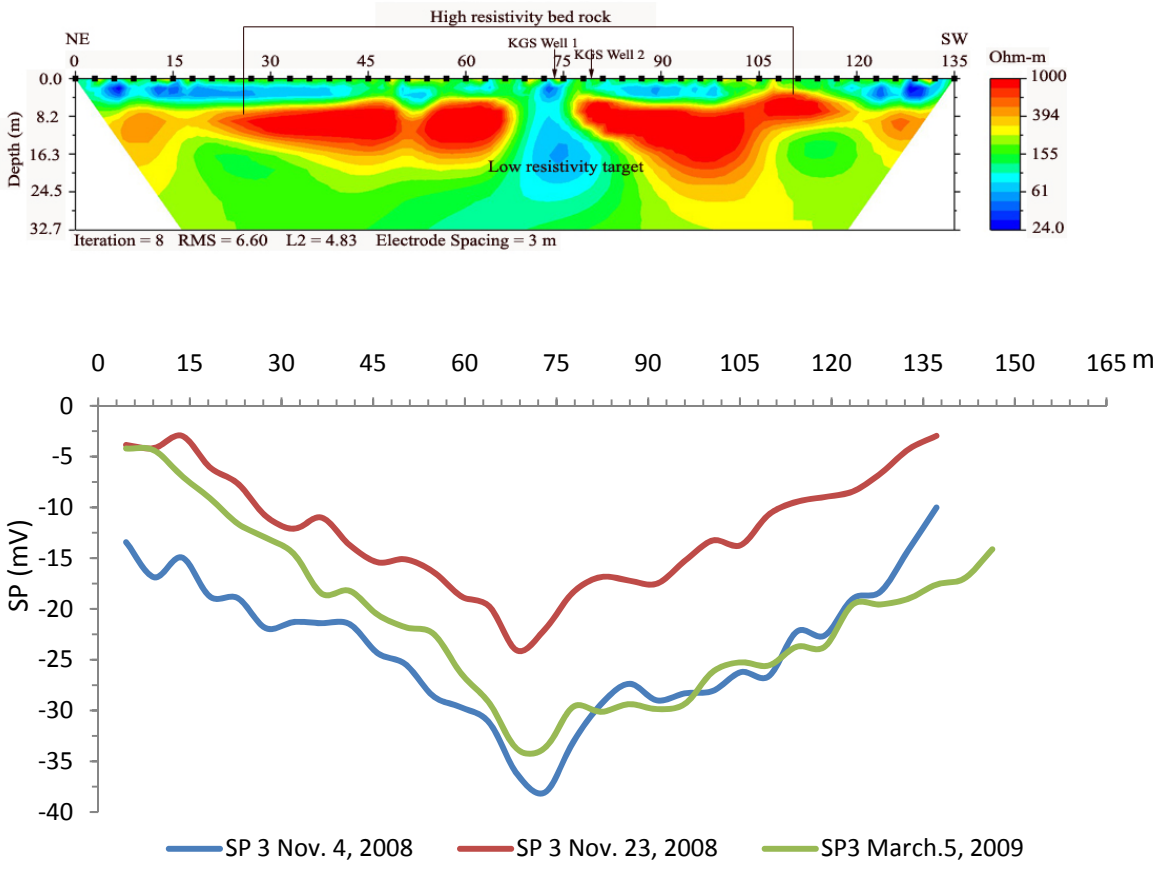

Figure 3.16. ER and SP responses along line 3 at Berea Road (Site 2).

The ER profile along line 4 (Fig. 3.17) at this site shows a prominent resistivity low at an approximate depth of 19 m around 144 m along the transect. The large resistivity contrast relative to the background makes this a potential target for the conduit, but it has not been drilled yet. The SP measurements along the same line begin as station 0 corresponding to station 97 m on the ER profile. In contrast to other sites, the SP profile did not show any anomaly corresponding to the ER anomaly. The inconsistency in SP results could be the result of emplacing fill to make the soccer field level or the existence of the inferred fault. The low- and intermediate-resistivity layers along line 4, in contrast to the sections at other sites, are not distinguishable into two layers. However, the top of the underlying high-resistivity layer is almost uniform on either side of the fault (with 3-m vertical offset) inferred between stations 105 and 111 m. Many other small scale faults have been documented in the vicinity (Kentucky Geologic Map Information Service 2009).

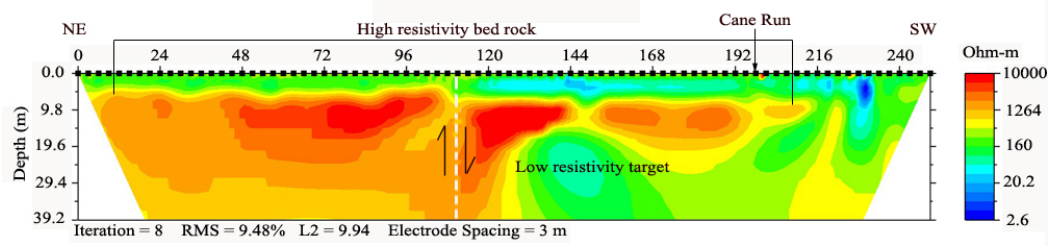

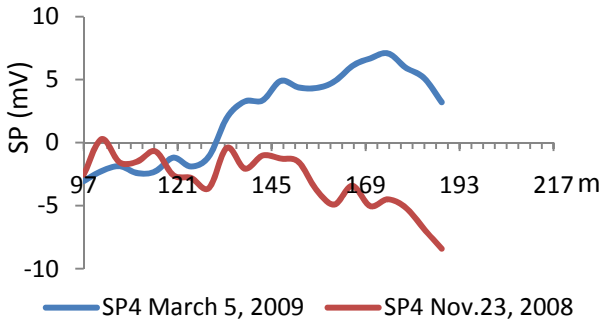

Figure 3.17. ER and SP responses along line 4 at Berea Road (Site 2).

3.3.3 Kentucky Horse Park (Site 3)

The three low-resistivity anomalies along line 5 (Fig. 3.19) correspond roughly with the negative SP anomalies along the same line, although a fourth anomaly (at about 64 m along the transect) does not have a matching ER anomaly. The low-resistivity anomalies are located approximately at 17 m depth. The apparent resistivity for the anomaly located between stations 33 and 42 m is about 441 ohm-m, which exceeds the typical range for fresh groundwater; however, the high contrast between the anomaly and the background resistivity (1000 to 2000 ohm-m) could have a masking effect on the anomaly. The apparent resistivity is the volumetric average for the particular location and the surrounding high resistivity might have raised a true low-resistivity value in this case. The second anomaly (345 ohm-m) is located between stations 75 and 108 m. The proximity of the low-resistivity anomaly at 123 m to a sinkhole and the typical sinkhole-like ER response (Ahmed and Carpenter 2003, Jardani et al. 2007) suggest an ongoing process of sinkhole formation below ground surface. The top of the medium resistivity layer (200 to 520 ohm-m) in this section is not distinct but the bottom of this intermediate layer is clear and continuous throughout the section.

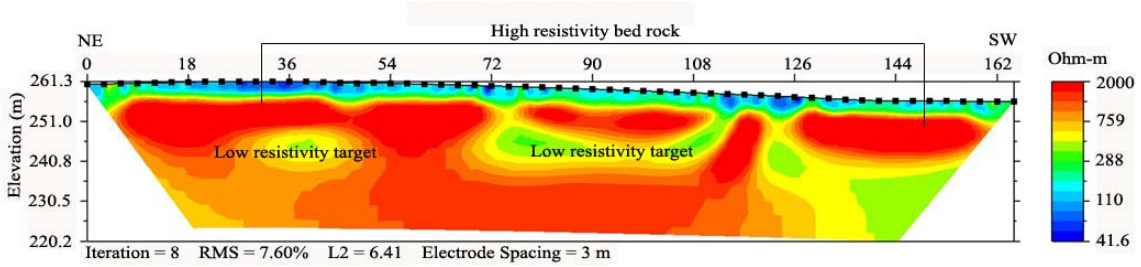

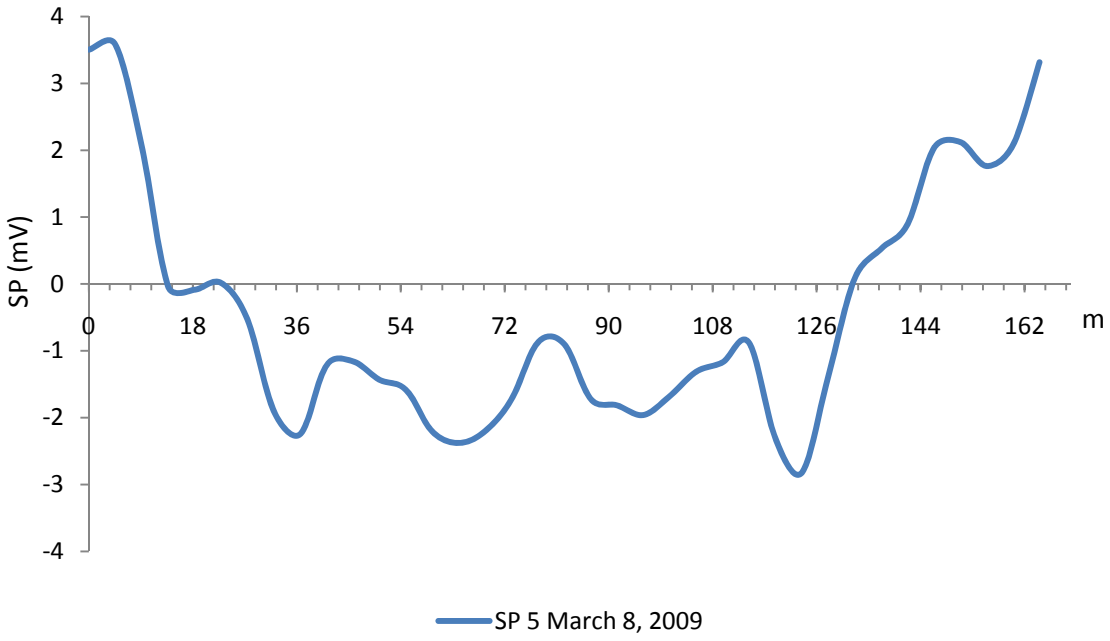

Figure 3.18. ER and SP responses along line 5 at the Kentucky Horse Park (Site 3).

Along line 6 low ER signatures correspond with negative SP anomalies in most cases. However, the resistivity low (107.6 ohm-m) visible between stations 14 and 17 m along line 6(a) (Fig. 3.19) is not visible in the SP plots. The SP plots show an overall negative anomaly along approximately the middle third of the transect (Fig. 3.19). The resistivity low (around 500 ohm-m) located at about 15 m depth between stations 72 and 111 m (line 6(a)) was also reflected in the SP profile. The three wells (W-1, W-2 and W-3) drilled into this anomaly encountered water. Average depth to static water levels at these wells was around 14 m, while a well (W-4) drilled slightly away, at station 68.58 m along the transect, was dry. The target depth obtained from the ER section is about 7% higher than the measured depth in the well. The differences in true and calculated depth could be the result of oblique orientation of survey line to the conduit, insufficient sample data points or over-processing during the inversion. Another ER anomaly at the SW end

of line 6(a) was also drilled but the conduit was not encountered at the expected depth. This anomaly is located adjacent to a sinkhole and the resistivity signature could be the effect of ongoing sinkhole formation.

ER line 6(b) overlaps line 6(a) at station 84 m and continues toward the SW. The ER section shows distinct low-resistivity anomalies (around 200 ohm-m) between stations 99 to 126 m, located at a depth of 15 to 20 m, and below the station at 138 m, which might be a result of the nearby sinkhole. Similarly, the ER signature between stations 198 and 210 m at the SW end of the transect could also be a result of a sinkhole about 3 m away. The anomaly at station 138 m along line 6(a) and 6(b) exactly matches, but the anomaly between stations 72 and 111 m along line 6(a) only partly matches with the anomaly between stations 99 and 126 m along line 6(b). The mismatch between 72 to 99 m and 111 to 126 m along the line may be the result of edge effects due to insufficient data and relative misfit data removal. The SP profiles also show negative anomalies for these targets, but they have not been drilled to verify the result.

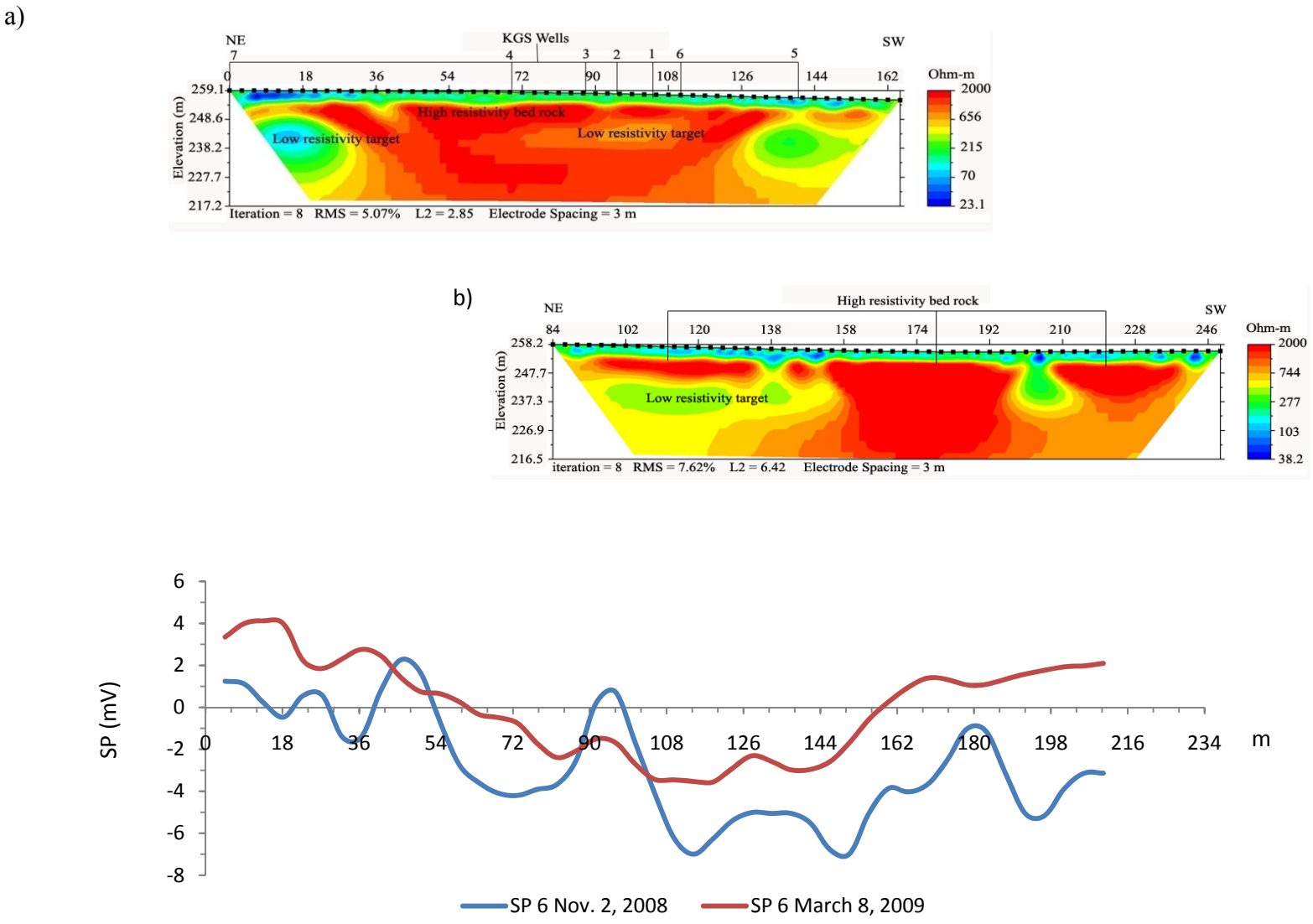

Figure 3.19. ER and SP responses along line 6 at the Kentucky Horse Park (Site 3).

The upper 5 meters of the sections along lines 5 and 6 show similar ER responses of low to medium resistivity with discrete low-resistivity patches near the surface. The contact between the medium-resistivity layer and the underlying high-resistivity layer is located at a nearly uniform depth throughout the section, which suggests that the bedrock and the surface slope are dipping in the same direction. The maximum soil (overburden) thickness at this site is perhaps 2 m from the surface.

3.4 Temporal Variability in SP Results

Qualitative comparison of profiles collected on different dates indicates that the relative magnitude of SP anomalies tends to vary with soil dryness. The anomalous SP values along the same profile on different dates vary up to 8 mV but the principal anomaly for all the profile is at least 5 mV higher than the background SP. Excepting line 5, for which results were erratic, and the March 5, 2009 for line 3, which was offset by 3 m from previous surveys, SP anomalies became less negative as one-week antecedent precipitation increased. Similarly, anomalies became less negative as temperature decreased (except for line 7, where the anomalies became more negative as both precipitation and temperature decreased between August 29 and September 12, 2008). For lines 1, 2, 4, 6, and (considering the final two surveys) 7, the elapsed time between SP surveys spanned at least one season through the cool portion of the year (i.e., from late summer to early winter, early winter to late winter, autumn to late winter, or late summer to late winter). Consequently, the differences in SP responses may reflect not merely short-term (i.e., weekly) variability in weather, but also seasonal variability in soil moisture (i.e., soil moisture recharge during autumn, winter, and spring [Domenico and Schwartz 1998, Fig. 1.5]). Such recharge is consistent with GIS estimates for Fayette

County showing that, as of 1997, average precipitation exceeded pan evaporation from November through April (UK Agricultural Weather Center 2009).

Chapter 4. Conclusions

Six coincident ER and SP lines (86 to 249 m) and an additional SP line (230 m) were surveyed on different dates at three sites within the Inner Bluegrass karst region, Kentucky. The two different geophysical techniques were applied along coincident survey lines to correlate the interpreted results. The ER and SP methods complement each other in the delineation of anomalies that may correspond to karst conduits. Combined use of these methods can potentially decrease the ambiguities inherent in the geophysical data interpretation. The following conclusions can be drawn from the present study:

- Four out of six ER sections and SP profiles along lines 1, 2, 3 and 5 closely corresponded with each other.
- In most of the cases, the low-resistivity anomalies are reflected as negative SP anomalies. Holes drilled into these anomalies along line 3 (between stations 69 and 81 m along the transect) at Berea Road and along line 6 (between stations 72 and 111 m along the transect) at the Horse Park encountered water-bearing conduits.
- The holes drilled over matched low-resistivity and negative SP anomalies at the University of Kentucky Agricultural Research Farm did not encounter the water-bearing target. However, the core log suggests the anomaly along line 1 may represent soil-filled sinkholes. The target on line 2 needs to be verified with additional ER and SP profiles.

- Low-resistivity anomalies around 144 m along line 4, low ER and negative SP targets between stations 33–42 m and 72–111 m along line 5, low ER targets betweens stations 14–18 m along line 6, and the negative SP anomaly around 150 m along line 7 are potential targets for future drilling.

- SP data change over time but the overall trends remain similar. In general, SP responses become less negative as precipitation increases and soil temperature decreases. Therefore, under wet field conditions, a negative SP anomaly generated by groundwater flow could be masked by the positive SP response generated by infiltration.

- Further investigation, such as drilling the potential targets identified in this study and running a few more geophysical lines across the inferred conduit at other locations, are needed to determine whether the anomalies represent the main conduit or tributary conduits in the Royal Spring groundwater basin.

Appendices

Appendix I

A. Inverted resistivity sections with and without relative data misfit removed.

Site – 1: University of Kentucky Agricultural Research Farm

Line – 1, without relative misfit data removed

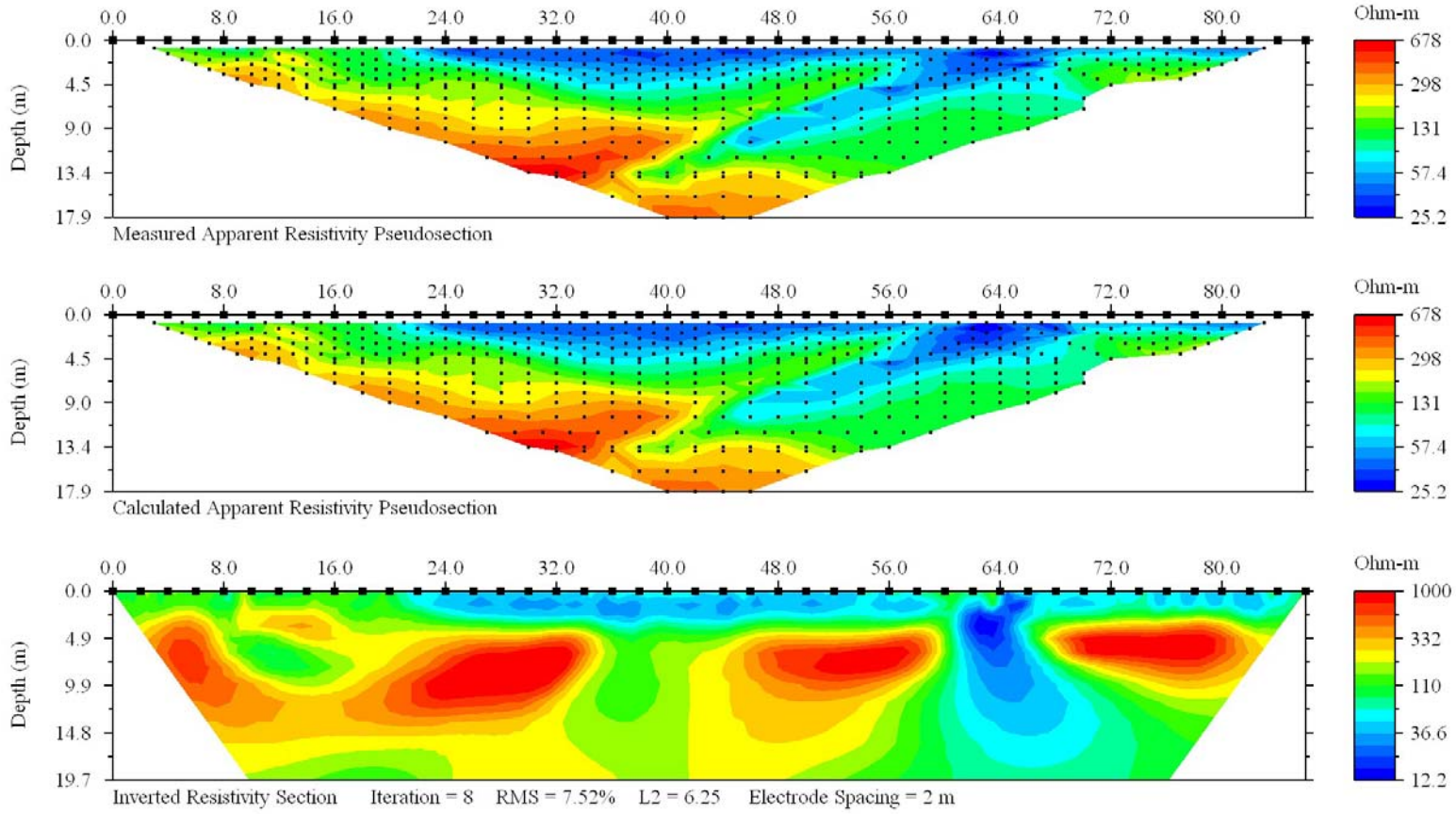

Line – 1, relative data misfit above 12% removed

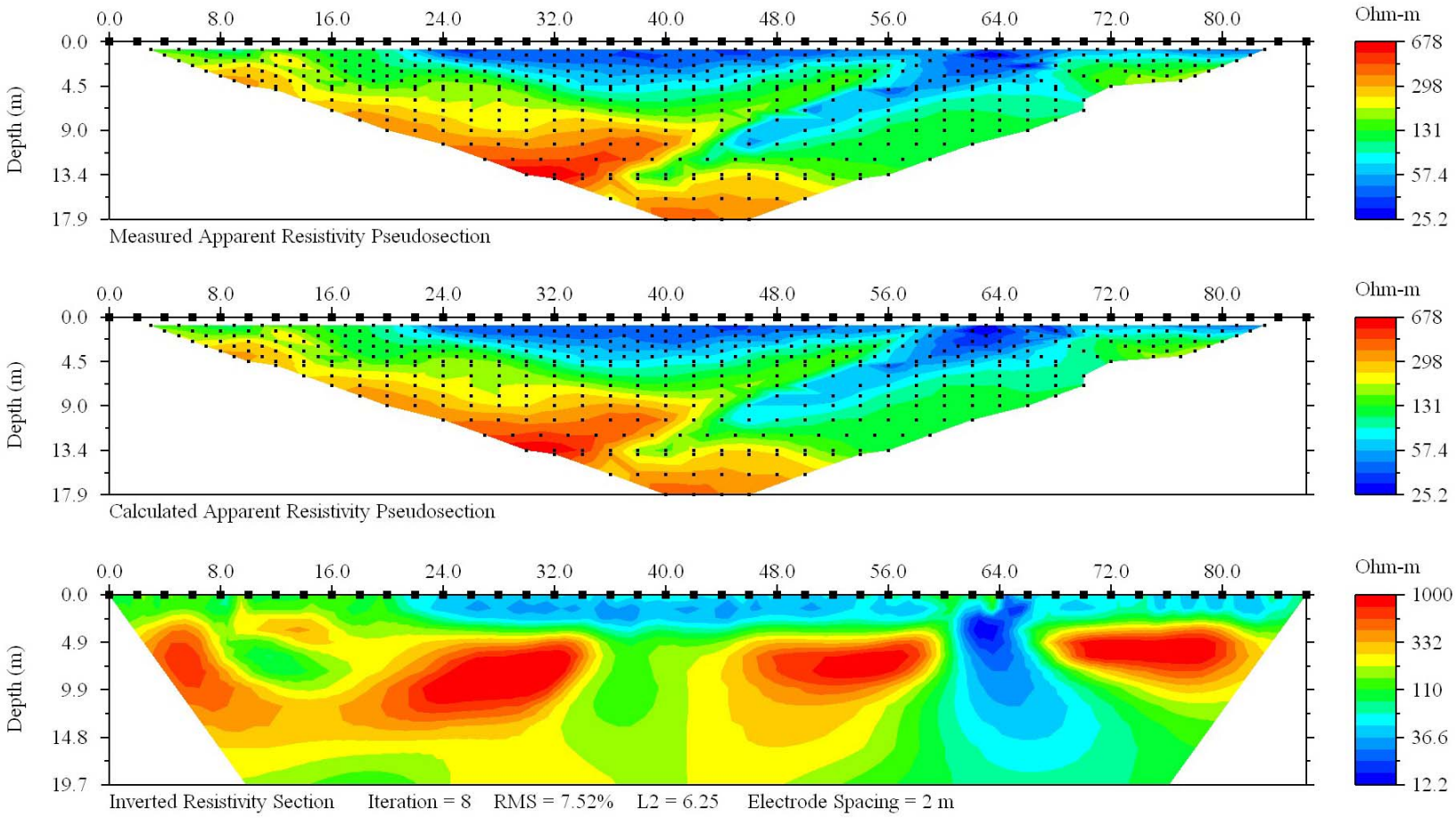

Line – 2, without relative misfit data removed

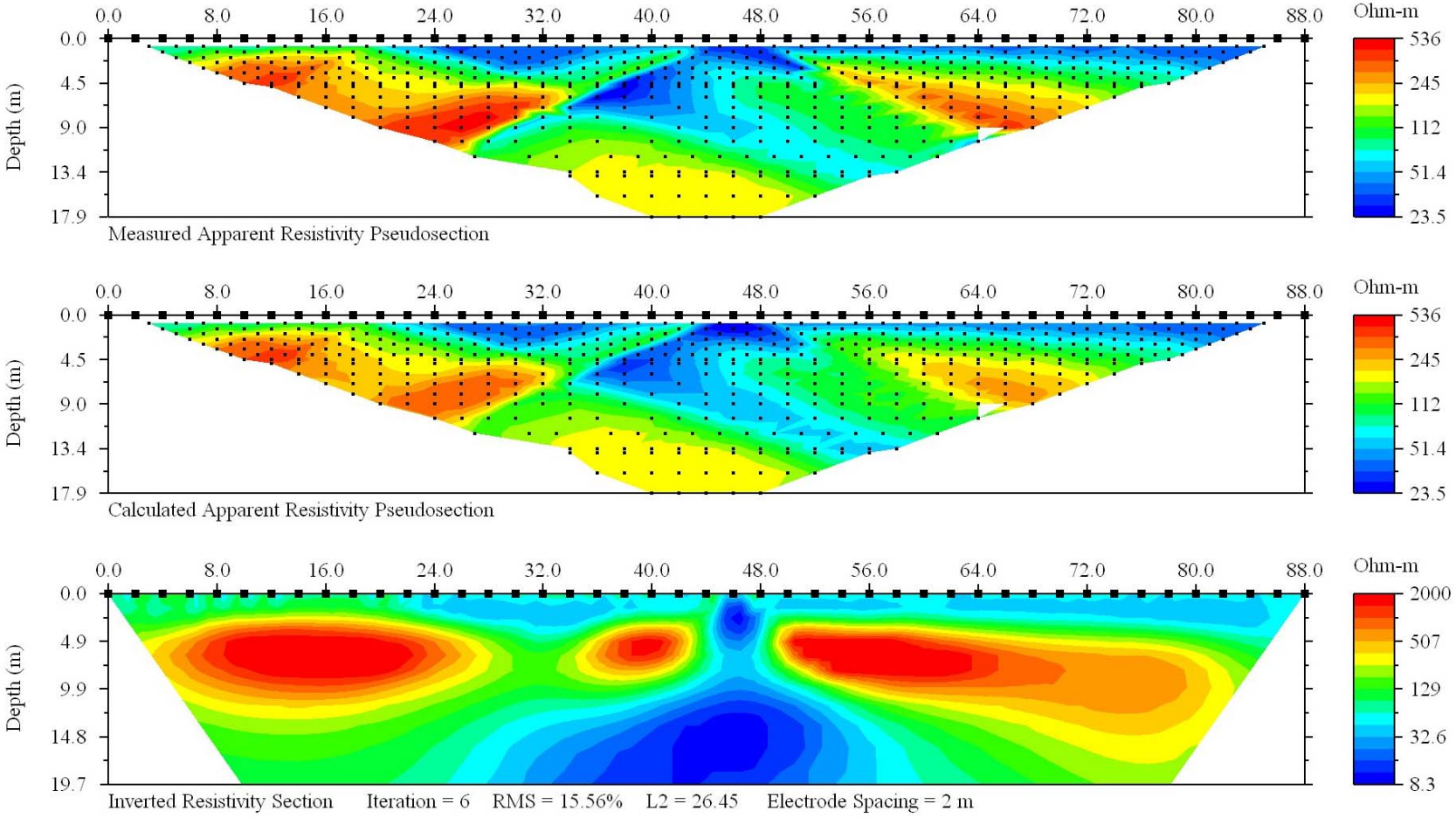

Line – 2, with relative data misfit above 24% removed

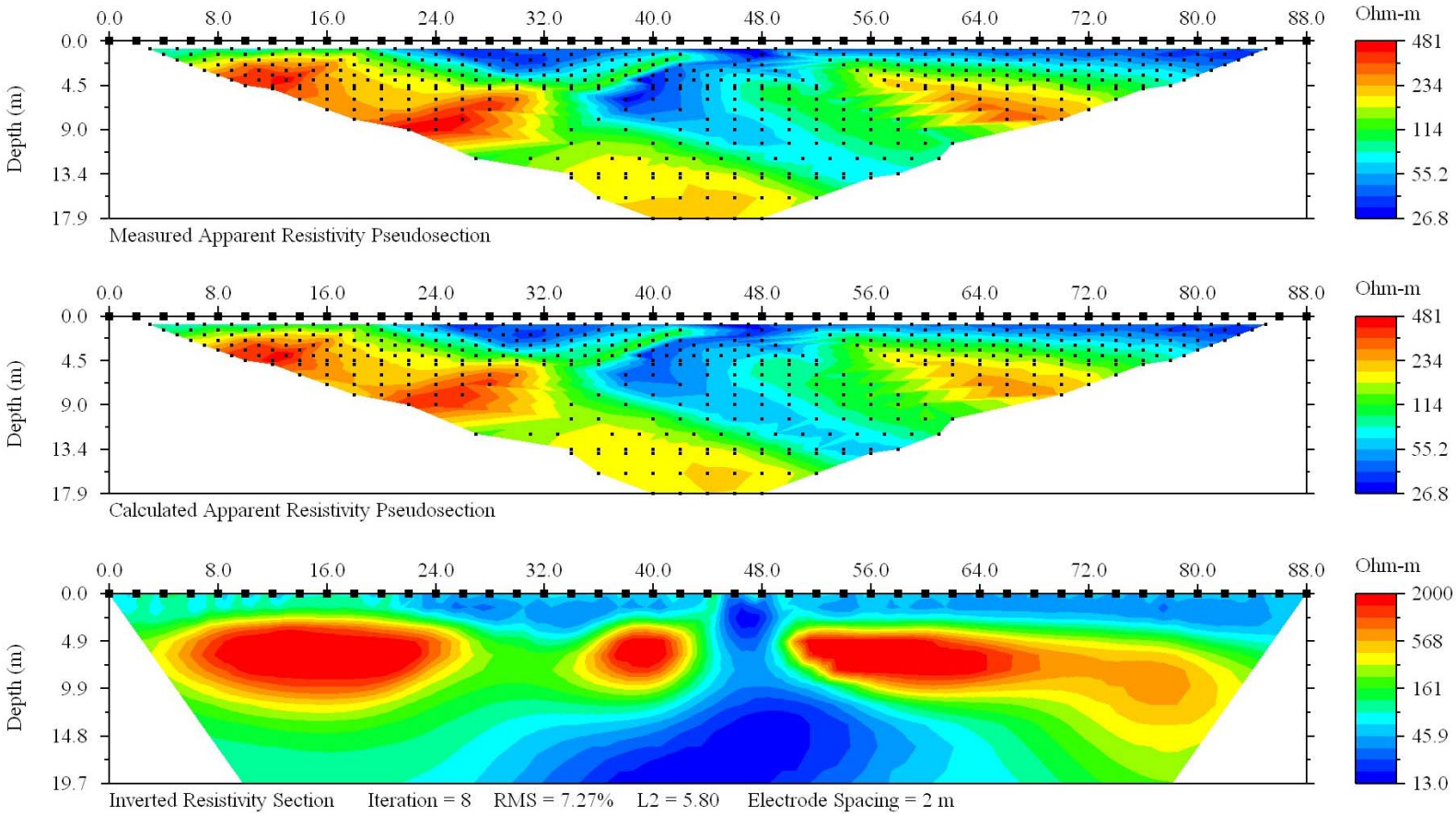

Site – 2: Berea Road

Line – 3, without relative misfit data removed

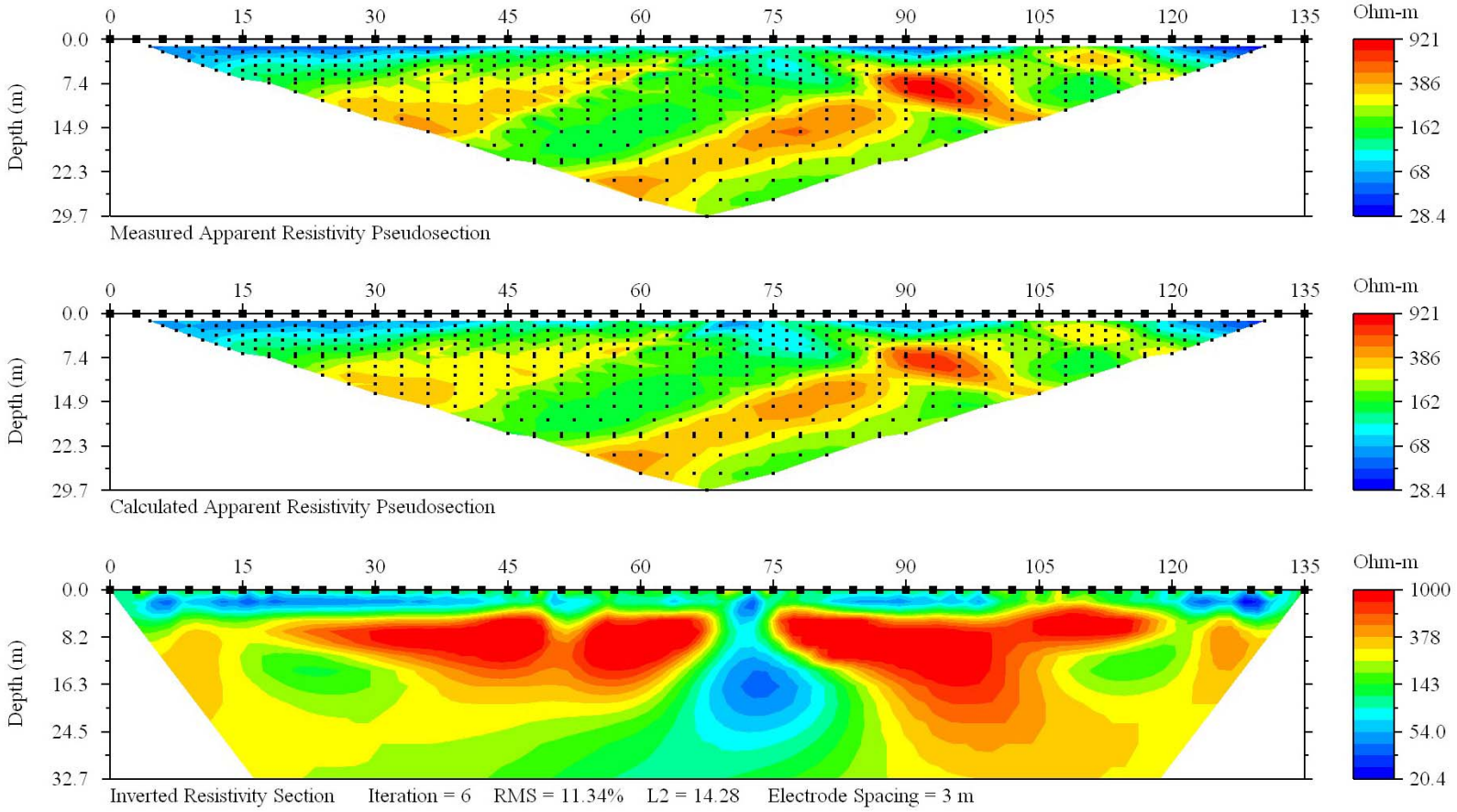

Line - 3, with relative data misfit above 15% removed

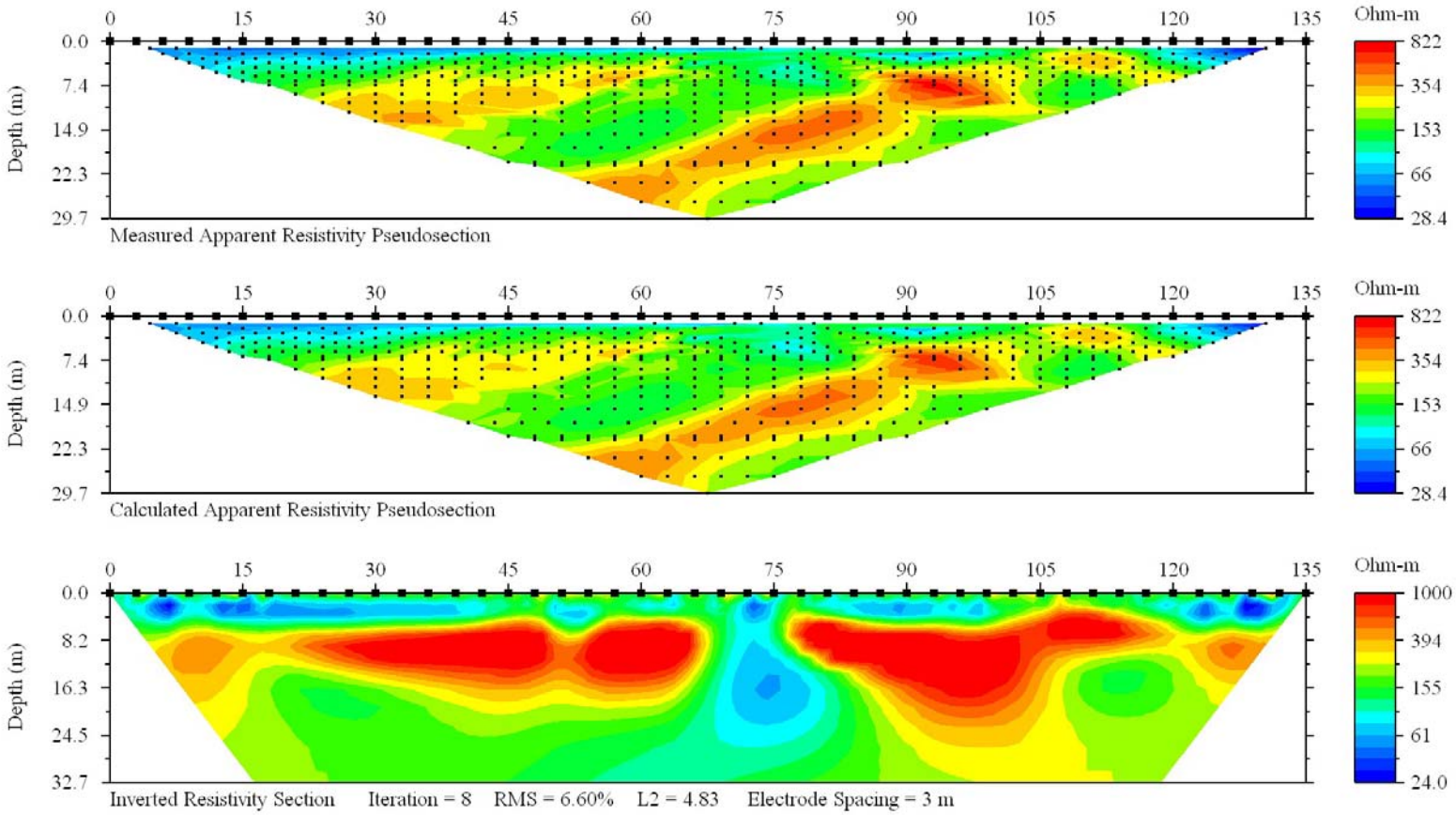

Line - 4, without relative misfit data removed

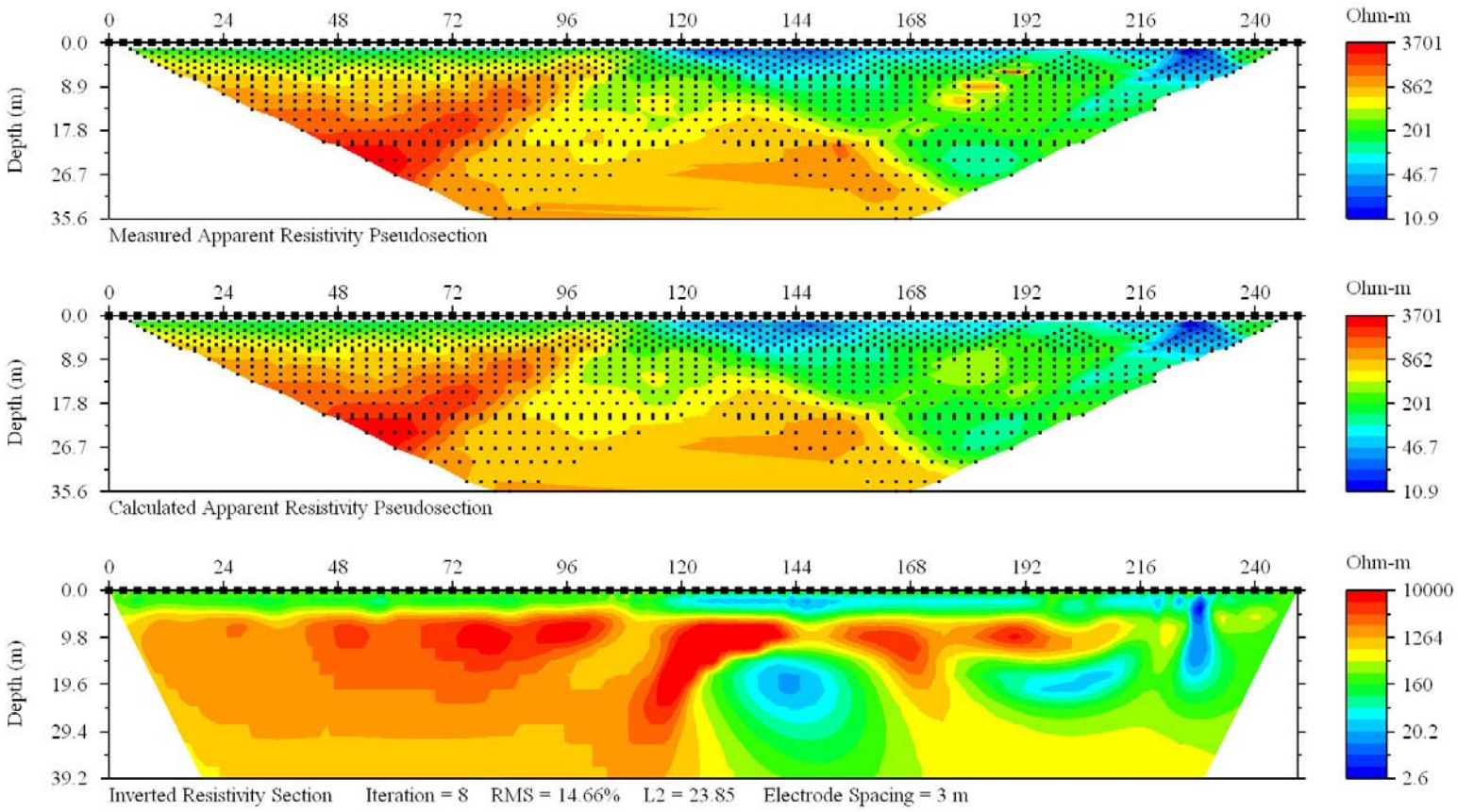

Line - 4, with relative data misfit above 5% removed

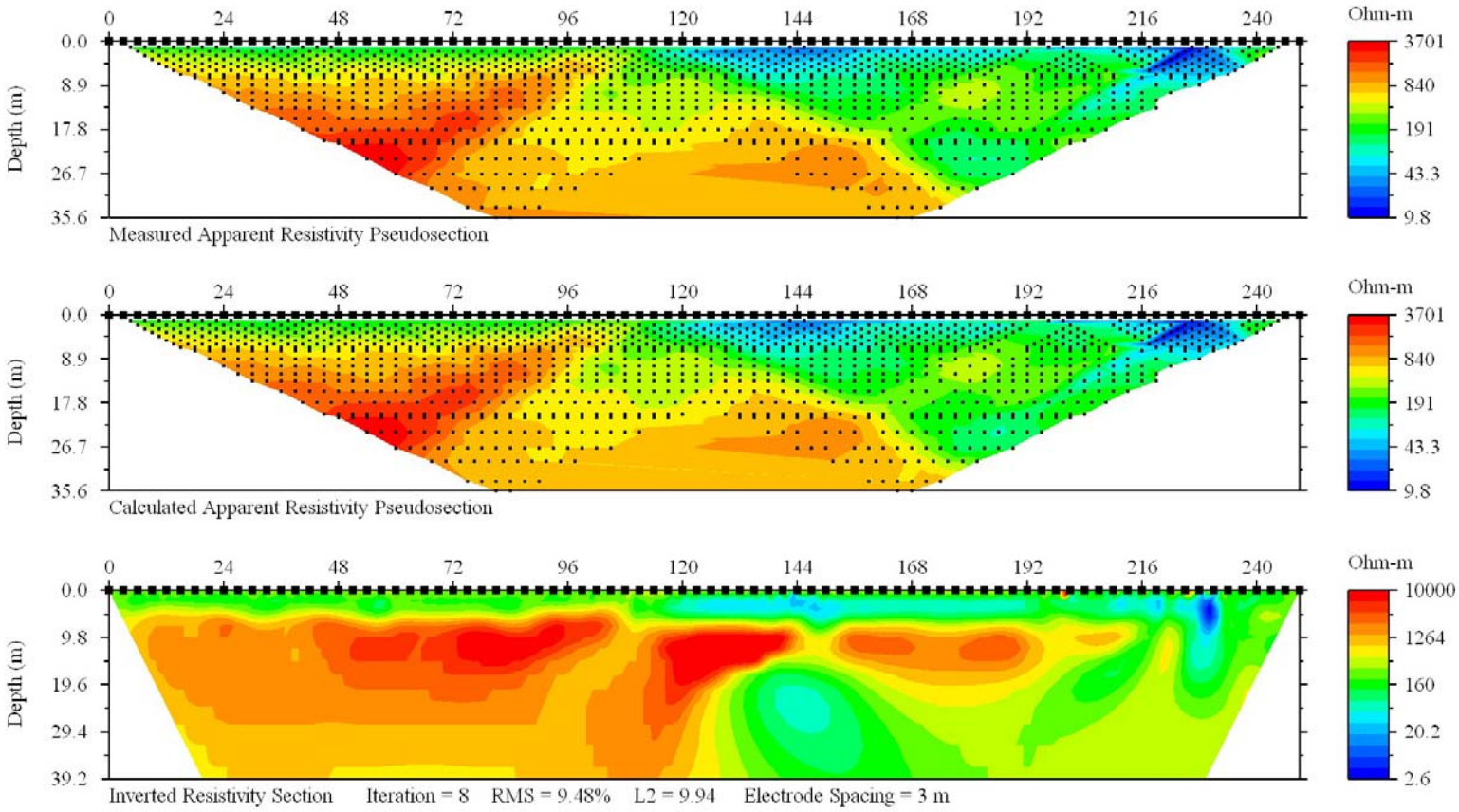

Site – 3: Kentucky Horse Park

Line - 5, without relative misfit data removed

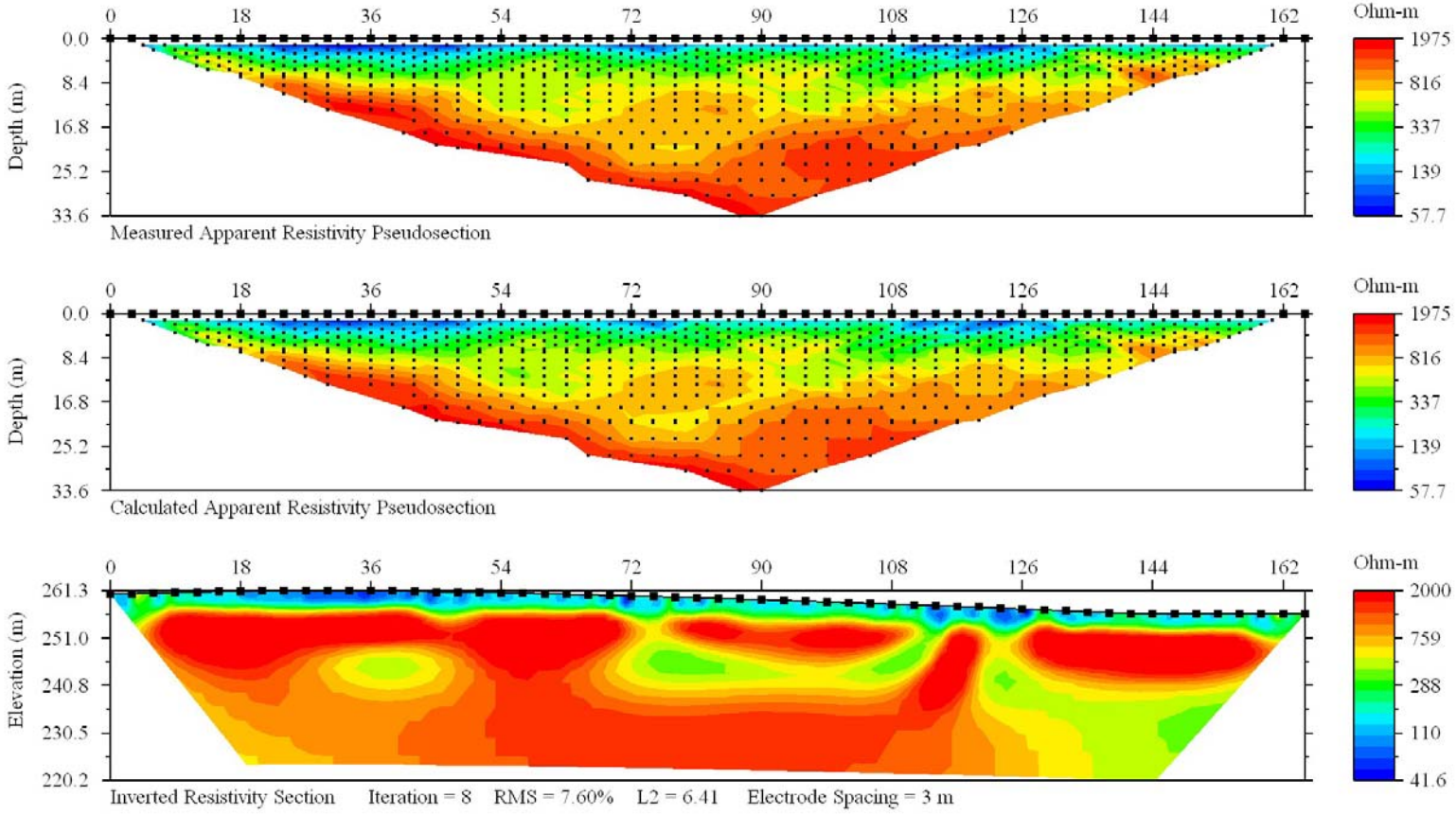

Line - 5, with relative data misfit above 15% removed

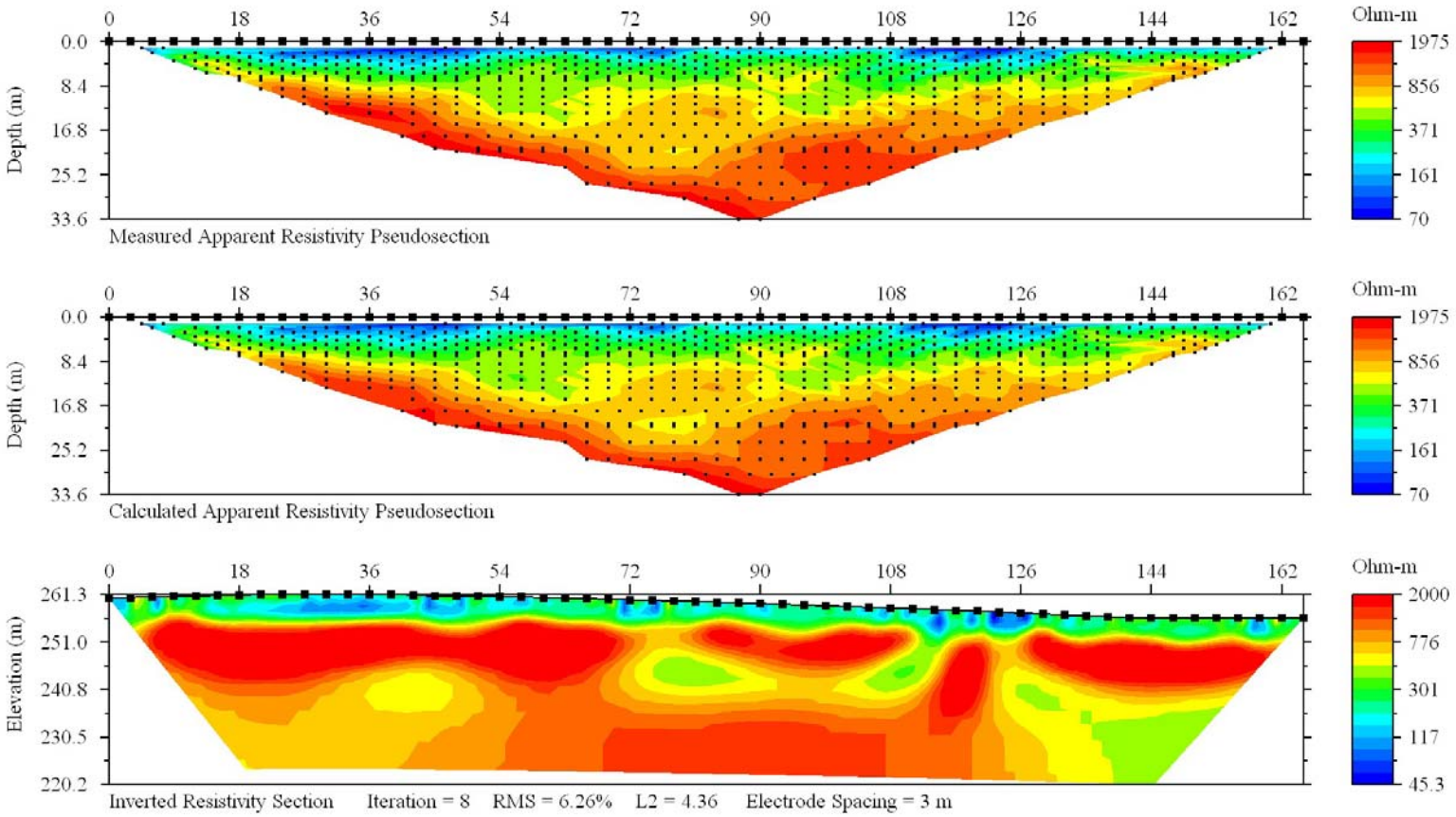

Line – 6(a), without relative misfit data removed

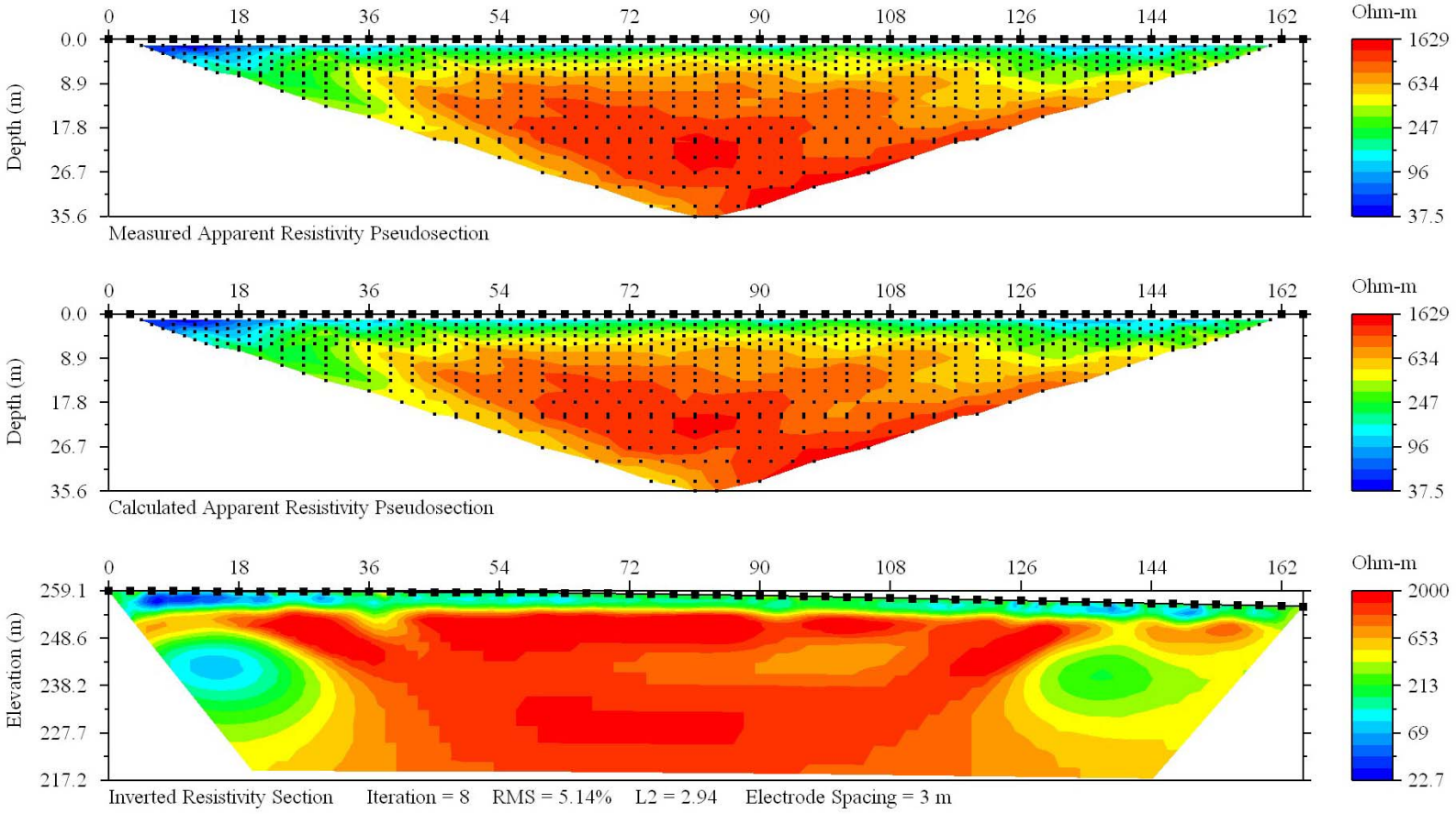

Line – 6(a), with relative data misfit above 10.5% removed

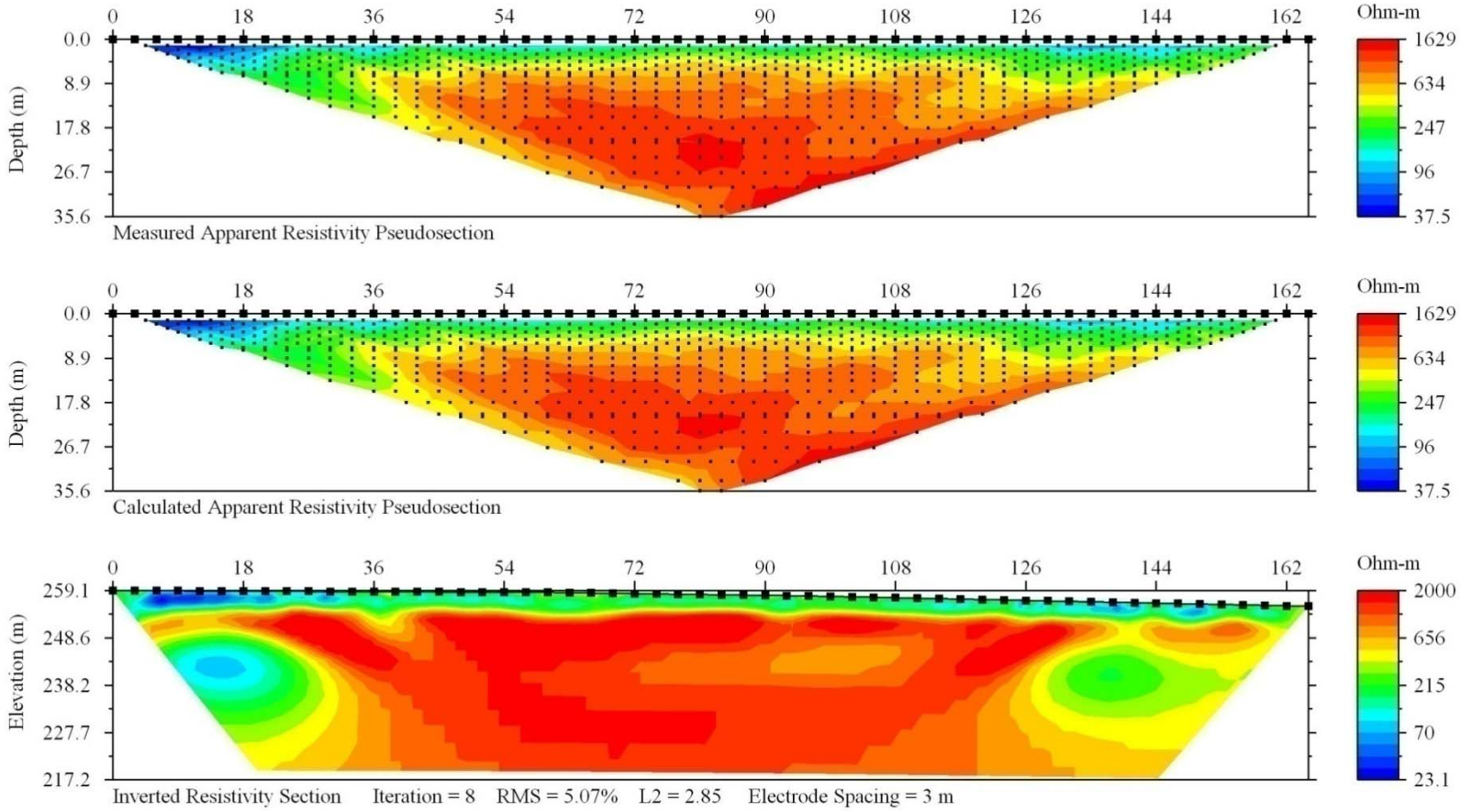

Line – 6(b), without relative misfit data removed

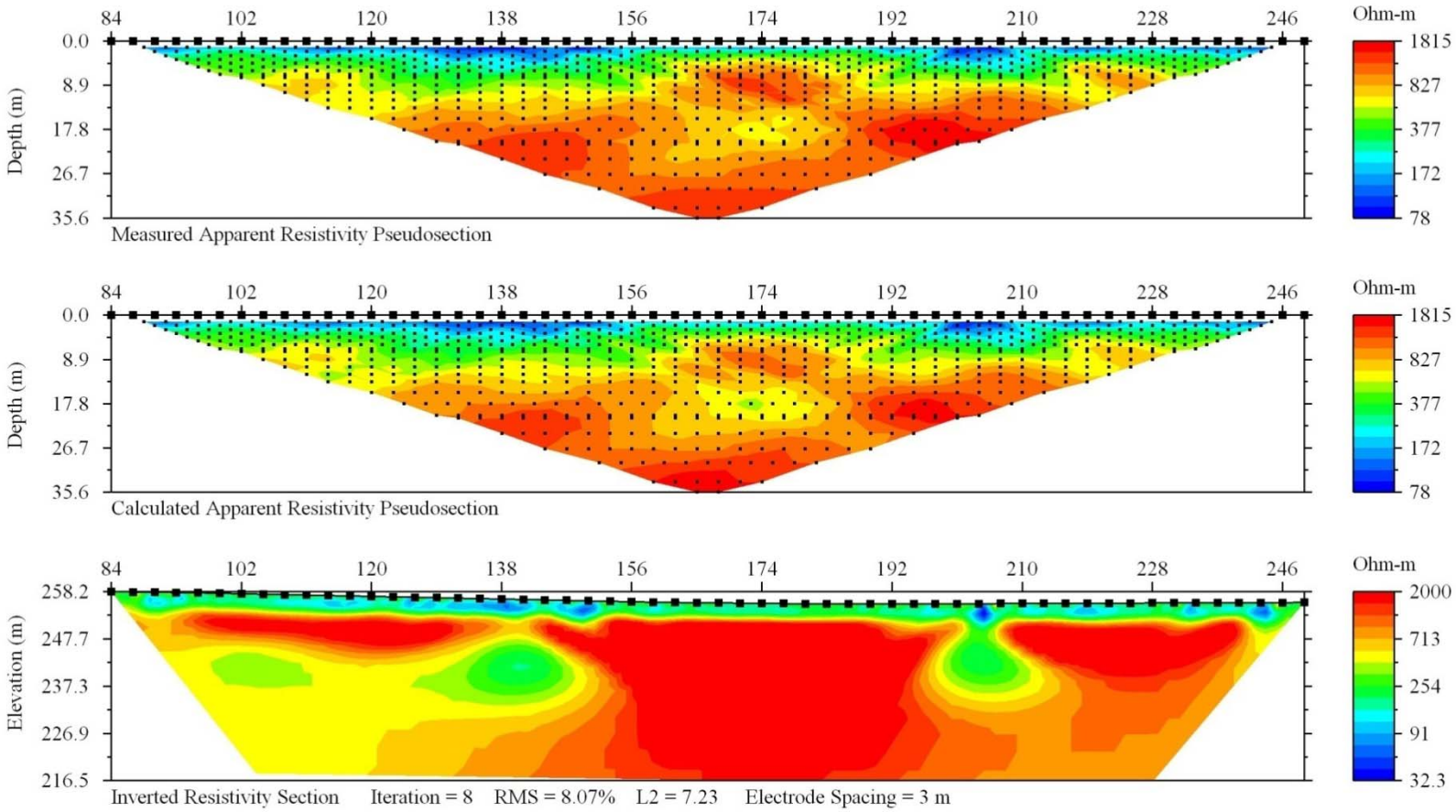

Line – 6(b), with relative data misfit above 5% removed

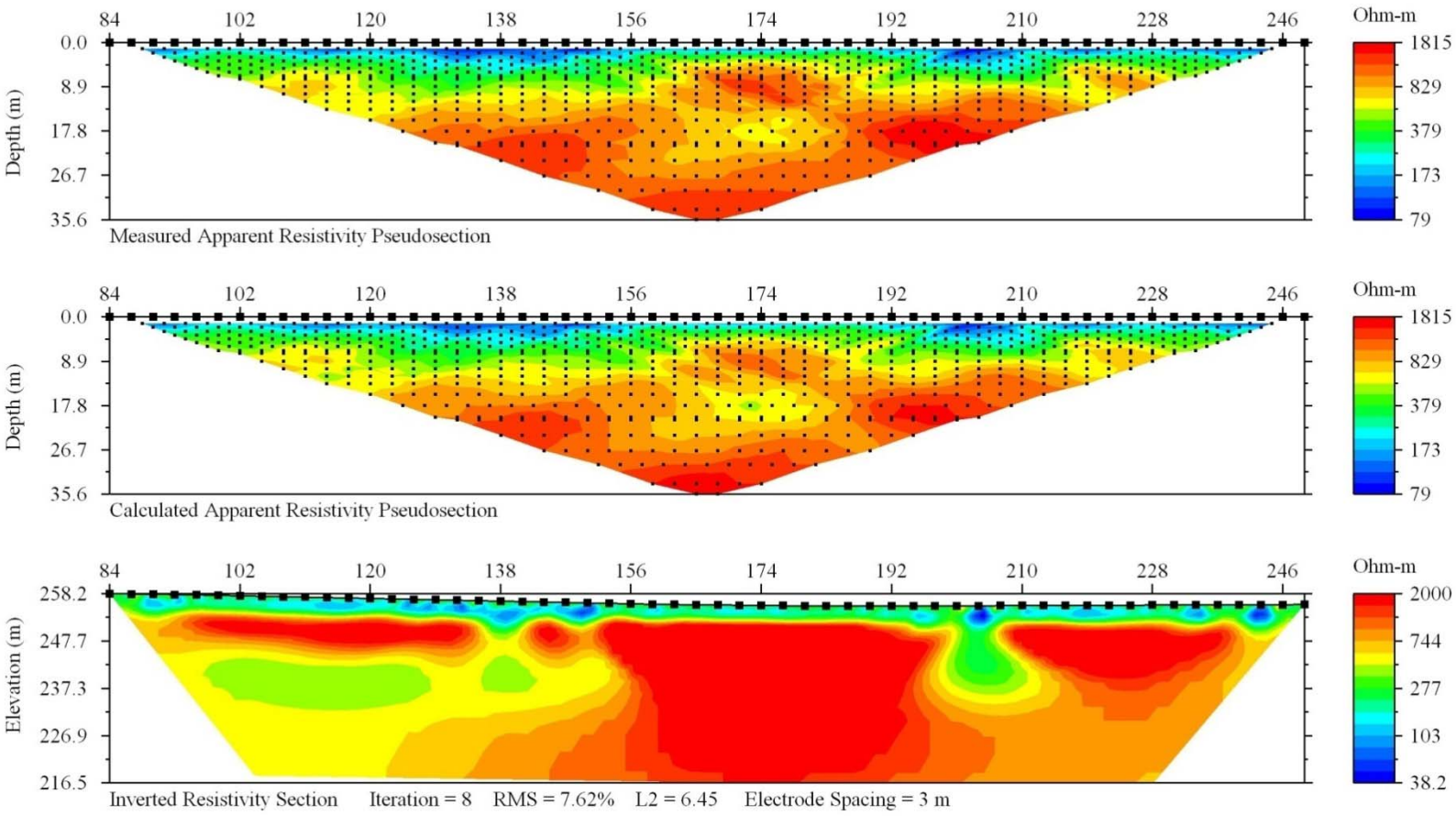

Appendix I

B. Convergence curves of root mean square (RMS) versus number of iterations.

Site – 1: University of Kentucky Agricultural Research Farm

Line – 1, without relative misfit data removed

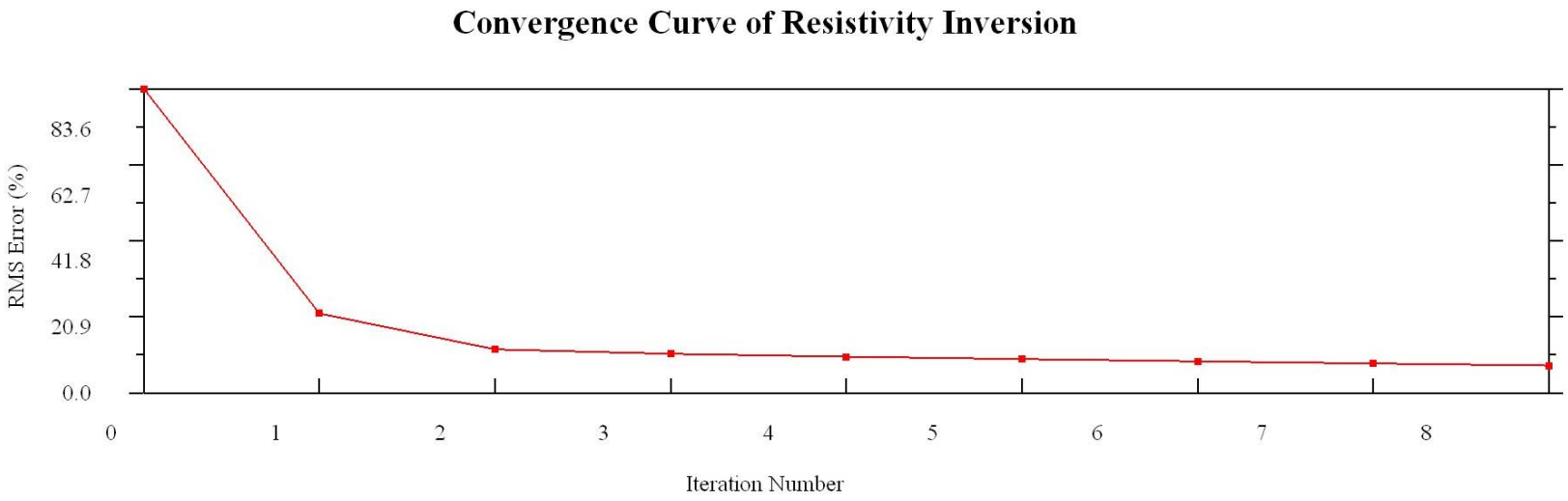

Line – 1, with relative data misfit above 12% removed

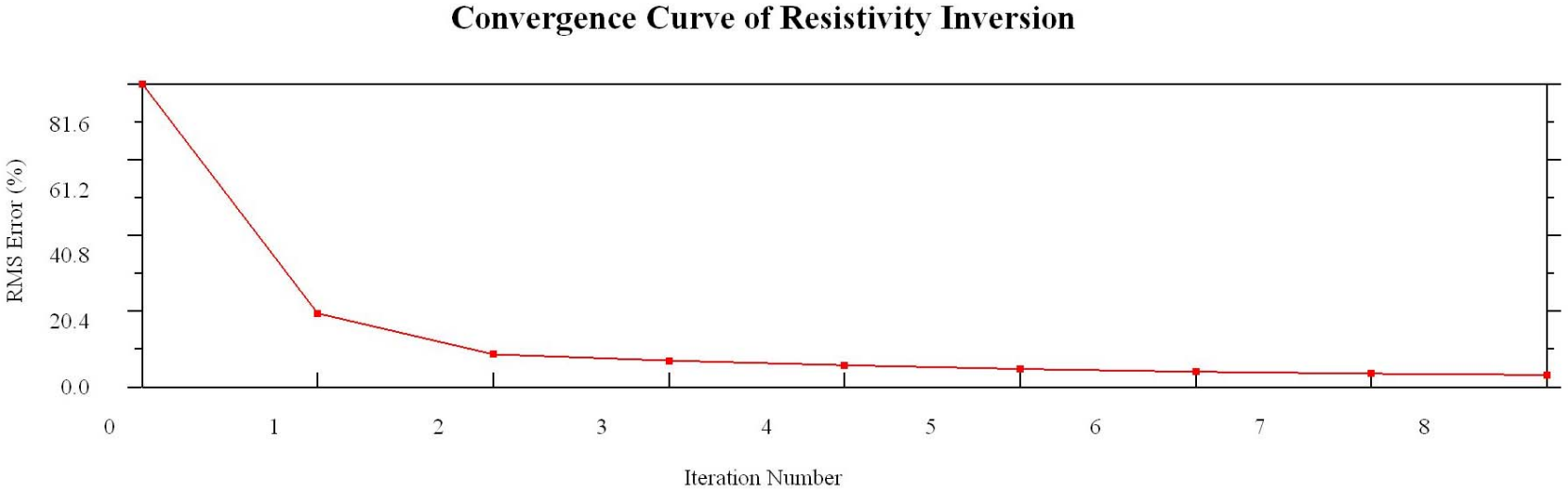

Line – 2, without relative misfit data removed

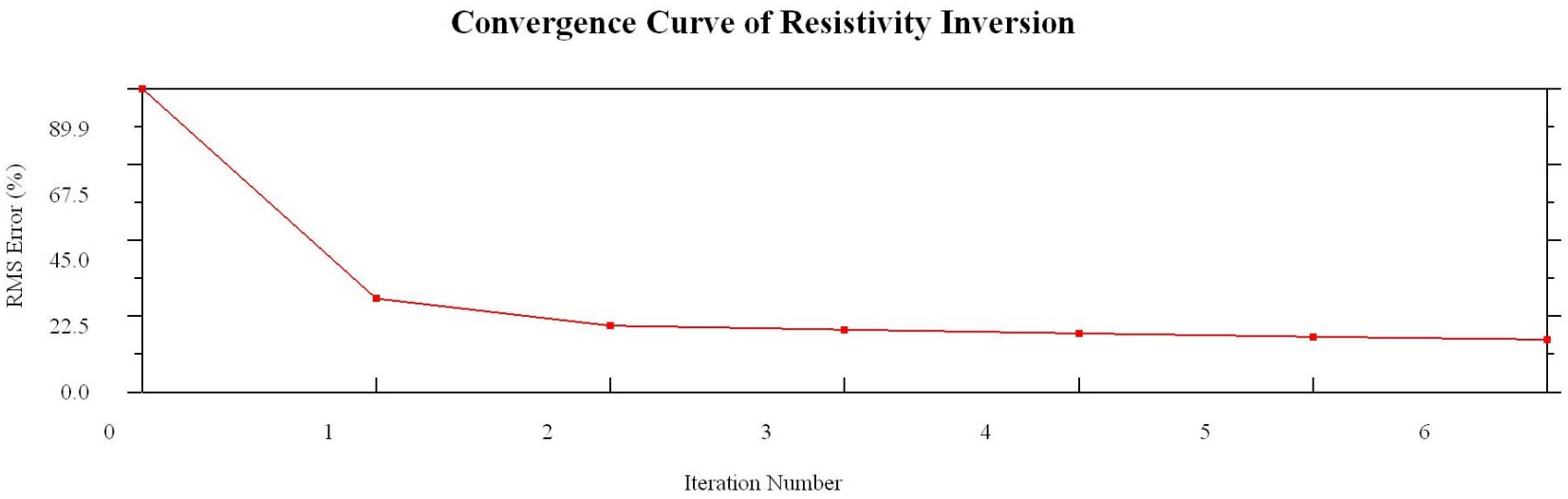

Line – 2, with relative data misfit above 24% removed

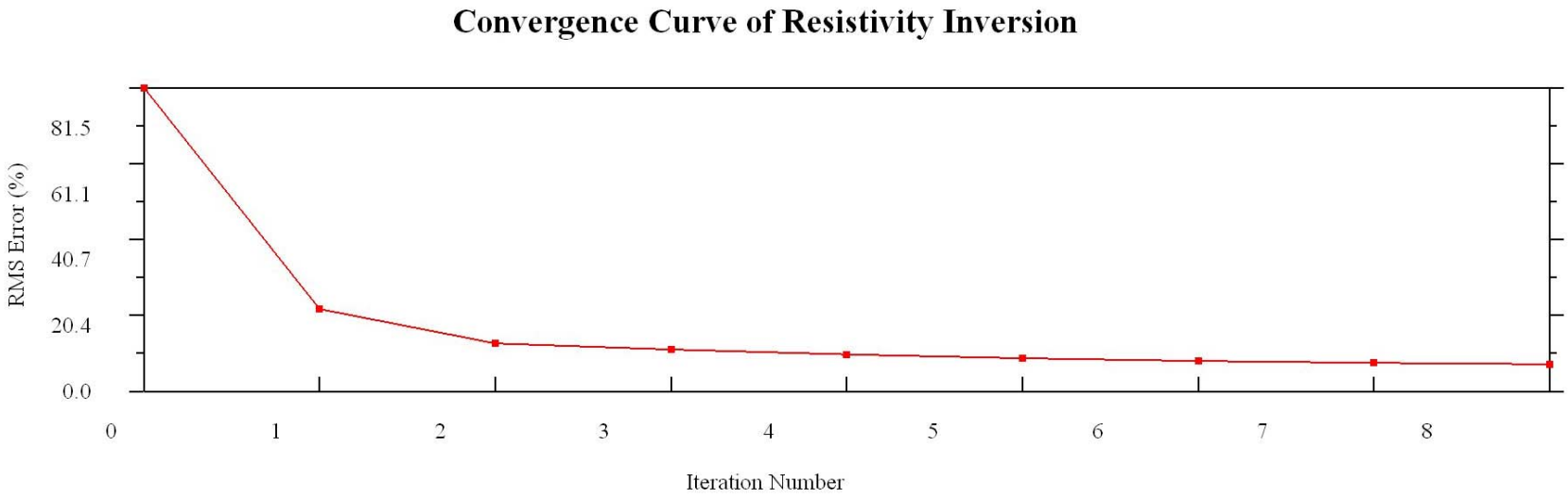

Site – 2: Berea Road

Line – 3, without relative misfit data removed

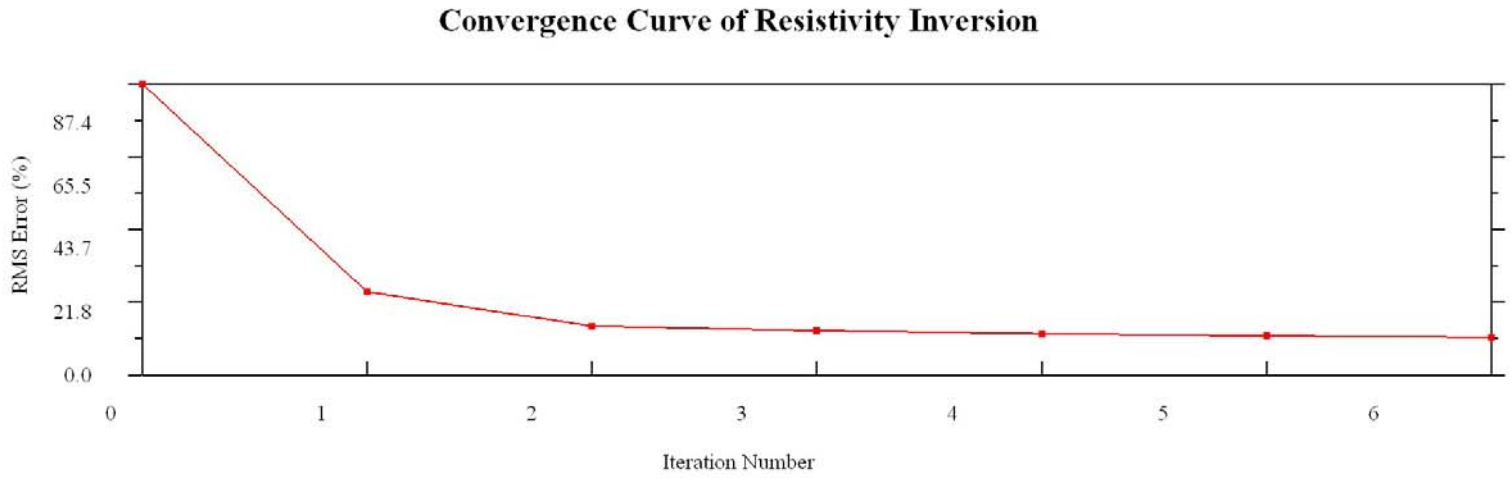

Line – 3, with relative data misfit above 15% removed

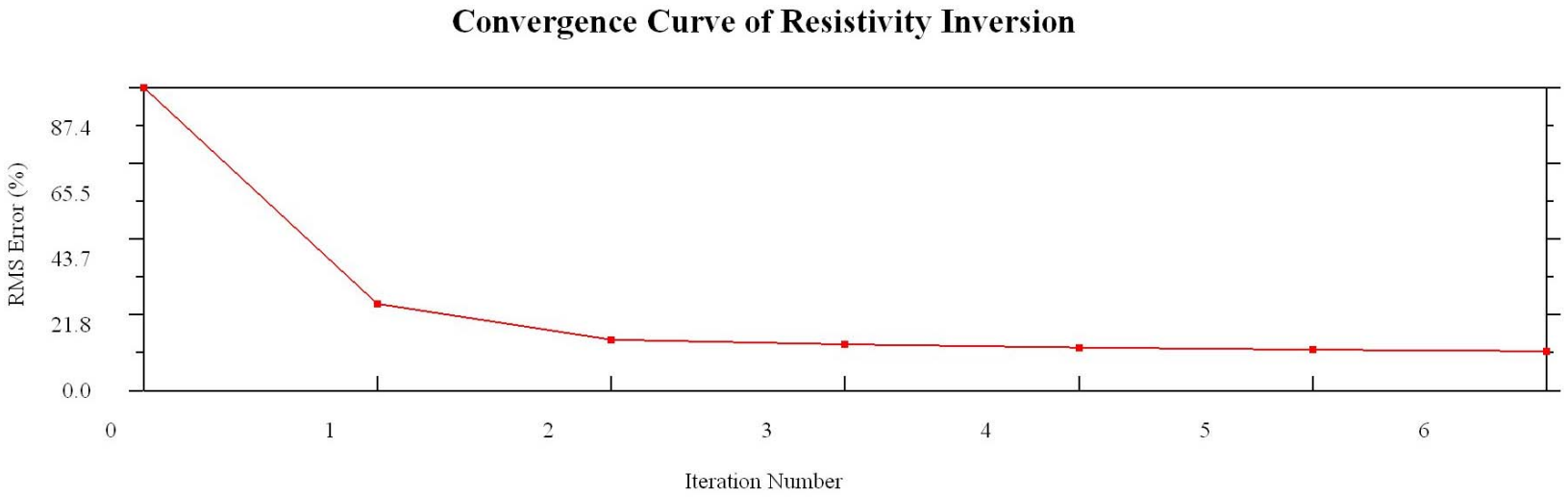

Line – 4, without relative misfit data removed

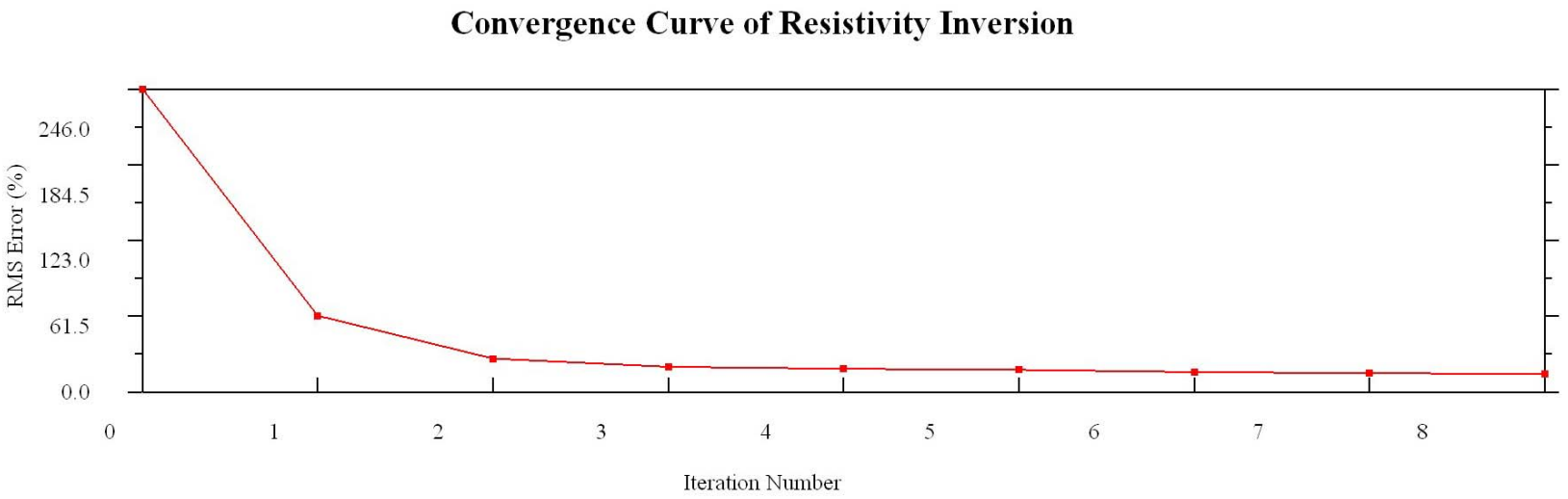

Line – 4, with relative data misfit above 5% removed

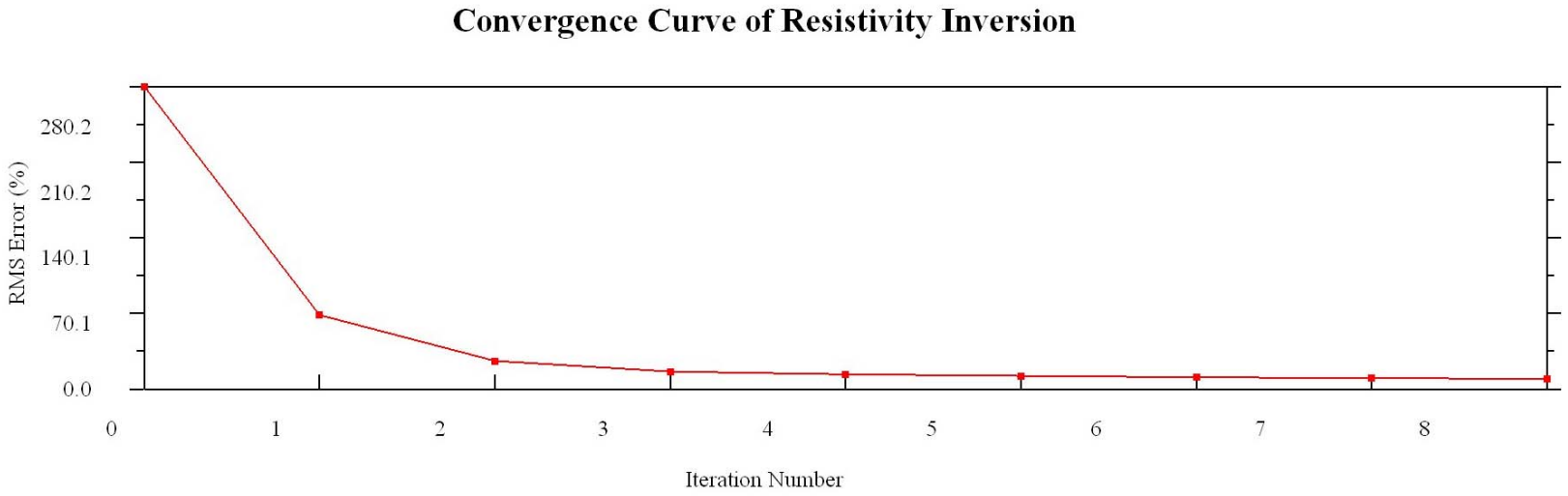

Site – 3: Kentucky Horse Park

Line - 5, without relative misfit data removed

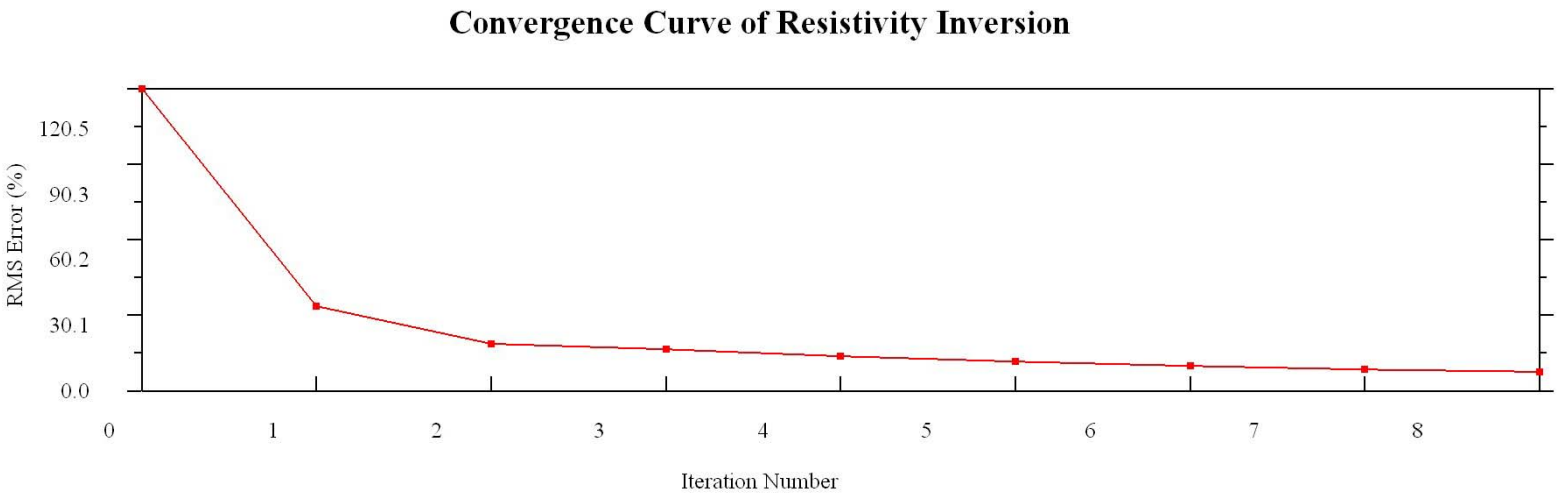

Line - 5, with relative data misfit above 15% removed

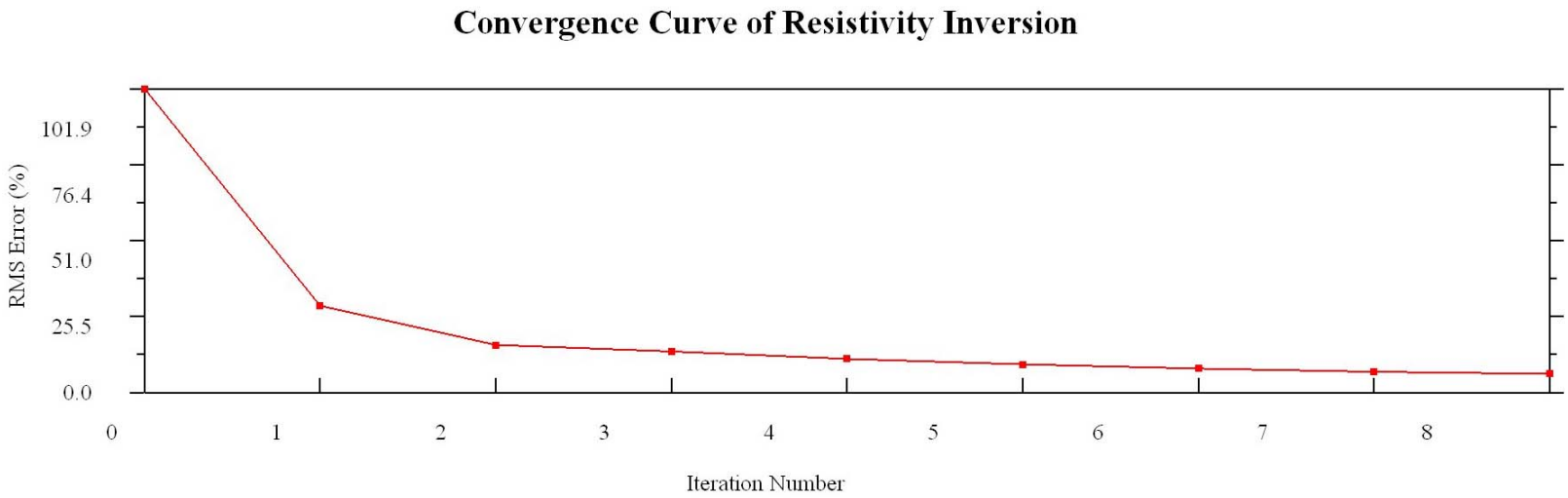

Line – 6(a), without relative misfit data removed

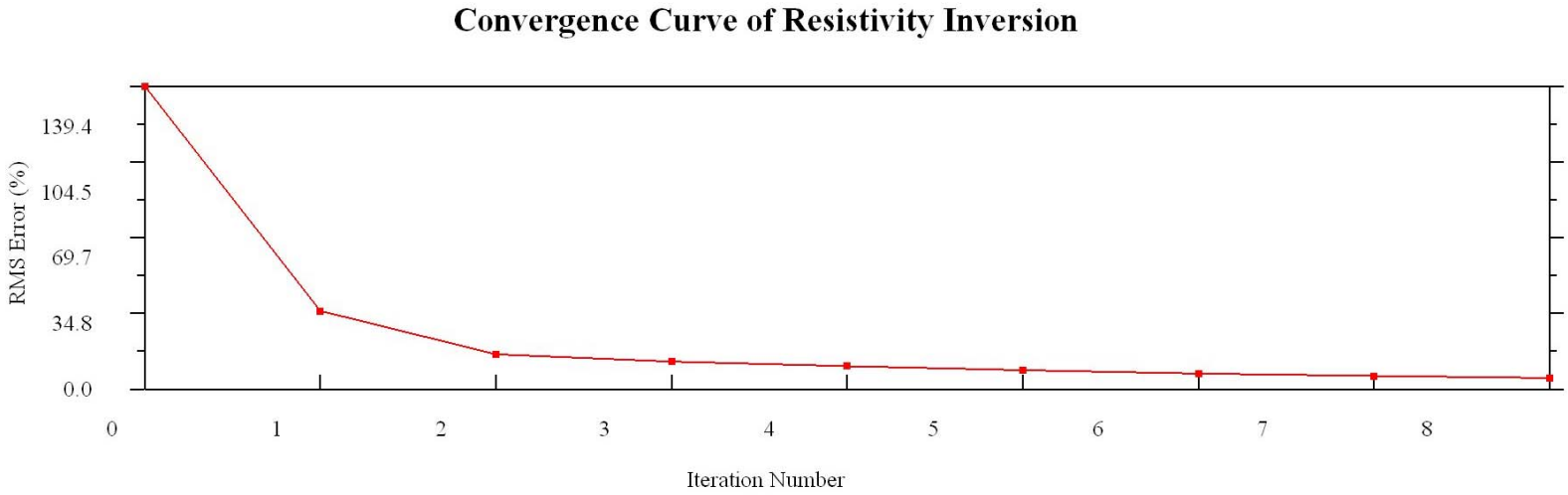

Line – 6(a), with relative data misfit above 10.5% removed

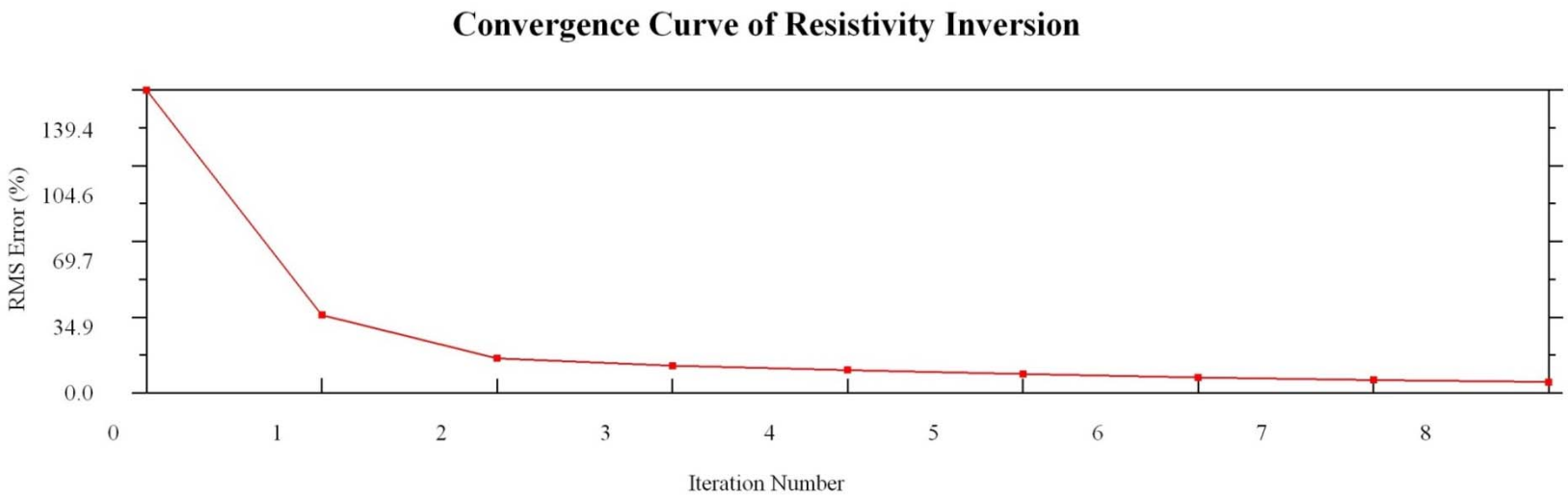

Line – 6(b), without relative misfit data removed

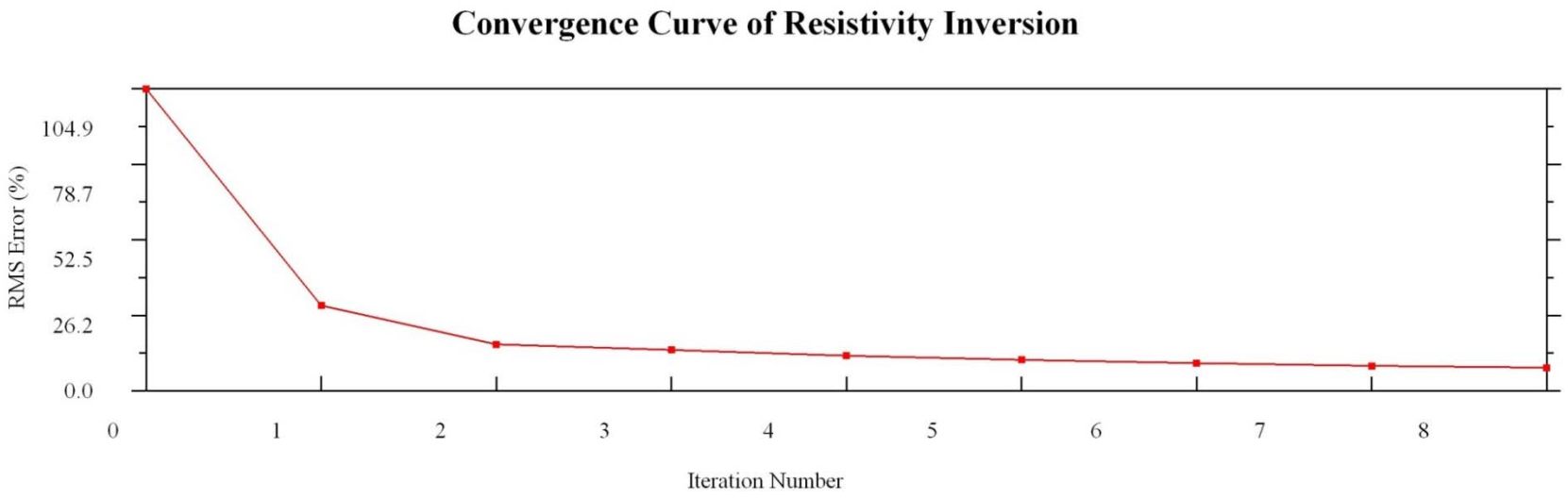

Line – 6(b), with relative data misfit above 19.5% removed

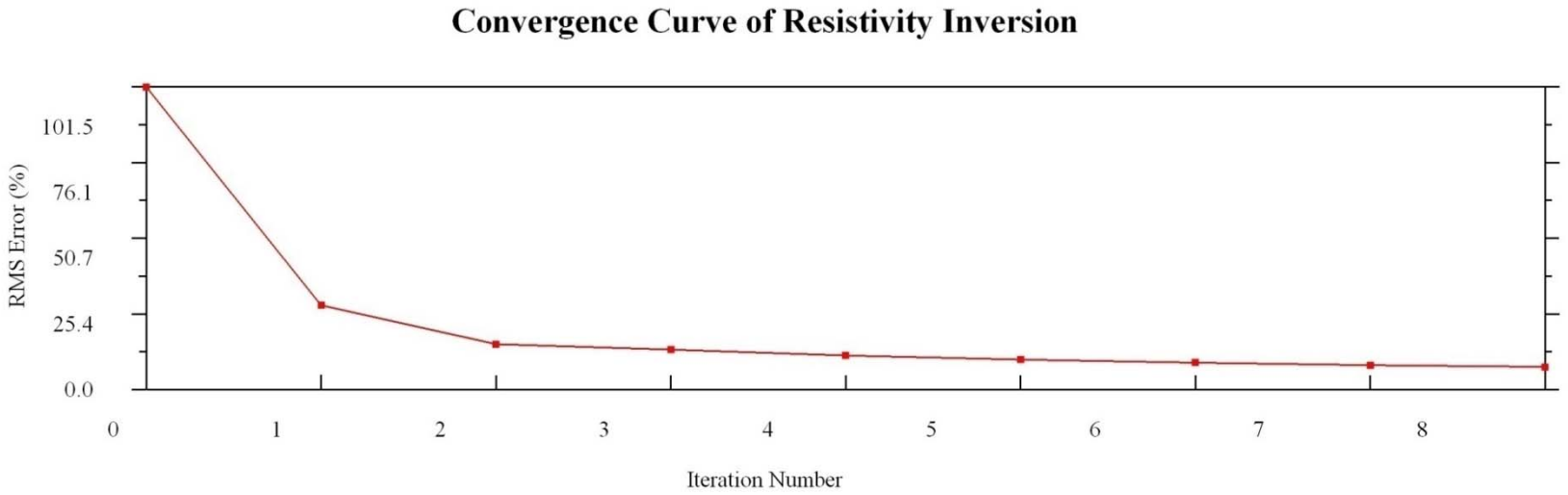

Appendix I

C. Data misfit crossplots. These plots show relative fitness between calculated and measured apparent resistivity.

Site – 1: University of Kentucky Agricultural Research Farm

Line – 1, with relative data misfit above 12% removed

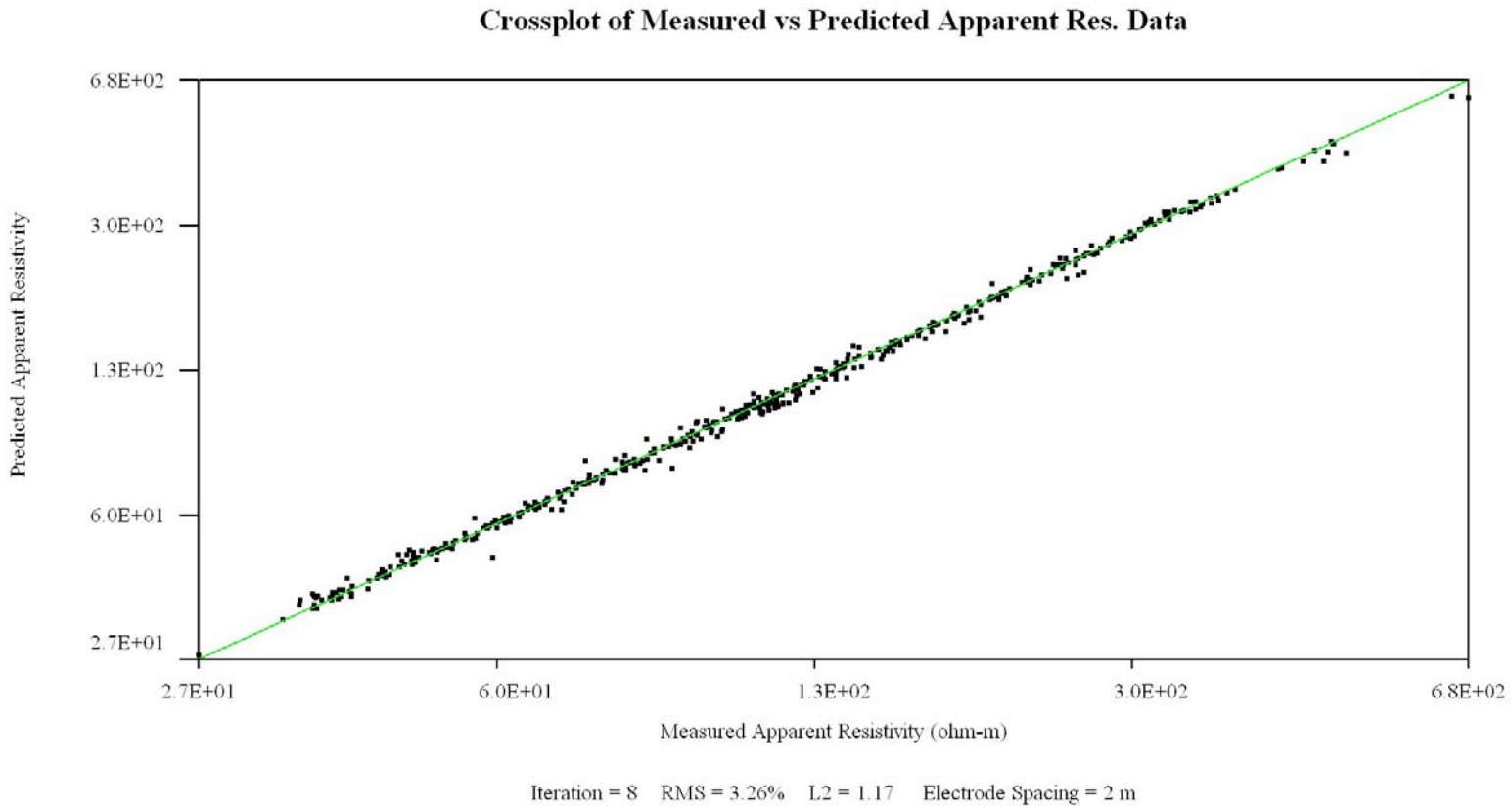

Line – 2, without relative misfit data removed

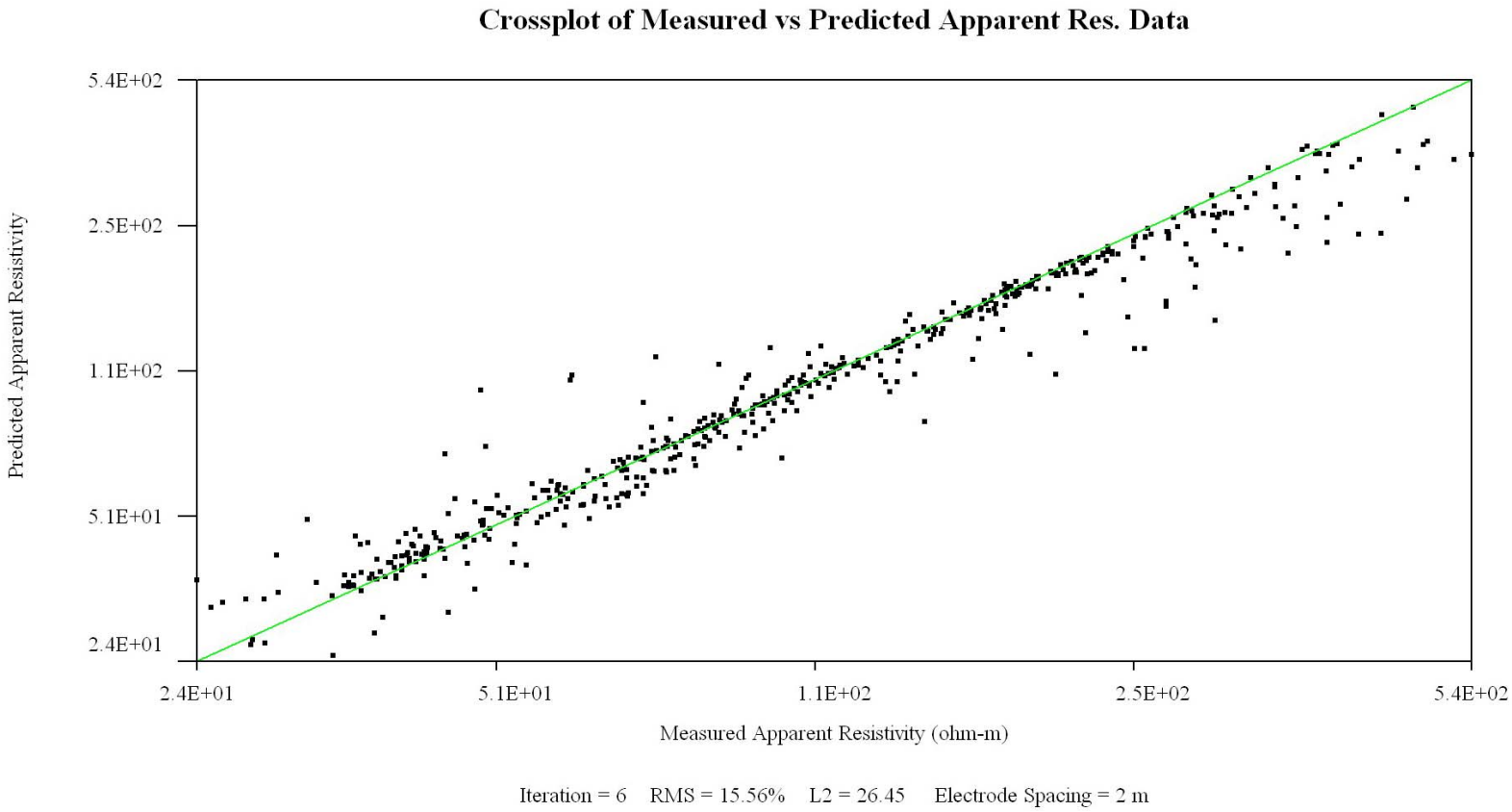

Line – 2, with relative data misfit above 24% removed

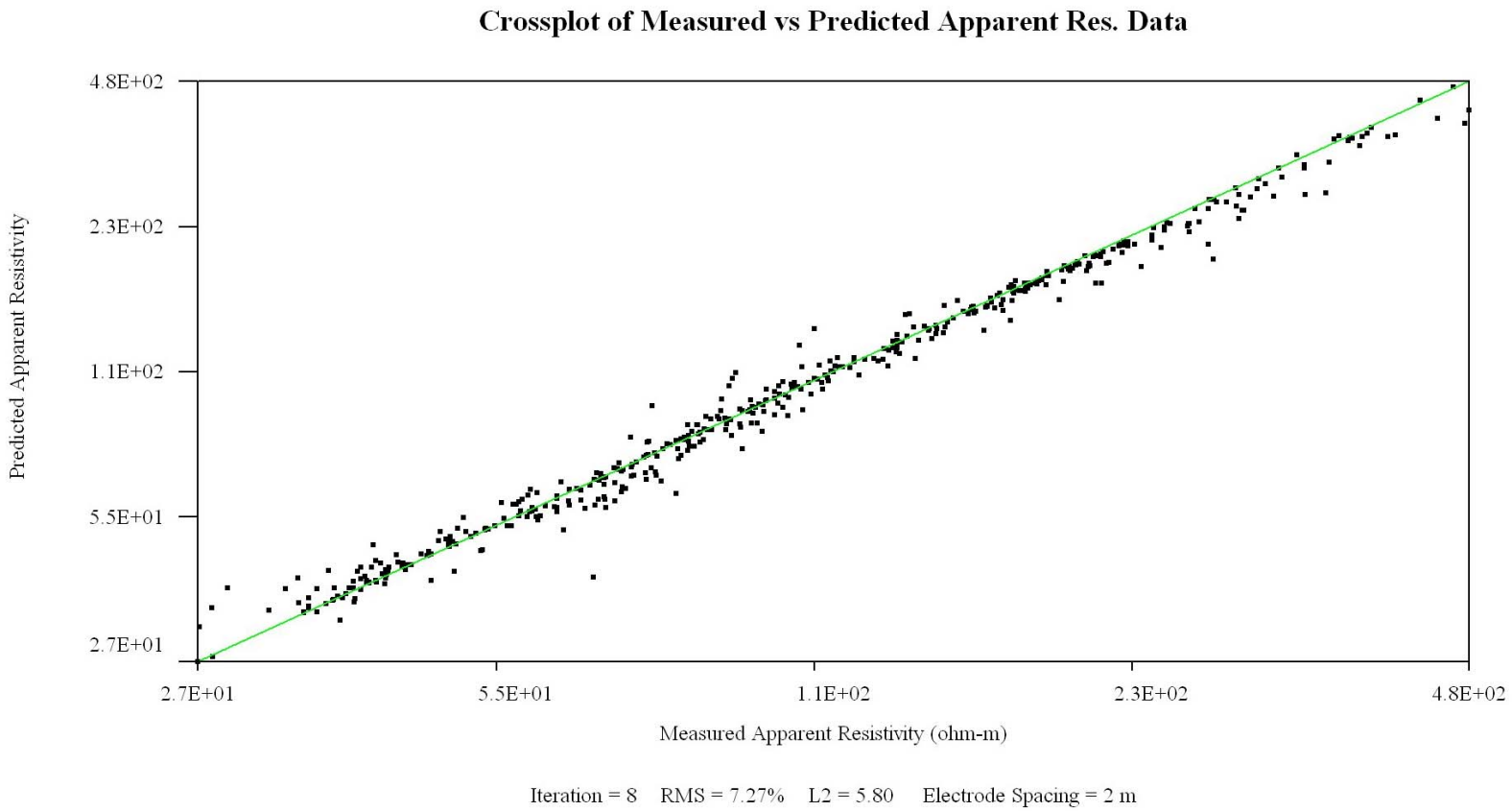

Site – 2: Berea Road

Line – 3, without relative misfit data removed

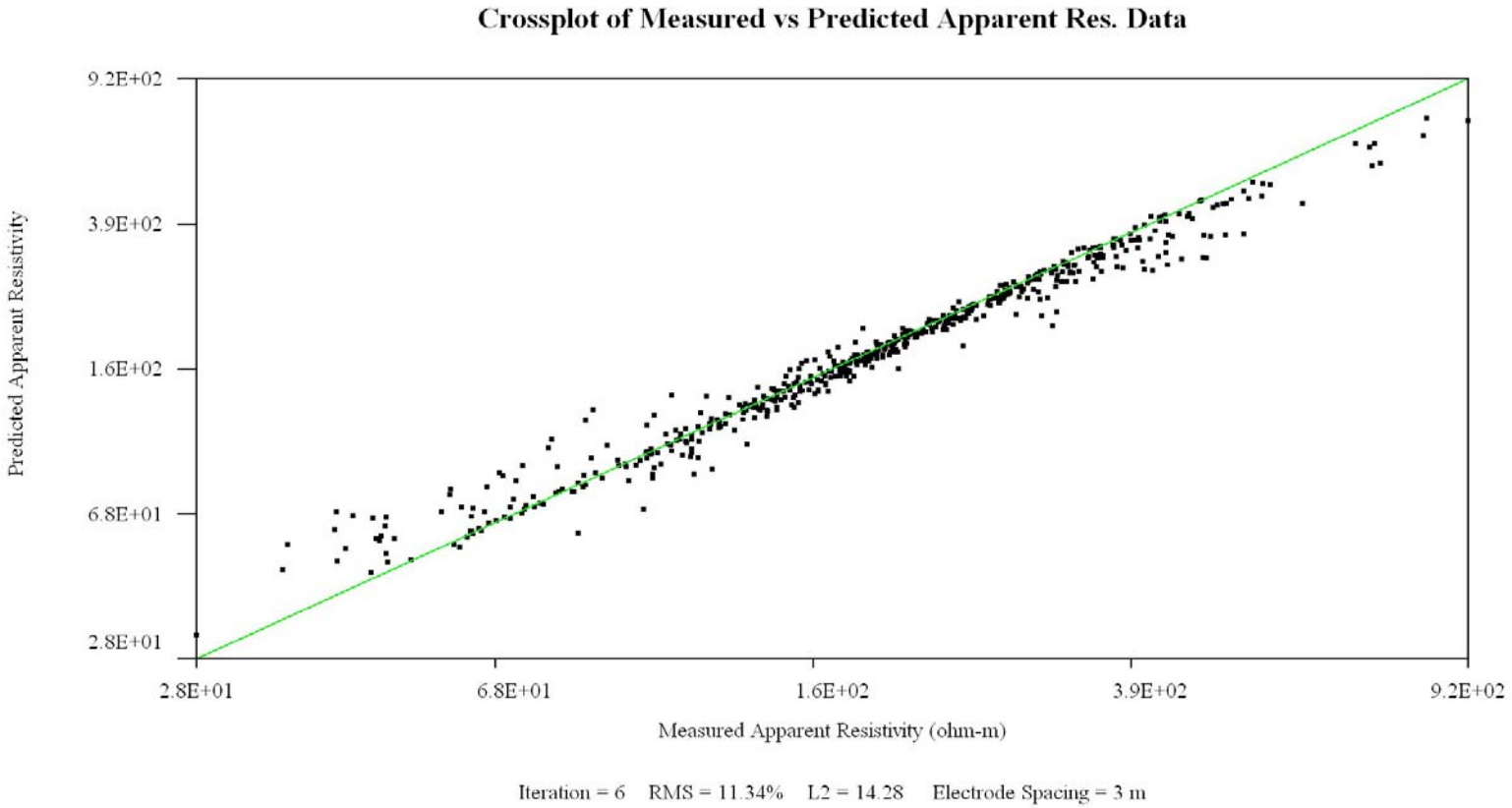

Line – 3, with relative data misfit above 15% removed

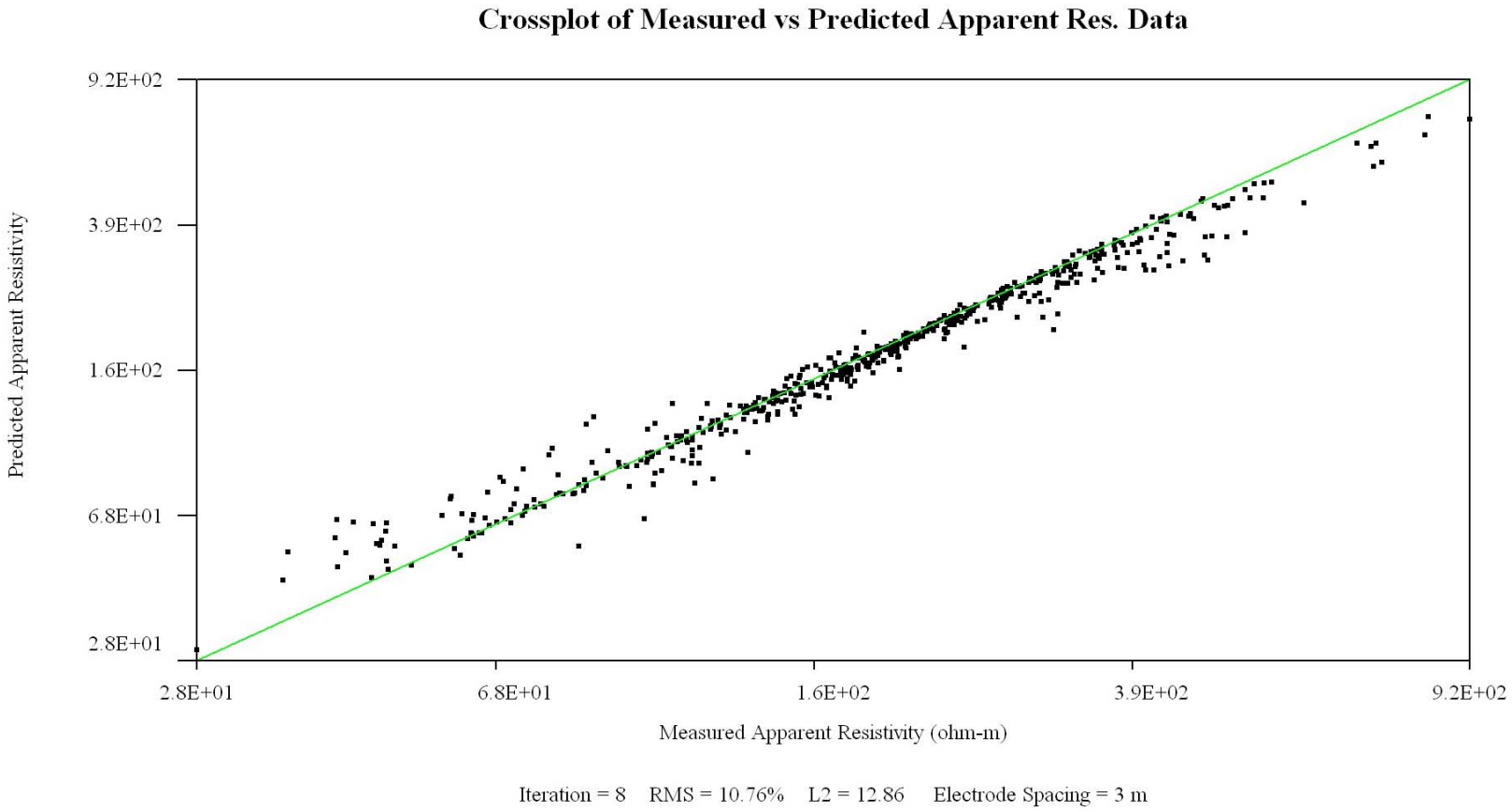

Line – 4, without relative misfit data removed

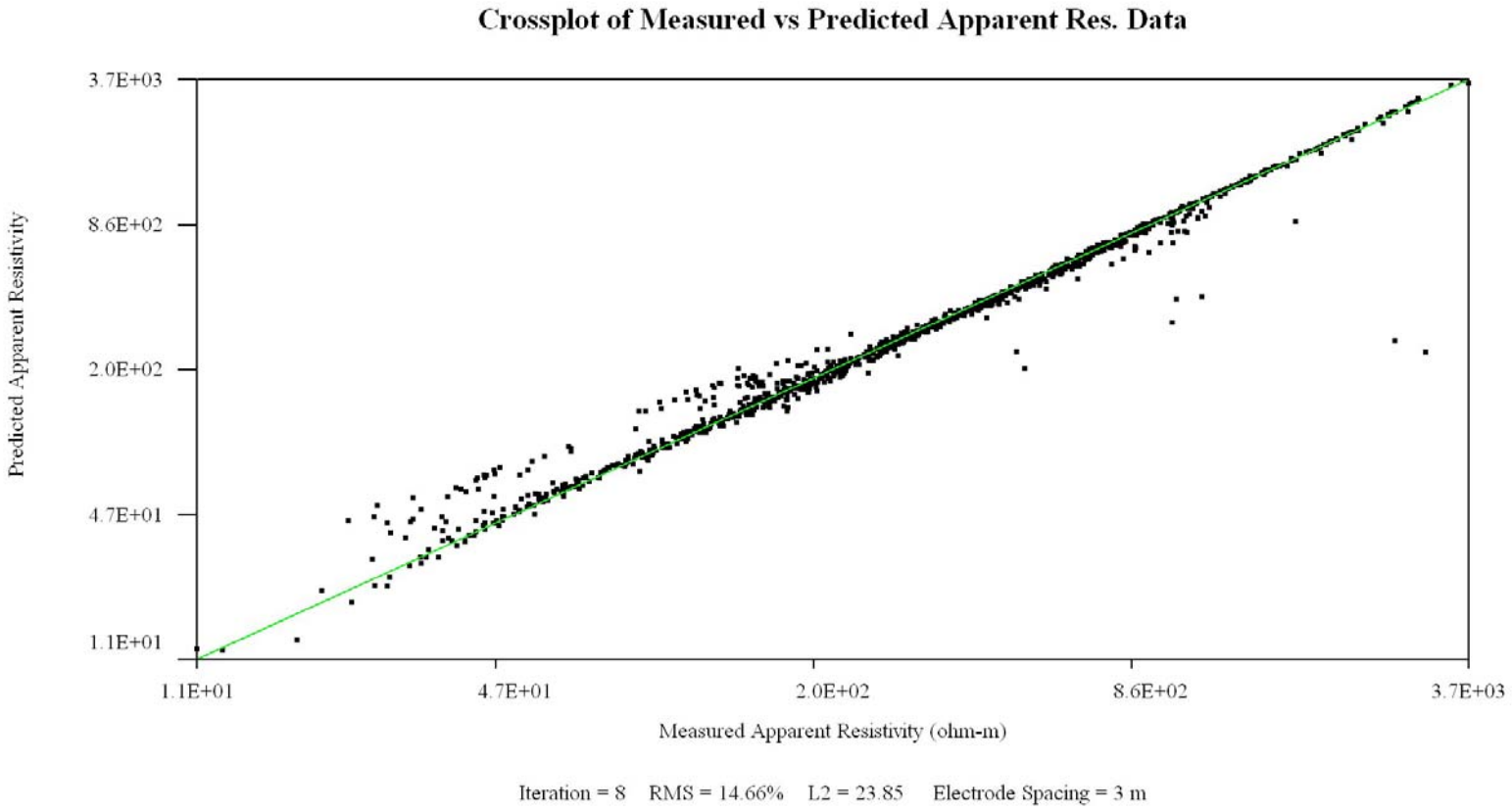

Line – 4, with relative data misfit above 5% removed

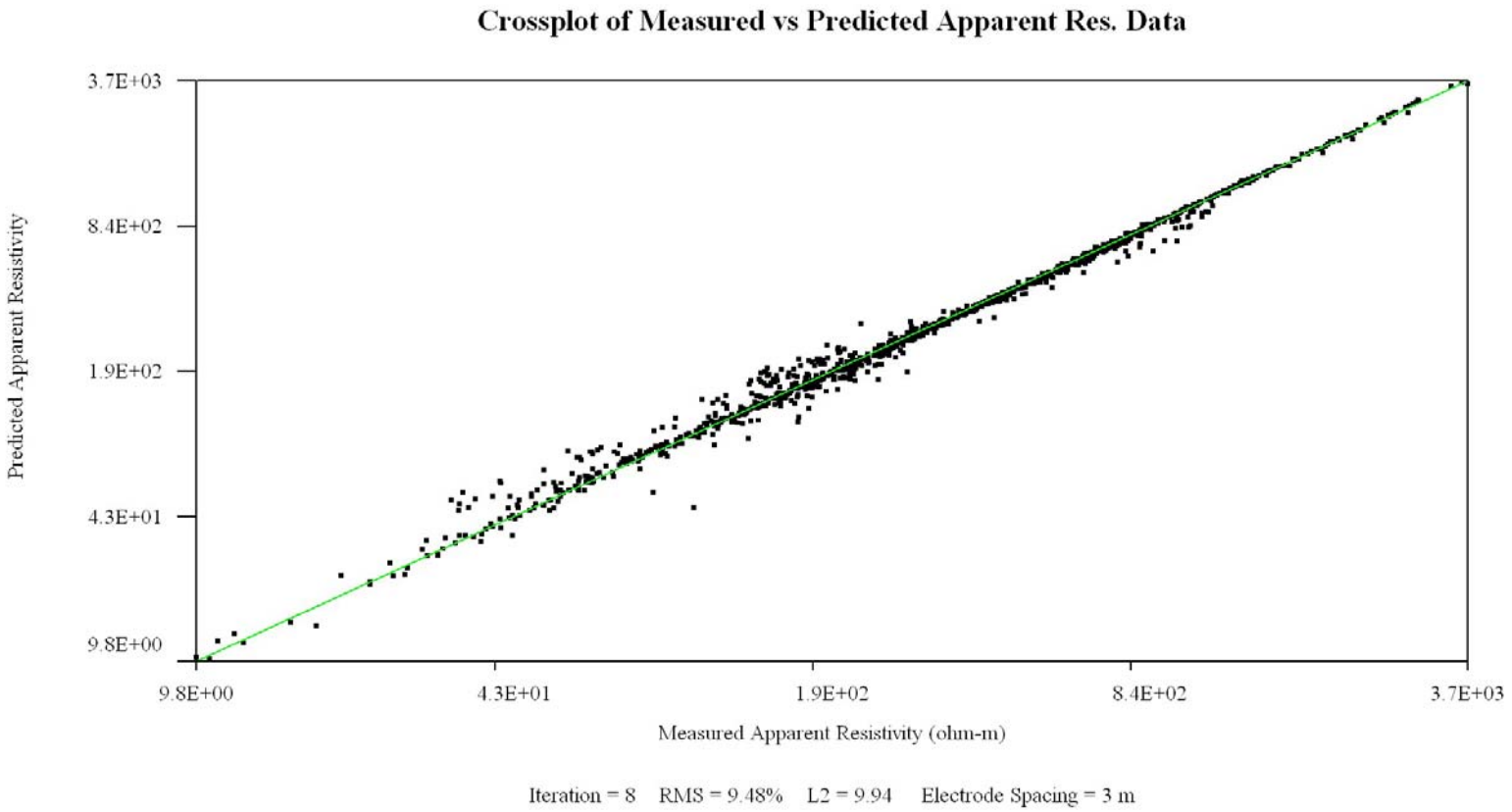

Site – 3: Kentucky Horse Park

Line - 5, without relative misfit data removed

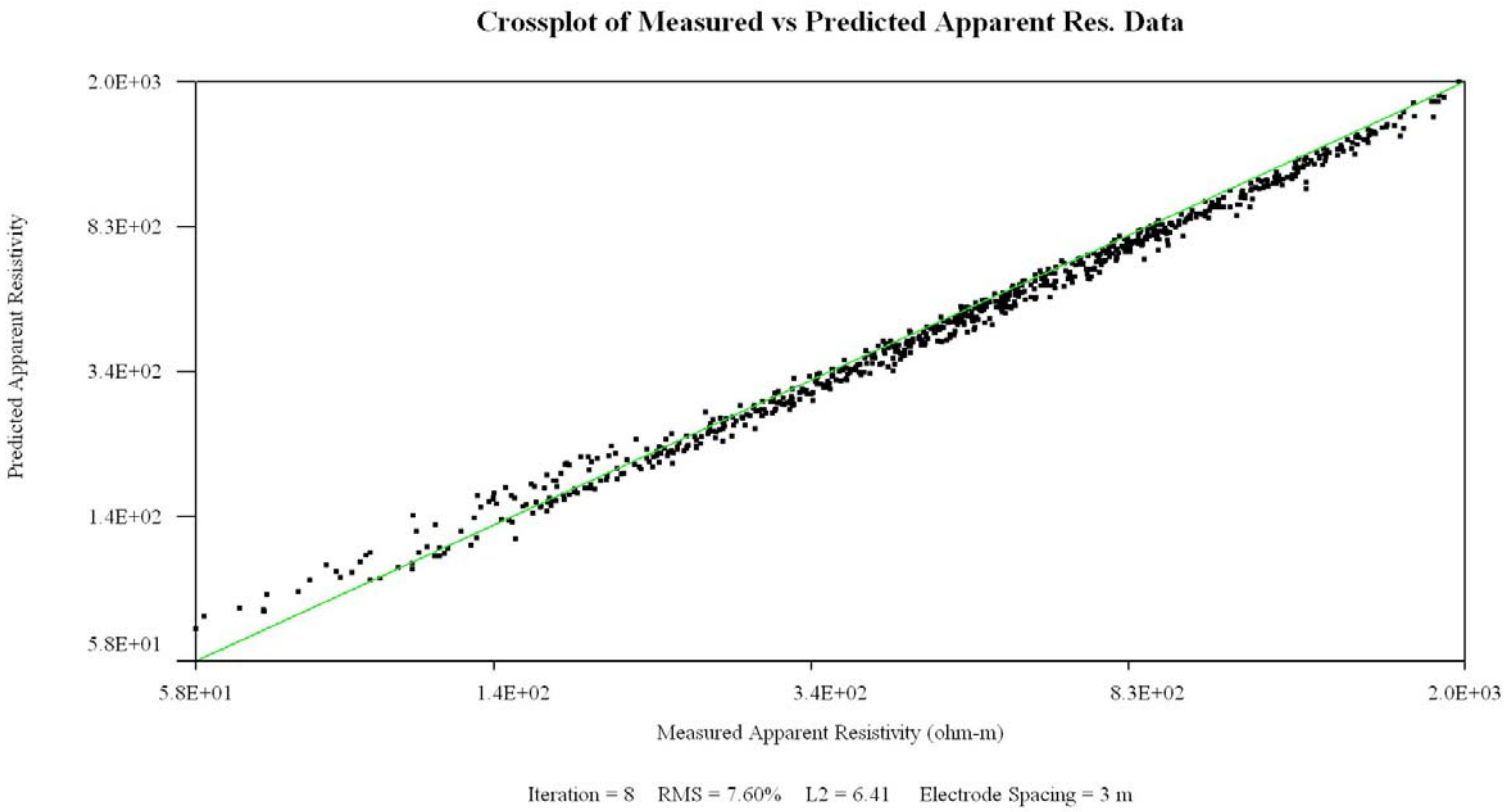

Line – 5, with relative data misfit above 15% removed

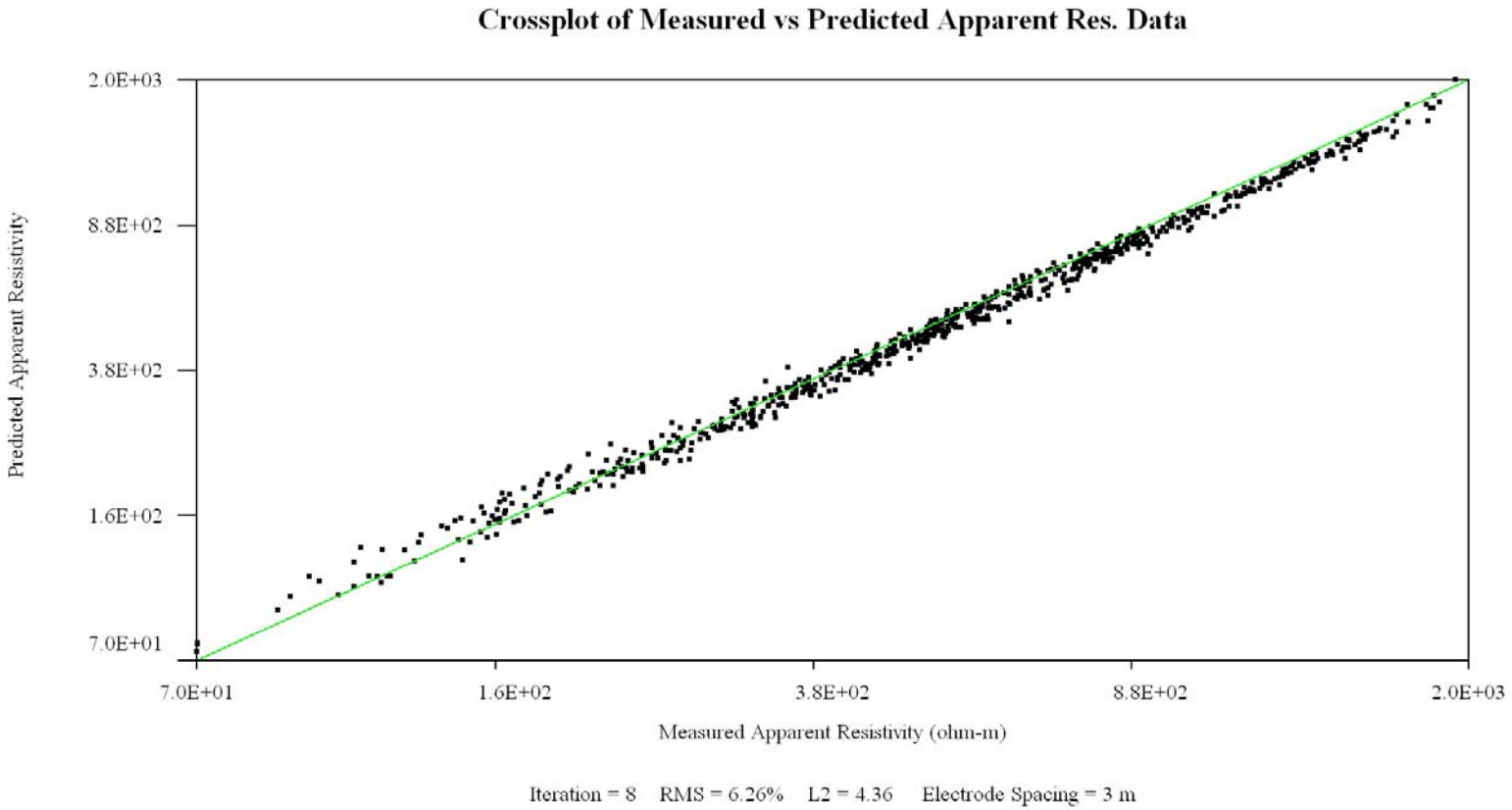

Line – 6(a), without relative misfit data removed

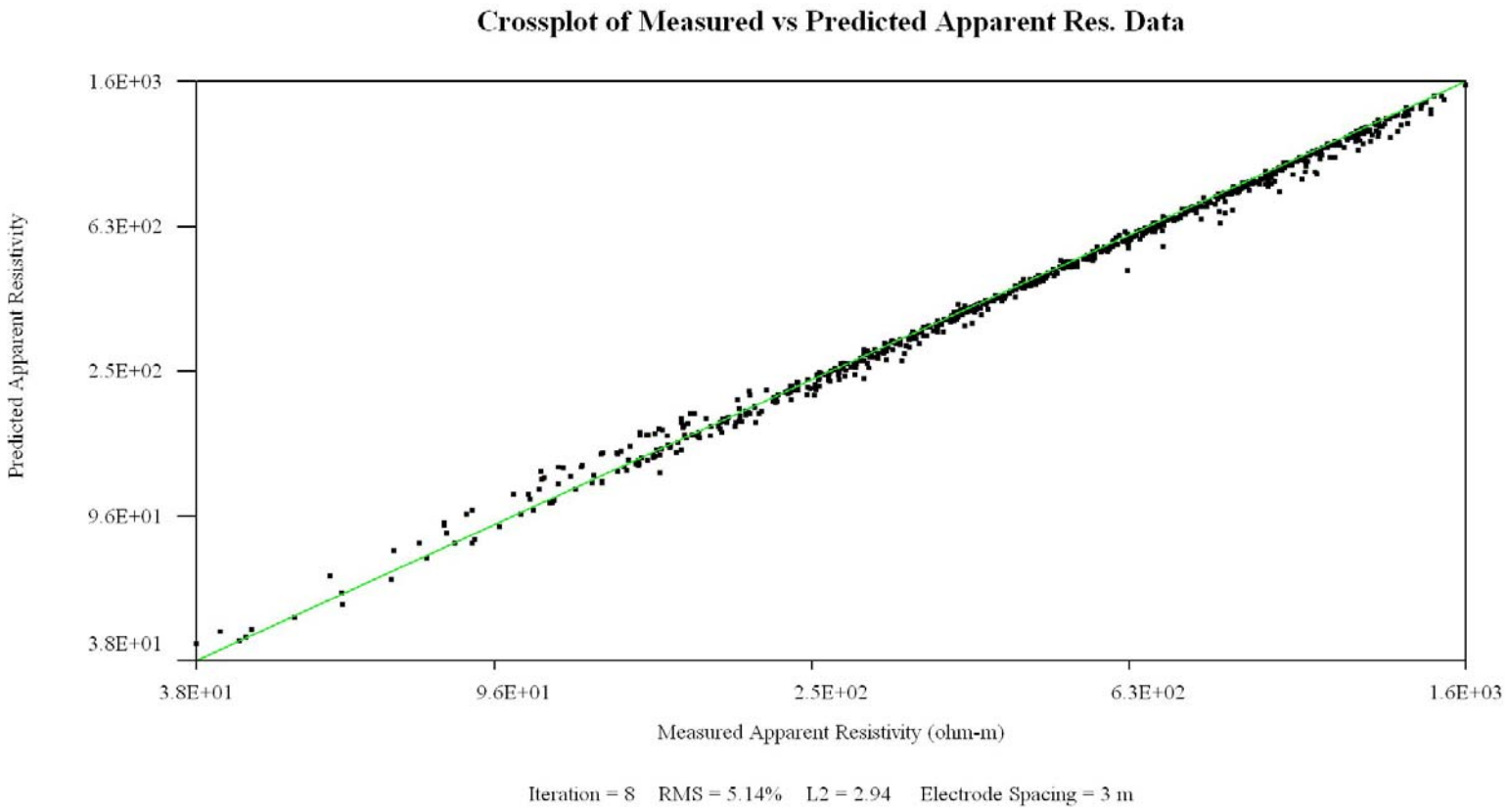

Line – 6(a), with relative data misfit above 10.5% removed

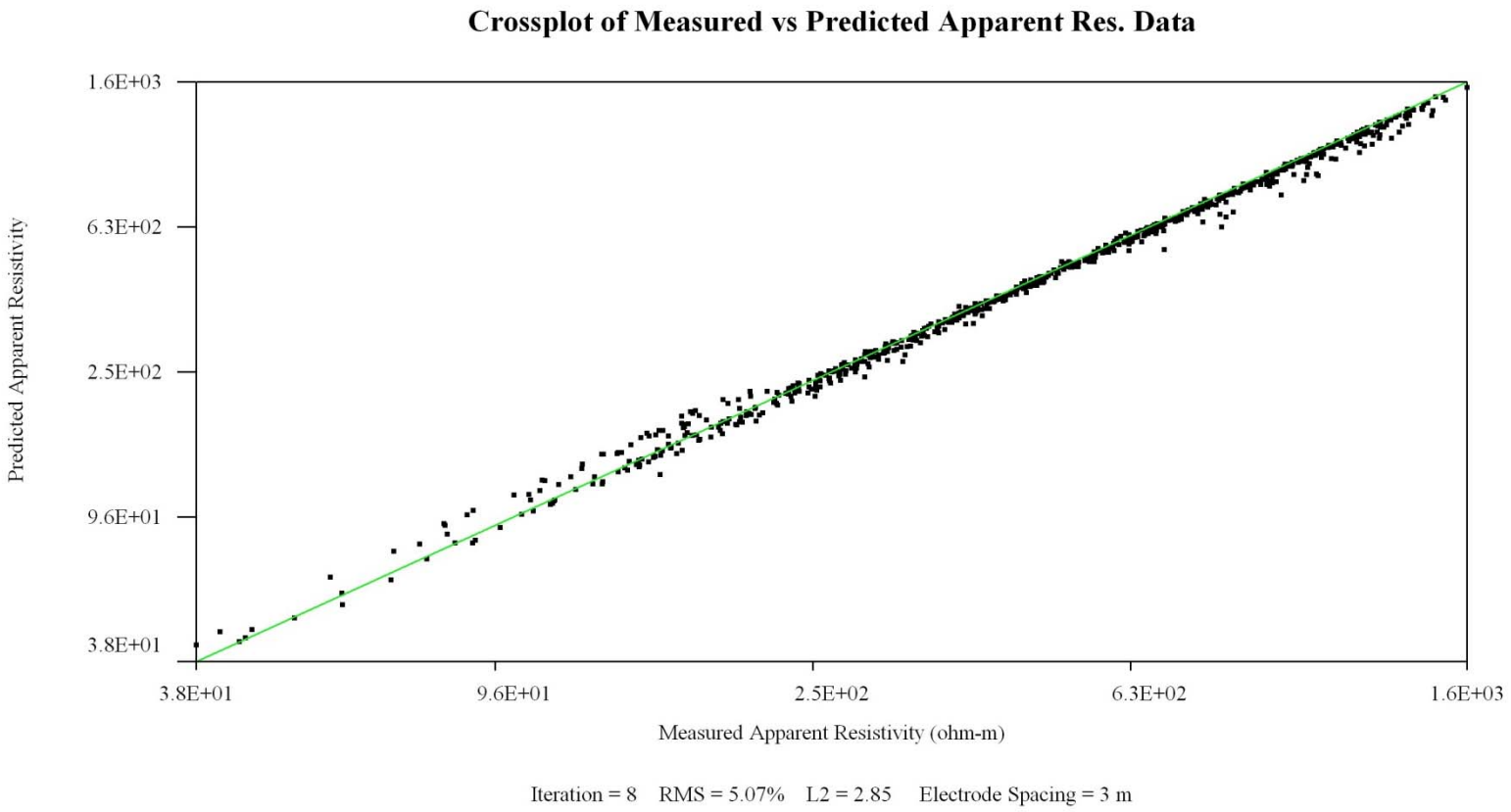

Line – 6(b), without relative misfit data removed

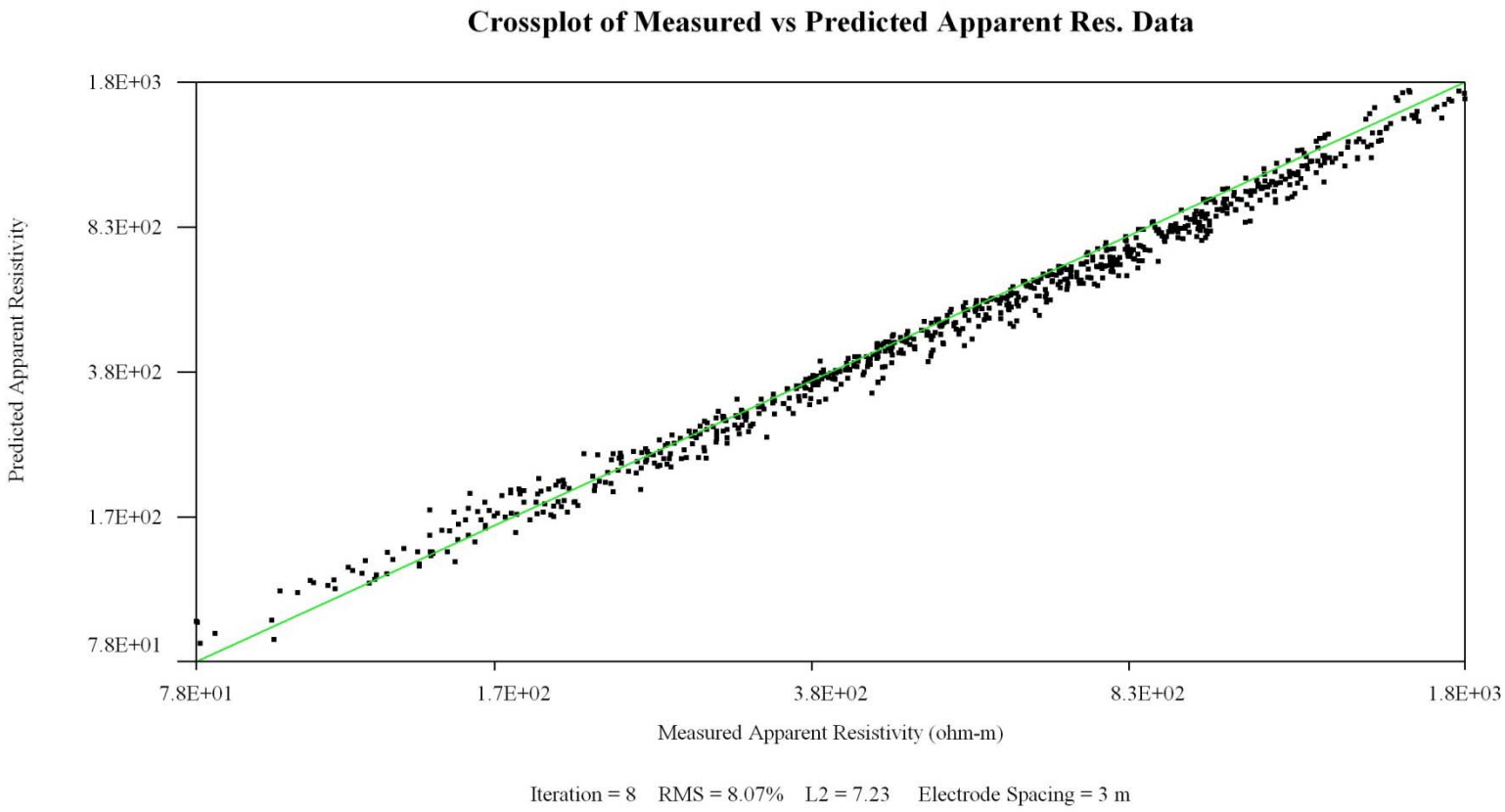

Line – 6(b), with relative data misfit above 19.5% removed

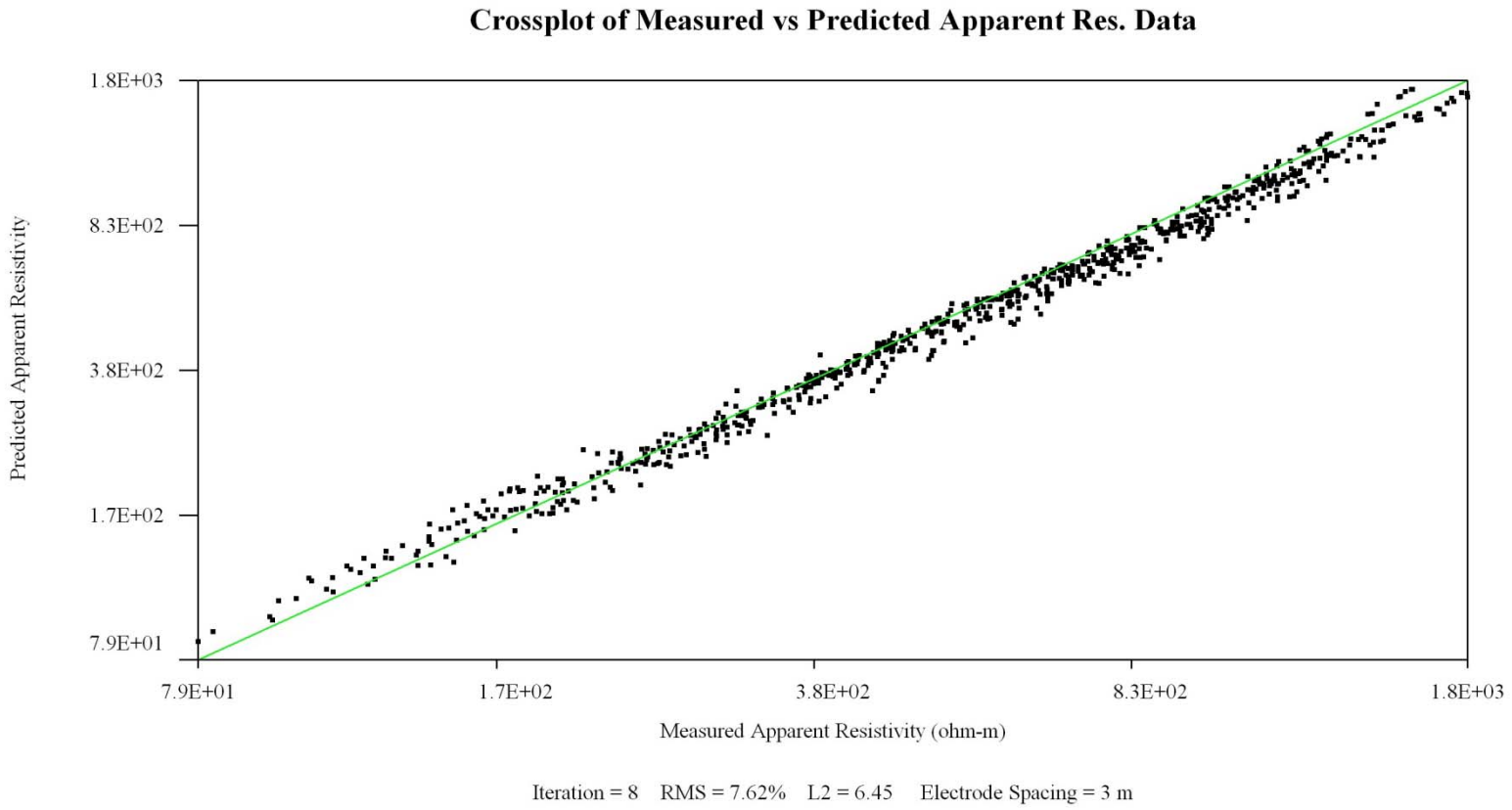

Appendix II

Self-potential field data

Site - 1

UK Agricultural Research Farm (Line - 1)							
Sept. 14, 2008				Dec. 28, 2008			
Electrode Spacing (ft.)	SP reading1 (mV)	SP reading2 (mV)	Average SP (mV)	Electrode Spacing (ft.)	SP reading1 (mV)	SP reading2 (mV)	Average SP (mV)
10	8.6	9.7	9.15	10	0.4	0.5	0.45
20	7.9	8	7.95	20	-1.1	-1.2	-1.15
30	4.8	5.5	5.15	30	2.5	2.6	2.55
40	6.7	7.2	6.95	40	3.1	3.4	3.25
50	1.6	2.2	1.9	50	4.4	4.7	4.55
60	2.1	3.5	2.8	60	-0.4	-0.5	-0.45
70	3.8	5.1	4.45	70	1	1.3	1.15
80	0.5	2.4	1.45	80	3	3.1	3.05
90	1.8	3.3	2.55	90	2.3	2.5	2.4
100	1.7	3.8	2.75	100	2.5	2.7	2.6
110	0.9	3.4	2.15	110	2.6	2.9	2.75
120	2.1	5.6	3.85	120	1.3	1.7	1.5
130	1.2	3.9	2.55	130	2.7	2.9	2.8
140	0.1	1.8	0.95	140	1.7	1.9	1.8
150	0.4	3.2	1.8	150	0.1	0.4	0.25
160	-2.2	-0.2	-1.2	160	1.2	1.6	1.4
170	-2.1	0.3	-0.9	170	1.9	2.4	2.15
180	-5.4	-1.9	-3.65	180	0.8	1.2	1
190	-2.2	-0.6	-1.4	190	1.4	2.1	1.75
200	-6.5	-5.5	-6	200	1.7	1.9	1.8
210	-13.2	-10.5	-11.85	210	4.6	3.7	4.15
220	-13.4	-11.6	-12.5	220	4.5	4.8	4.65
230	-16.1	-13.8	-14.95	230	6.4	6.9	6.65
240	-15.7	-14.4	-15.05	240	6.9	7.3	7.1
250	-15.1	-11.9	-13.5	250	7.9	8.1	8
260	-13.5	-11.6	-12.55	260	5.3	6	5.65
270	-14	-12.6	-13.3	270	5.3	6.1	5.7
280	-11.3	-10.4	-10.85	280	4.1	5.6	4.85

UK Agricultural Research Farm (Line - 2)									
Sept. 14, 2008				Dec. 28, 2008			March 10, 2009		
Electrode Spacing (ft.)	SP reading1 (mV)	SP reading2 (mV)	Average SP (mV)	SP reading1 (mV)	SP reading2 (mV)	Average SP (mV)	SP reading1 (mV)	SP reading2 (mV)	Average SP (mV)
10	-4.2	-4.2	-4.2	-2.8	-2.7	-2.75	-1.8	-2.2	-2
20	-0.7	-0.8	-0.75	-3.4	-3.5	-3.45	0.7	0.7	0.7
30	-0.7	-0.9	-0.8	-2.7	-2.6	-2.65	0.1	0	0.05
40	-0.4	-0.8	-0.6	-2.7	-2.9	-2.8	1.4	1.5	1.45
50	-3.5	-4.8	-4.15	-3.5	-3.7	-3.6	1.2	1.5	1.35
60	-3.9	-4.8	-4.35	-2.6	-2.7	-2.65	0.9	1.2	1.05
70	-0.2	-0.4	-0.3	-2.7	-2.9	-2.8	1.4	1.8	1.6
80	-5.6	-6	-5.8	-0.1	-0.2	-0.15	-0.6	-0.1	-0.35
90	-7.7	-8.1	-7.9	-2	-2.3	-2.15	0.8	1.2	1
100	-7.7	-8	-7.85	-2.5	-2.6	-2.55	0.4	0.8	0.6
110	-7.1	-7.7	-7.4	-2.6	-2.9	-2.75	1.8	2.3	2.05
120	-11.2	-11.8	-11.5	-0.8	-0.9	-0.85	-0.1	0.7	0.3
130	-14.1	-14.5	-14.3	-0.1	-0.2	-0.15	-0.2	0.4	0.1
140	-13.9	-14.1	-14	1.4	1.7	1.55	-0.8	-1.7	-1.25
150	-18.2	-18.6	-18.4	5.1	5.4	5.25	-3.7	-5	-4.35
160	-14.9	-15.4	-15.15	2.7	3	2.85	-1.7	-2.4	-2.05
170	-10.2	-10.9	-10.55	0.8	1.1	0.95	-0.5	0.2	-0.15
180	-8.6	-9.3	-8.95	-0.1	0.2	0.05	0.5	1	0.75
190	-5.6	-6.4	-6	-0.1	-0.6	-0.35	2.4	3.1	2.75
200	-5.6	-6.2	-5.9	-1.1	-1.4	-1.25	2.4	3.1	2.75
210	-4.9	-5.7	-5.3	-0.9	-1.2	-1.05	1.7	2.7	2.2
220	-3.9	-4.3	-4.1	-1.1	-1.5	-1.3	3.7	4.1	3.9
230	-5.6	-6.1	-5.85	-2.7	-3	-2.85	4.8	5.2	5
240	-3.4	-4.2	-3.8	-3.3	-2.9	-3.1	5.8	6.2	6
250	-2.7	-3.5	-3.1	-5.3	-5.5	-5.4	6.4	7.2	6.8
260	-5	-6.1	-5.55	-5.7	-6	-5.85	6.5	7.1	6.8

Site - 2

Berea Road (Line - 3)									
Nov. 4, 2008				Nov. 23, 2008			March 5, 2009		
Electrode Spacing (ft)	SP Reading 1 (mV)	SP Reading 2 (mV)	Average SP (mV)	SP Reading 1 (mV)	SP Reading 2 (mV)	Average SP (mV)	SP Reading 1 (mV)	SP Reading 2 (mV)	Average SP (mV)
15	-12.4	-12.4	-12.4	-4.2	-3.5	-3.85	-5	-5.3	-5.15
30	-15.9	-15.8	-15.85	-4.3	-4.4	-4.35	-5.2	-5.5	-5.35
45	-14	-13.8	-13.9	-3.1	-3.3	-3.2	-7.6	-8.2	-7.9
60	-17.7	-17.8	-17.75	-6.4	-6.5	-6.45	-9.8	-10.4	-10.1
75	-17.8	-18	-17.9	-8	-8.2	-8.1	-12.1	-13.2	-12.65
90	-20.8	-20.9	-20.85	-11.4	-11.6	-11.5	-13.7	-14.4	-14.05
105	-20.1	-20.4	-20.25	-12.7	-13	-12.85	-15.1	-16.2	-15.65
120	-20.7	-20	-20.35	-11.6	-12	-11.8	-19.1	-20.1	-19.6
135	-20.6	-20.2	-20.4	-14.3	-14.8	-14.55	-18.6	-20.1	-19.35
150	-23.1	-23.4	-23.25	-16.2	-16.6	-16.4	-21.9	-22.4	-22.15
165	-24.2	-24.5	-24.35	-15.9	-16.5	-16.2	-22.7	-24.1	-23.4
180	-27.6	-27.4	-27.5	-17.1	-17.9	-17.5	-23.8	-24.3	-24.05
195	-28.8	-28.4	-28.6	-19.7	-20.2	-19.95	-27.7	-28.3	-28
210	-29.9	-30.3	-30.1	-20.7	-21.2	-20.95	-30.6	-31.2	-30.9
225	-35.2	-34.9	-35.05	-25.3	-25.8	-25.55	-34.7	-36.2	-35.45
240	-36.5	-37.1	-36.8	-23.5	-24	-23.75	-34.6	-36	-35.3
255	-32.2	-31.5	-31.85	-20.2	-20.8	-20.5	-30.7	-31.9	-31.3
270	-28.3	-27.9	-28.1	-18.9	-19.5	-19.2	-31.4	-32.2	-31.8
285	-26.4	-26	-26.2	-19.6	-20.2	-19.9	-30.5	-32.1	-31.3
300	-27.5	-28	-27.75	-20.2	-20.8	-20.5	-30.5	-33.1	-31.8
315	-27.3	-26.8	-27.05	-18.2	-18.8	-18.5	-30.6	-32	-31.3
330	-27.1	-26.5	-26.8	-16.5	-17.3	-16.9	-26.7	-29.6	-28.15
345	-25.4	-24.5	-24.95	-17.2	-18	-17.6	-26.6	-27.9	-27.25
360	-25.8	-24.9	-25.35	-14.2	-15.1	-14.65	-26.2	-29.4	-27.8
375	-21.5	-20.4	-20.95	-12.9	-14.2	-13.55	-24.4	-27.6	-26
390	-21.8	-20.7	-21.25	-12.1	-13.2	-12.65	-24.3	-27.8	-26.05
405	-18.4	-16.9	-17.65	-11.2	-12.2	-11.7	-20.6	-23.3	-21.95
420	-17.1	-16.8	-16.95	-8.9	-10.1	-9.5	-21.3	-22.7	-22
435	-13.8	-11.9	-12.85	-6.1	-7.3	-6.7	-20.1	-22.9	-21.5
450	-9.1	-8.3	-8.7	-4.3	-5.8	-5.05	-18.6	-21.7	-20.15

Berea Road Soccer Field (Line - 4)							
Nov. 23, 2008				March 5, 2009			
Electrode Spacing (ft)	SP Reading 1 (mV)	SP Reading 2 (mV)	Average SP (mV)	Electrode Spacing (ft)	SP Reading 1 (mV)	SP Reading 2 (mV)	Average SP (mV)
15	-3.4	-3.5	-3.45	15	-1.8	-1.9	-1.85
30	-0.4	-0.6	-0.5	30	-2	-2.2	-2.1
45	-3.1	-3.3	-3.2	45	-0.7	-0.8	-0.75
60	-1.9	-2.1	-2	60	-1.1	-1.6	-1.35
75	-0.9	-1.2	-1.05	75	-0.9	-1.6	-1.25
90	-2.6	-3	-2.8	90	-0.1	-0.3	-0.2
105	-1.2	-1.6	-1.4	105	-0.7	-1.2	-0.95
120	-2	-2.4	-2.2	120	-0.1	-0.3	-0.2
135	0.8	1.2	1	135	2	2.2	2.1
150	-0.5	-0.8	-0.65	150	3.2	3.5	3.35
165	0.2	0.6	0.4	165	3.1	3.7	3.4
180	0.1	0.3	0.2	180	4.6	5.2	4.9
195	0	-0.2	-0.1	195	4.1	4.6	4.35
210	-2.1	-2.6	-2.35	210	3.9	4.6	4.25
225	-3.3	-3.8	-3.55	225	4.2	5.2	4.7
240	-1.8	-2.4	-2.1	240	5.6	6.2	5.9
255	-3.5	-4	-3.75	255	6.1	6.8	6.45
270	-3	-3.5	-3.25	270	5.7	6.1	5.9
285	-4.2	-4.8	-4.5	285	4.3	5.1	4.7
300	-7.9	-8.4	-8.15	300	3.6	4.1	3.85
315	-9.5	-10	-9.75	315	1.7	2	1.85

Site - 3

Kentucky Horse Park (Line - 5)			
March 8, 2009			
Electrode Spacing (ft)	SP Reading 1 (mV)	SP Reading 2 (mV)	Average SP (mV)
15	3.6	2.8	3.2
30	3.9	4	3.95
45	4.3	4.1	4.2
60	4.1	5	4.55
75	5	5.3	5.15
90	8.4	9	8.7
105	10.3	10.6	10.45
120	9.8	10	9.9
135	11.2	11.5	11.35
150	12	12.2	12.1
165	15.1	15.3	15.2
180	13.8	14	13.9
195	15.1	15.3	15.2
210	15.7	16	15.85
225	16.7	17	16.85
240	17.1	17.4	17.25
255	19	19.4	19.2
270	18.4	19	18.7
285	19.7	20.2	19.95
300	18.7	19	18.85
315	19.2	19.5	19.35
330	19.7	20.3	20
345	21.9	22.3	22.1
360	21.1	21.5	21.3
375	23	24	23.5
390	22.6	23.2	22.9
405	24.7	25.1	24.9
420	23.2	24.1	23.65
435	25.1	25.6	25.35
450	27.1	28	27.55
465	26.9	27.9	27.4
480	25.4	26	25.7
495	25.1	25.9	25.5
510	25.5	26.2	25.85
525	25.4	26.2	25.8
540	24	25.2	24.6
555	26.5	26.8	26.65
570	25.8	26.9	26.35
585	26.5	27.6	27.05
600	24.4	25.4	24.9
615	21.2	23.4	22.3

Kentucky Horse Park (Line - 6)							
Nov. 2, 2008				March 8, 2009			
Electrode Spacing (ft)	SP Reading 1 (mV)	SP Reading 2 (mV)	Average SP (mV)	Electrode Spacing (ft)	SP Reading 1 (mV)	SP Reading 2 (mV)	Average SP (mV)
15	-1.2	-1.3	-1.25	15	5	5.1	5.05
30	-1.9	-2	-1.95	30	8.3	8.5	8.4
45	-4.5	-4.8	-4.65	45	9.6	9.9	9.75
60	-1.6	-2	-1.8	60	9.3	9.9	9.6
75	-1	-1.5	-1.25	75	9.3	9.6	9.45
90	-5.6	-6	-5.8	90	8.9	9.4	9.15
105	-5.3	-6.1	-5.7	105	10.7	11	10.85
120	-1.6	-2.1	-1.85	120	13	13.3	13.15
135	-0.6	-1.9	-1.25	135	13.3	13.6	13.45
150	-1.3	-1.1	-1.2	150	13	13.4	13.2
165	-4.5	-5.4	-4.95	165	15.2	15.6	15.4
180	-6.8	-8.1	-7.45	180	16	16.4	16.2
195	-7.3	-7.8	-7.55	195	15.9	16.3	16.1
210	-8.6	-9.1	-8.85	210	16.6	17.1	16.85
225	-8.7	-8.9	-8.8	225	20	20.3	20.15
240	-8.3	-9	-8.65	240	19.5	19.8	19.65
255	-8.8	-9.4	-9.1	255	19.5	19.8	19.65
270	-8.5	-9.5	-9	270	19	19.3	19.15
285	-4.2	-5	-4.6	285	20.2	20.7	20.45
300	-2.2	-2.8	-2.5	300	25.7	25.9	25.8
315	-8.4	-8.9	-8.65	315	25.5	26.2	25.85
330	-7.4	-8	-7.7	330	25.4	26.1	25.75
345	-11.8	-12.6	-12.2	345	26.8	27.4	27.1
360	-11.1	-11.6	-11.35	360	27.3	28.1	27.7
375	-10.9	-11.6	-11.25	375	25.7	26.3	26
390	-9.6	-10.1	-9.85	390	26	27	26.5
405	-9.5	-10	-9.75	405	28.1	29	28.55
420	-11.4	-12.2	-11.8	420	28.1	29.1	28.6
435	-11.3	-11.6	-11.45	435	28.6	29.1	28.85
450	-11.5	-12.3	-11.9	450	29.2	29.8	29.5
465	-12.9	-13.9	-13.4	465	27	28.2	27.6
480	-14.9	-15.5	-15.2	480	27.3	28	27.65
495	-10.8	-11.3	-11.05	495	27.1	27.8	27.45
510	-10.5	-11.1	-10.8	510	26.7	27.3	27
525	-12.3	-12.8	-12.55	525	28.2	28.6	28.4
540	-10.4	-11.1	-10.75	540	29.1	30	29.55
555	-10.5	-11.5	-11	555	30.1	30.8	30.45
570	-7.1	-8	-7.55	570	30.2	30.6	30.4
585	-7.7	-8.5	-8.1	585	30.4	31.3	30.85
600	-9.3	-10.1	-9.7	600	30.9	31.2	31.05
615	-11.5	-12	-11.75	615	31.2	32	31.6
630	-12	-12.8	-12.4	630	31.4	32.1	31.75
645	-8.9	-9.7	-9.3	645	32.2	32.7	32.45
660	-9.1	-10.1	-9.6	660	33	33.7	33.35
675	-7.5	-8.5	-8	675	32.2	31.3	31.75
690	-8.3	-9	-8.65	690	31.3	31.4	31.35

Kentucky Horse Park (Line - 7)									
Aug. 29,2008				Sept. 12,2008			March 18, 2009		
Electron Spacing (ft.)	SP reading 1 (mV)	SP reading 2 (mV)	Average SP (mV)	SP reading 1 (mV)	SP reading 2 (mV)	Average SP (mV)	SP reading 1 (mV)	SP reading 2 (mV)	Average SP (mV)
15	7.7	8.2	7.95	-2.1	-2.2	-2.15	5.4	5.6	5.5
30	-1.5	-0.7	-1.1	-2.7	-4.1	-3.4	5.4	5.8	5.6
45	7.6	8.8	8.2	-1.6	-2.8	-2.2	9.7	10.2	9.95
60	10.5	11.5	11	-0.2	1.8	0.8	9.6	10.3	9.95
75	23.1	24.1	23.6	3.2	6.4	4.8	11.5	12.4	11.95
90	10	10.8	10.4	0.2	2.6	1.4	14.2	15.4	14.8
105	10.4	11.7	11.05	0.7	4.1	2.4	14.8	16.2	15.5
120	12.2	13.6	12.9	1.8	6.4	4.1	18.3	19.2	18.75
135	18.5	19.9	19.2	3.2	10.5	6.85	19.8	21.2	20.5
150	15.8	17.5	16.65	-0.1	7.3	3.6	20.5	21.4	20.95
165	15.9	18.5	17.2	0.8	8.8	4.8	21.1	23.6	22.35
180	23.7	25.1	24.4	2.4	10.3	6.35	23.7	25.2	24.45
195	16.1	18.4	17.25	0.4	10.5	5.45	23.4	25.3	24.35
210	15.4	17.1	16.25	2.1	9.2	5.65	26.4	28	27.2
225	21	23.9	22.45	4.1	13.6	8.85	26.6	28.1	27.35
240	15.7	18.5	17.1	1.4	11.8	6.6	28.6	29.4	29
255	9	12.7	10.85	1.4	13.9	7.65	28.8	31.7	30.25
270	18.3	21.5	19.9	5.2	16.4	10.8	30.9	33.2	32.05
285	13.8	16.6	15.2	4.9	16.6	10.75	33.5	35.8	34.65
300	22.9	25.8	24.35	7.8	16.5	12.15	35.7	38.3	37
315	18.3	21.8	20.05	6.9	17.5	12.2	33.3	36.5	34.9
330	18.8	23	20.9	11.9	25.5	18.7	36.5	38.4	37.45
345	22.8	26.1	24.45	9.3	21.9	15.6	35.8	38.3	37.05
360	16.7	21.3	19	11.6	25.7	18.65	39.6	41.2	40.4
375	26.8	29.1	27.95	13.3	24.1	18.7	39.8	42.3	41.05
390	24.3	29.2	26.75	11.9	23.9	17.9	39.1	42.4	40.75
405	24.5	28.1	26.3	15.4	24.4	19.9	40.1	43.5	41.8
420	26.3	31.4	28.85	16.2	25.3	20.75	40.9	42.6	41.75
435	24.7	28.4	26.55	14.4	26.9	20.65	39.7	41.8	40.75
450	24.2	2.9	13.55	16.8	27.1	21.95	42.8	44.5	43.65
465	36	42	39	18.5	30.9	24.7	41.5	44	42.75
480	28.7	32.7	30.7	13.7	24.6	19.15	39.7	42.6	41.15
495	26.9	31.4	29.15	12.5	23.2	17.85	36.4	41.4	38.9
510	22.2	27.6	24.9	11.3	22.1	16.7	40.7	43.2	41.95
525	22.8	27.3	25.05	13.9	25.1	19.5	42.6	45.8	44.2
540	27.3	32.4	29.85	16.2	29.2	22.7	42.6	46.1	44.35
555	26.8	32.2	29.5	14.6	26.5	20.55	43.7	47.2	45.45
570	26.1	31.2	28.65	16.7	28.4	22.55	42.7	46.5	44.6
585	27.7	33.3	30.5	15.8	30.4	23.1	42.8	46.4	44.6
600	26	30.7	28.35	18	32.5	25.25	44.7	46.4	45.55
615	28	32.2	30.1	12.1	26.7	19.4	43.9	46.3	45.1
630	18.3	23.8	21.05				41.4	45.7	43.55
645	13.6	18.3	15.95				38.9	43.1	41

References

Adeyemi, A., Idornigie, A. & Olorunfemi, M. 2006. Spontaneous potential and electrical resistivity response modelling for a thick conductor. *Journal of Applied Sciences Research* **2**, 691-702.

AGI, 2005. Instruction manual for the SuperSting^{TM} with Swift^{TM} automatic resistivity and IP system: Austin, TX, Advanced Geosciences, Inc., 87 p.

AGI, 2007. Seminar on resistivity imaging, *AGI Resistivity Imaging Seminar*, Sept. 11-12, Austin, TX.

Ahmad, M. 1964. A laboratory study of streaming potentials. *Geophysical Prospecting* **12**, 49-64.

Ahmed, S. & Carpenter, P. 2003. Geophysical response of filled sinkholes, soil pipes and associated bedrock fractures in thinly mantled karst, east-central Illinois. *Environmental Geology* **44**, 705-716.

Aubert, M. & Atangana, Q. 1996. Self-potential method in hydrogeological exploration of volcanic areas. *Ground Water* **34**, 1010-1016.

Bakalowicz, M. 2005. Karst groundwater: a challenge for new resources. *Hydrogeology Journal* **13**, 148-160.

Bogoslovsky, V. & Ogilvy, A. 1972. The study of streaming potentials on fissured media models. *Geophysical Prospecting* **20**, 109-117.

Bonita, J.A. 1993. An electrical resistivity and fracture trace study in the Inner Bluegrass karst region of north-central Kentucky. *University of Kentucky, M. S. Thesis*, 155 p.

Carpenter, P.J. & Ekberg, D.W. 2006. Identification of buried sinkholes, fractures and soil pipes using ground-penetrating radar and 2D electrical resistivity tomography. *Proceedings of the 2006 Highway Geophysics - NDE Conference*, 437-449.

Corwin, R. 1990. The self-potential method for environmental and engineering applications. *Geotechnical and Environmental Geophysics* **1**, 127-145.

Cressman, E. 1965. Geologic map of the Keene quadrangle, central Kentucky: *U. S. Geological Survey Geologic Quadrangle Map GQ-440*.

Cressman, E. 1967. Geologic map of the Georgetown quadrangle, Scott and Fayette Counties, Kentucky: *U. S. Geological Survey Geologic Quadrangle Map GQ-605*.

Cressman, E. 1973. Lithostratigraphy and depositional environments of the Lexington Limestone (Ordovician) of central Kentucky. *U. S. Geological Survey Professional Paper 768,* 61 p.

Currens, J., Paylor, R. & Ray, J.A. 2002. Mapped karst ground-water basins in the Lexington 30 by 60 quadrangle. *Map and Chart 10, Series XII, Kentucky Geological Survey, University of Kentucky, 1 sheet*.

Dahlin, T. & Zhou, B. 2004. A numerical comparison of 2D resistivity imaging with ten electrode arrays. *Geophysical Prospecting* **52**, 379–398.

Domenico, P.A. & Schwartz, F.W. 1998. *Physical and Chemical Hydrogeology*, John Wiley, New York, 506 p.

El-Araby, H. 2004. A new method for complete quantitative interpretation of self-potential anomalies. *Journal of Applied Geophysics* **55**, 211-224.

El-Qady, G., Hafez, M., Abdalla, M. & Ushijima, K. 2005. Imaging subsurface cavities using geoelectric tomography and ground-penetrating radar. *Journal of Cave and Karst Studies* 67(3), 174-181.

Ernstson, K. & Scherer, H. 1986. Self-potential variations with time and their relation to hydrogeologic and meteorological parameters. *Geophysics* **51**, 1967-1977.

Eslinger, E. & Pevear, D. 1988. *Clay minerals for petroleum geologists and engineers*. Society of Economic Paleontologists and Mineralogists, Tulsa, OK.

Fagerlund, F. & Heinson, G. 2003. Detecting subsurface groundwater flow in fractured rock using self-potential (SP) methods. *Environmental Geology* **43**, 782-794.

Faust, R. 1977. Ground-water resources of the Lexington, Kentucky, area. *U. S. Geological Survey Water-Resources Investigations Report 76-113,* 24 p.

Graham, C.D.R. 2000. Electrical resistivity studies in the Inner Bluegrass Karst Region, Kentucky. *University of Kentucky, M. S. Thesis*, 92.

Hamilton, D. 1950. Areas and principles of ground-water occurrence in the Inner Bluegrass Region, Kentucky: *Series IX, Bulletin* **5**, *Kentucky Geological Survey,* 68 p.

Hiltunen, D., Hudyma, N., Quigley, T. & Samakur, C. 2007. Ground proving three seismic refraction tomography programs. *Transportation Research Record* **2016**, 110-120.

Ishido, T. & Mizutani, H. 1981. Experimental and theoretical basis of electrokinetic phenomena in rock-water systems and its applications to geophysics. *Journal of Geophysical Research* **86**, 1763-1775.

Jardani, A., Dupont, J. & Revil, A. 2006. Self-potential signals associated with preferential groundwater flow pathways in sinkholes. *Journal of Geophysical Research-Solid Earth* **111**, B09204.

Jardani, A., Revil, A., Santos, F., Fauchard, C. & Dupont, J. 2007. Detection of preferential infiltration pathways in sinkholes using joint inversion of self-potential and EM-34 conductivity data. *Geophysical Prospecting* **55**, 749-760.

John, J.Q., David, T. & James, A.K. 2006. Modeling of complex flow in a karst aquifer. *Sedimentary Geology* **184**, 343-351.

Kentucky Geologic Map Information Service, 2009. Kentucky Geological Survey. http://kgsmap.uky.edu/website/KGSGeology/viewer.asp

Kiraly, L. 2003. Karstification and groundwater flow. *Speleogenesis and Evolution of Karst Aquifers* **1**.

Lange, A. & Kilty, K. 1991. Natural-potential responses of karst systems at the ground surface. *Proceedings of the Third Conference on Hydrogeology, Ecology, Monitoring, and Management of Hydrogeology in Karst Terrains,* 179-196.

Lange, A.L. 1999. Geophysical studies at Kartchner Caverns State Park, Arizona. *Journal of Cave and Karst Studies* **61**, 68-72.

Leucci, G. & De Giorgi, L. 2005. Integrated geophysical surveys to assess the structural conditions of a karstic cave of archaeological importance. *Natural Hazards and Earth System Sciences* **5**, 17-22.

Loke, M. 2001. Tutorial: 2-D and 3-D electrical imaging surveys. *Geotomo Software, Malaysia*.

Matson, G. 1909. Water resources in the Blue Grass region, Kentucky: *US Geological Survey Water Supply Paper 233, 42–45.*

Mochales, T., Casas, A., Pueyo, E., Pueyo, O., Román, M., Pocoví, A., Soriano, M. & Anson, D. 2008. Detection of underground cavities by combining gravity, magnetic and ground penetrating radar surveys: a case study from the Zaragoza area, NE Spain. *Environmental Geology* **53**, 1067-1077.

Motyka, J. 1998. A conceptual model of hydraulic networks in carbonate rocks, illustrated by examples from Poland. *Hydrogeology Journal* **6**, 469-482.

Nosow, E. & McFarlan, A. 1960. Geology of the central Bluegrass area. *Series X, Guidebook 12*, *Kentucky Geological Survey,* 56 p.

Palacky, G.V. 1987. Resistivity characteristics of geologic targets. *Applied Geophysics* **1**, ,1351.

Palmquist, W.M. & Hall, F.R. 1961. Reconnaissance of ground-water resources in the Blue Grass Region of Kentucky. *U. S. Geological Survey Water Supply Paper 1553*, 39 p.

Parasnis, D. 1986. *Principles of Applied Geophysics*, Chapman and Hall, New York, 402 pp.

Paylor, R. & Currens, J. 2004. Royal spring karst groundwater travel time investigation. *Report prepared for Georgetown Municipal Water and Sewer Services, Kentucky Geological Survey, University of Kentucky*, 15p.

Romanov, D., Dreybrodt, W. & Gabrovsek, F. 2002. Interaction of fracture and conduit flow in the evolution of karst aquifers. In Martin, J.B, Wicks, C.M., and Sasowsky, I.D (eds.), *Hydrogeology and Biology of Post-Paleozoic Carbonate Aquifers, Karst Waters Institute Special Publication 7,* Charles Town, West Virginia.

Roth, M. & Nyquist, J. 2003. Evaluation of multi-electrode earth resistivity testing in karst. *Geotechnical Testing Journal* **26**, 167-178.

Schwartz, B. & Schreiber, M. 2009. Quantifying potential recharge in mantled sinkholes using ERT. *Ground Water* **47**, 370 - 381.

Sheehan, J.R., Doll, W.E., Watson, D.B. & Mandell, W.A. 2005. Application of seismic refraction tomography to karst cavities. *U. S. Geological Survey Scientific Investigation Report 5160*, 29-38.

Spangler, L., Troester, J. & Thrailkill, J. 1982. Northern Fayette and southern Scott Counties area p. 38 to 54, in J. Thrailkill et al., Groundwater in the Inner Bluegrass karst region, Kentucky. *Available from the National Technical Information Service, Springfield VA 22161 as PB 83-108126. Research Report*.

Stevanovic, Z. & Dragisic, V. 1998. An example of identifying karst groundwater flow. *Environmental Geology* **35**, 241-244.

Styles, P., McGrath, R., Thomas, E. & Cassidy, N. 2005. The use of microgravity for cavity characterization in karstic terrains. Vol. 38, pp. 155-169. Geological Soc London.

Sullivan, S. 1983. An investigation of flow in two groundwater basins in the Inner Bluegrass karst region, Kentucky using fluorescent dyes. *University of Kentucky, M. S. Thesis*, 85 p.

Telford, W.M., Geldart, L.P., Sheriff, R.E. & Keys, D.A. 1983. *Applied Geophysics.* Cambridge University Press.

Thrailkill, J. & Gouzie, D. 1984. Discharge and travel time determinations in the Royal Spring groundwater basin, Kentucky. *Available from the National Technical*

Information Service, Springfield, VA 22161 as PB 85-214765/AS. Research Report.

Thrailkill, J., Spangler, L., Hopper, W. & Troester, J. 1982. Groundwater in the Inner Bluegrass karst region, Kentucky. *Available from the National Technical Information Service, Springfield, VA 22161 as PB 83-108126. Research Report*.

UK Agricultural Weather Center, 2009. Climatology data. http://wwwagwx.ca.uky.edu/climdata.html

Wanfang, Z., Beck, B. & Stephenson, J. 1999. Investigation of groundwater flow in karst areas using component separation of natural potential measurements. *Environmental Geology* **37**, 19-25.

White, W. 2002. Karst hydrology: recent developments and open questions. *Engineering Geology* **65**, 85-105.

White, W. & White, E. 2005. Ground water flux distribution between matrix, fractures, and conduits: constraints on modeling. *Speleogenesis and Evolution of Karst Aquifers* **3**, 2–8.

Zhou, W., Beck, B. & Adams, A. 2002. Effective electrode array in mapping karst hazards in electrical resistivity tomography. *Environmental Geology* **42**, 922-928.

VITA

Ganesh Nath Tripathi, permanent resident of Nepal, was born on June 15, 1974. After completing Master's of Science in Geology from Tribhuvan University in 2001, he joined the Nepal Electricity Authority, Kathmandu, Nepal, as a geologist for two years. He has been appointed as a geologist at the Department of Mines and Geology since 2003. He served as a teaching and research assistant at the Department of Earth and Environmental Sciences, University of Kentucky from 2007 to 2009.

Publications:

- Phillips, J. D., McCormack, S., Duan, J., Russo, J. P., Schumacher, A. M., Tripathi, G. N., Brockman, R. B., Mays, A. B., Pulugurtha, S., 2009. Origin and interpretation of knickpoints in the Big South Fork River basin, Kentucky-Tennessee. In press: Geomorphology. Available online 8 July 2009.
- Tripathi, G.N., Fryar, A.E., Paylor, R.L., Dinger, J.S., Currens, J.C., and Strohmeyer, J.S., 2009, Use of integrated geophysical techniques to locate a karst conduit in the Inner Bluegrass region, Kentucky: Geological Society of America Abstracts with Programs, v. 41, no. 4, p. 15.
- Tripathi, G.N., Fryar, A.E., Paylor, R.L., Dinger, J.S., Currens, J.C., and Strohmeyer, J.S., 2009, Use of surface geophysical techniques to locate a karst conduit in the Cane Run – Royal Spring basin, Kentucky, *in* Kentucky Water Resources Annual Symposium Proceedings: Lexington, University of Kentucky, Kentucky Water Resources Research Institute, p. 73.